ACOUSTIC EMISSION FOR FATIGUE CRACK MONITORING IN NUCLEAR PIPING SYSTEM

PhD Thesis

Shukri Mohd

Cardiff School of Engineering
Cardiff University, Cardiff
UK
2012

SUMMARY OF THESIS

Candidate's Name: Shukri Mohd
Candidate's for the Degree of: PHD
Institution at which study pursued: School of Engineering, Cardiff University
Full title of Thesis: Acoustic Emission for Fatigue Crack Monitoring in Nuclear Piping System

Summary:

Accurate Acoustic Emission (AE) source location is crucial for monitoring the thermal fatigue crack in nuclear piping systems. Conventional Time of Arrival (TOA) location techniques can provide estimated location of fatigue cracks but are not accurate enough to allow crack size estimation. This thesis examines the role of AE as a Non-destructive Testing (NDT) tool for thermal fatigue damage monitoring in nuclear piping system. The work focuses on developing an accurate AE source location technique. The works is divided into three main areas of research:

1. **Development of Wavelet Transform analysis and Modal Location (WTML) method**

A novel location method was successfully developed using modal location theory and wavelet transform analysis. Source location was performed on a steel plate of 790 x 300 mm with nominal thickness of 5 mm under a planar location setup using H-N sources. The accuracy of the new technique was compared with the major location methods (the time of arrival (TOA) technique, triple point filtering and DeltaT location methods). The result of the study shows that the WTML method produces more accurate location result compared with other AE location methods.

2. **Validation of WTML method for accurate location of fatigue crack growth in steel plate**

Laboratory fatigue tests were conducted on steel plate in order to monitor and locate fatigue crack growth, and validate the workability of WTML method. WTML was successful in locating the AE signal released from fatigue crack growth. The accuracy of WTML is much better than TOA, DeltaT and triple point filtering location methods.

3. **Crack size measurement using WTML method**

The capability of the WTML location method to measure crack length due to fatigue crack growth under tensile-tensile loading is investigated. The WTML method successfully used to determine the crack length in the steel pipe with the maximum measurement error of 5 mm.

Key Words: Acoustic Emission, Damage detection, Fatigue Crack Growth, Source location, Modal Analysis, Wavelet Transform Analysis, Crack-length measurement

ACKNOWLEDGEMENTS

Praise to God, The Almighty, who gave me this opportunity to complete this research work.

I take this opportunity to express my deep gratitude to Prof. K. Holford for her great supervision throughout my study. Her guidance and encouragement are much appreciated. I am also grateful to Dr. Rhys Pullin for his excellent guidance and support throughout this study.

My thanks also to all Acoustic Emission (AE) group members especially Dr. Mark Eaton, Matthew Pearson and Hisyam for their technical advice and help. Many thanks to all staff of the Cardiff University Mechanical and Structural Engineering Divisions; particularly Harry Lane, Len Czekaj, Des Sanford and Brian Hooper for their continuous support during my experimental work.

Finally I extend my deepest thanks to my dearest wife Juliawati and my lovely daughter Nurul Afifah and all of my family members for their patient and support throughout my study.

GLOSSARY OF TERM

Acoustic Emission:

Acoustic Emission Signal: The electrical signal obtained by an instrumented computer system through the detection of Acoustic Emission

Hit: A hit is the term used to indicate that a given AE channel has detected and processed an acoustic emission transient.

Event: A single AE source produces a transient mechanical wave that propagates in all direction in medium. The AE wave is detected in the form of hits on one or more channels. An event therefore, is a group of AE hits that was received from a single source.

Source: Place where the event takes place.

Noise: The signal obtained in the absence of any acoustic emission.

Sensor: Device that converts the physical parameter of wave into an electrical parameter.

Resonant Sensor: High sensitivity over a narrow frequency band.

Wideband Sensors: High sensitivity over a large frequency band.

Source location: Computed origin of the acoustic source.

Location Plot: Representation of sources of acoustic emission computed using an array of sensors.

INDEX OF CONTENTS

CHAPTER 1: INTRODUCTION

This chapter begins with relevant background information regarding structural integrity of nuclear piping (Section 1.1), followed by a brief explanation on Acoustic Emission (AE) and other non-destructive testing (NDT) techniques as structural integrity monitoring tools, their strengths and limitations (Section 1.2). The objective and scope of the research work is explained in Section 1.3 while Section 1.4 details the major contributions of this work. Finally, Section 1.5 presents an outline of the remaining chapters of the thesis.

1.1 Structural integrity of nuclear piping

Piping integrity is a major issue for nuclear plant safety. Piping systems in nuclear power plants are designed for pressures and mechanical loads originating from deadweight and seismic events and operating thermal transients using the equations in the ASME Boiler and Pressure Vessel Code, Section III (ASME, 2006).

In nuclear power plant, carbon steels and low alloy steels are usually used for various pipe components. These structures are not only subjected to mechanical loads, but are frequently exposed to aggressive thermal loads which induce the formation of fatigue cracks especially in the welded area. Thermal fatigue can occur in nuclear piping through a number of different mechanisms such as wall thermal gradient stress, piping thermal expansion and thermal stratification stress. Both thermal gradient stresses and thermal expansion is well considered in the ASME codes design stress analysis, however thermal stratification is not considered in this design code (Hirschberg, 2000).

Thermal fatigue cracks have been reported to occur in primary loop recirculation pipes and various other components of nuclear power plants (Hayashi, 1998). Thermal fatigue has also been identified as the major ageing mechanism of nuclear piping system such as in piping connected to Reactor Coolant System (RCS) especially for surge, spray and branch lines and their nozzles that are subject to

thermal transients during plant start-up and shut-down, thermal stratification, thermal shock, turbulent penetration, and thermal cycling (EPRI, 2005).

Thermal stratification may also cause leaks in normally stagnant lines connected to the reactor coolant loop in safety injection systems, reactor coolant drain lines, a residual heat removal suction line, and an excess letdown line. In addition, stratification has caused cracking of steam generator feed water nozzles and high piping displacements in pressuriser surge lines (Bieniussa, 1999).Thermal fatigue can lead to cracks formation and these cracks can be categorised as small leaks in piping or medium leaks in piping when crack opening is more than 1 mm (NEA/CSNI/R, 2005).

In normal practice, after detection of a fatigue crack during periodic non-destructive inspection, fracture mechanics methodology is used to estimate the safe operational life of the component or structure. Furthermore, a life prediction study can be useful to determine component flaw inspection intervals along with critical flaw shape and sizes for safety acceptance criteria. Based upon this information, maintenance and replacement schedules can be planned to ensure continued safe performance of the plant.

Section XI of ASME Boiler and Pressure Vessel Code provide the guidelines for nuclear power industry to evaluate the serviceability of piping component that is subject to cyclic stress such as thermal fatigue. One of the key parts of Section XI of this code is a damage tolerance analysis which postulates the flaw at thermal fatigue location and then performs thermal fatigue crack growth analysis to determine the inspection intervals that can detect the fatigue cracks before they exceed the critical size allowed by the governing code (Gosselin et. al., 2007).

Damage tolerance analysis of piping structural components is used to avoid catastrophic failure and to maintain the safe and reliable operation of piping structures especially for ageing nuclear power plants.

1.2 NDT and structural integrity monitoring

There is a comprehensive ageing management program in place for all the operating nuclear power plants. Periodic in-service inspection of critical components such piping system is very important for assuring their structural integrity and the safe operation of nuclear power plants. Non-destructive testing techniques play a crucial role in this regard and are conducted based on the guideline of Section XI of ASME Boiler and Pressure Vessel Code.

Acoustic Emission (AE) is considered as a passive NDT technique because AE detects emitted elastic waves within structure during deformation while most other traditional NDT methods such as radiography, ultrasound and eddy currents require a source input and are therefore defined as active testing technique. A major strength of AE is its ability to be used as a "global" monitoring tool (Holford et al. 1999) i.e. it can provide inspection on a wider area compared with other NDT techniques.

AE offers the opportunity to monitor the thermal fatigue damage continuously and cracks can be identified at early initiation stage of formation without intrusion on the test schedule. AE offers several advantages over other NDT techniques for monitoring fatigue crack growth on piping structure such as nuclear piping system:-

- It provides the ability to monitor the structure throughout the test period without interruption.
- It provides global monitoring of the structure.
- It requires minimum accessibility.
- It can provide an early warning before catastrophic failure, an option to stop the test, improving safety and saving cost.

Conventional acoustic emission testing methods, however, suffer from some draw- backs. Current AE location techniques only give estimated location of fatigue crack growth area. The exact size of fatigue crack growth cannot be determined using available commercial AE source location systems. The result of AE tests are usually followed by other conventional NDT methods such

ultrasonic testing for determining the accurate location and size of damage for further repairing processes.

1.3 Research objectives

The aim of this research work is to develop an accurate AE location technique for use in the global and local monitoring of thermal fatigue crack in steel pipes, in order to provide a commercial NDT tool for structural integrity monitoring of nuclear piping systems.

The main objectives are to evaluate and enhance current methods for locating the fatigue crack growth in the steel pipe member using standard artificial acoustic emission sources and validated these techniques using actual AE data from fatigue crack growth.

1.4 Major contribution of the research work

Major significant contribution of this research can be summarised as follows:

1. Development of novel AE location method based on wavelet transforms analysis and modal location method applied to fatigue cracks. This method is named 'Wavelet Transform analysis and Modal Location' (WTML). This method is found to be more accurate than available commercial location methods and comparable with advanced location methods such as the DeltaT (Baxter 2007) technique. However, WTML method is superior to the DeltaT method because it is easier to use and does not involve prior calibration. In addition, the proposed method could be applied using only a single sensor.

2. Validation of new methods for locating the actual fatigue crack growth on steel plate under cyclic tensile loading. The proposed method was successfully used to accurately locate fatigue crack growth in steel plate.

3. Deployment of discrete wavelet transforms (DWT) de-noising methodology to improve temporal measurement error in modal analysis. DWT de-noising

capability was found to significantly improve the accuracy of SSMAL for locating actual fatigue crack growth signal that contained excessive back ground noise.

1.5 Publication of research outcomes

The publications from this research are as follows:

Conference Papers

1. Shukri MOHD, Karen M. HOLFORD and Rhys PULLIN. "Acoustic Emission Source Location in Steel Structures Using a Wavelet Transform analysis and Modal Location Theory". In 7th International Conference on Acoustic Emission Testing, Granada, September 2012.

2. Shukri MOHD, Karen M. HOLFORD and Rhys PULLIN. "Planar Location of Simulated AE source on Steel Pipe using a Wavelet Transform analysis based on Modal Location Theory". International Conference on Humanities, Social Science, Science and Technology, Cardiff, July 2012

1.6 Outline of thesis

This chapter provides background information on thermal fatigue damage monitoring in nuclear piping. The benefits of AE monitoring for this application have been discussed and the objectives of this research have been identified.

Chapter Two presents relevant background information and theory. AE theory of source mechanisms, wave propagation and source location is provided along with wavelet transform analysis and thermal fatigue theory. A review of past failures in nuclear piping due to thermal fatigue is also included.

Chapter Three discusses experimental equipment, procedure and techniques utilised and developed throughout the research. This chapter also describes the software used for analysis of the AE data from artificial and actual sources.

Chapter Four describes a novel method developed to improve source location in plate like structure especially for nuclear power plant piping system based on Modal AE (MAE) theory and wavelet transform analysis. H-N tests on plate and pipe were completed to validate the method. The results are presented and discussed.

Chapter Five describe a fatigue test on a notched plate under tension loading. This test was carried out to validate the newly developed method to precisely locate the AE signal from fatigue crack growth in a plate under cyclic tensile loading and compare the location accuracy with other methods such as TOA planar location, DeltaT location and waveform filtering. The accuracy of location is then validated by a crack gauge measurement.

Chapter Six discusses a fatigue test on notched pipe under four point bend loading. This test was carried out to validate the newly developed method to precisely locating the AE signal from fatigue crack growth on a steel pipe. This chapter also discussed the application of the DWT denoisiong methodology for remove noise from the AE waveform and how this can then improve MAE source location for actual fatigue signal.

Finally, Chapter Seven summarises the overall conclusions and findings of the study and suggests directions for future research and development, and Chapter Eight contains all the references to research cited in this thesis.

CHAPTER2: BACKGROUND AND THEORY

2.1 Introduction

This chapter presents relevant background information and theory on AE source mechanisms, Lamb waves theory and wave propagation, and source location along with wavelet transform analysis and thermal fatigue. A review of past failures in nuclear piping due to thermal fatigue is also included.

2.2 Acoustic Emission (AE)

2.2.1 Background theory

AE is a transient elastic wave generated by the rapid release of energy from a localised source within a material (ASTM 1982). AE is a natural phenomenon and occurs in a wide range of materials, structures and processes. The largest-scale of AE is seismic events, while the smallest-scale processes that have been observed during AE tests are the movement of small numbers of dislocations in stressed metals (Miller and McIntire 1987).

The source of the AE is generally an elastic stress field in the material. Without stress, there is no emission. Therefore, an AE test is usually carried out during controlled loading of a structure (Pollock 1989). A typical AE test setup is illustrated in Fig. 2.1.

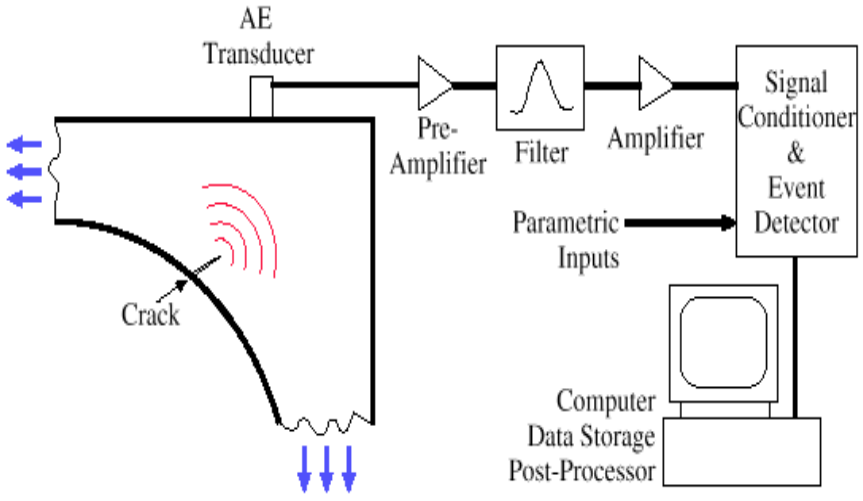

Fig. 2.1 A typical AE test set-up (Huang, 1998).

AE sensors mounted on the structure detect the displacement of the surface and convert this tiny movement to an electrical signal by using a piezoelectric crystal. After sensing and pre-amplification, the signal is transmitted to the main instrument, where it is amplified and filtered.

Detection of the signal is accomplished with a comparator circuit, which generates a digital output pulse whenever the AE signals exceeds a fixed threshold voltage. The threshold level is usually set by the operator and is the key variable that determines the test sensitivity (Miller and McIntire 2005).

AE equipment is highly sensitive to any kind of surface displacement within its operating frequency range, typically 20 to 1200 kHz. The equipment can detect not only crack growth and material deformation but also such processes as solidification, flow and phase transformation (Miller and McIntire, 1987).

Due to recent advancement in acquisition speeds and processors, the latest AE equipment is able to handle high rate data acquisition and faster signal processing. AE equipment with large data storage has enabled waveform data to be stored by the AE system which provide better understanding of AE wave propagation (Miller and McIntire, 2005).

2.2.2 Signal measurement parameters

The most widely used signal measurement parameters in AE signal analysis are counts, amplitude, duration, rise time, and the measured area under the rectified signal envelope which is also called relative energy (Fig. 2.2). Some tests and analysis use other parameter such as absolute energy, count-to-peak, average frequency, or spectral moment. However, the five principal parameters have become well standardised (Miller and McIntire, 2005).

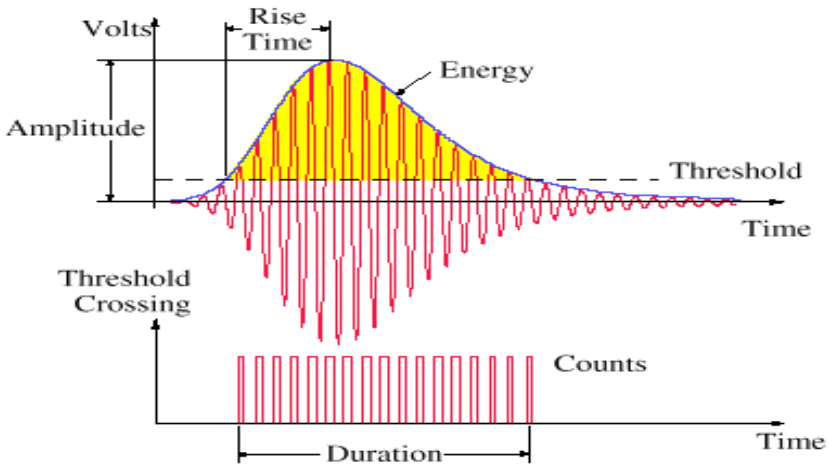

Fig. 2.2 Definitions used for recording acoustic-emission events (Huang, 1998).

Amplitude, A, is the highest peak voltage attained by an AE waveform. This is very important parameter because it directly determines the detectability of the AE event. AE amplitudes are directly related to the magnitude of the source event, and they vary over a wide range from micro-volts to volts. The amplitudes of AE are customarily expressed on a decibel scale, in which 1 μV at the transducer is defined as 0 dB, 10 μV as 20dB, 100 μV as 40dB and so on.

Counts, N, are the threshold-crossing pulses and sometimes are called ring-down counts. This is the one of the oldest and easiest ways to quantify the AE signal. Counts depend strongly on the acoustic properties and reverberant nature of both the specimen and sensor.

MARSE Energy, E, is the measured area under the rectified signal envelope. Energy is preferred over counts because it is sensitive to amplitude as well as duration, and it is less dependent on the threshold setting and operating frequency. *True Energy*, is a measure of the AE hit and is measured in atto-joules ($1x10^{-10}$ J = 1 aJ). *Absolute energy* is derived from integral of the squared voltage signal divided by reference resistance (10kΩ) over the duration of acoustic emission waveform packet. This parameter represents the true energy of an AE event from transient signals or of certain data rate interval of continuous AE signals (PAC 2005).

Duration, D, is the time from the first threshold crossing to the last. Duration is measured in microseconds. It is valuable for noise filtering and other type of signal qualification.

Rise time, R, is the elapsed time from the first threshold crossing to the signal peak.

In modern AE system, these parameters are known as feature data and are captured by signal processing software by extracting the value of these parameters from waveform data. This parameter can be used for several types of signal qualification and noise rejection and is dependent on wave propagation processes between source and sensor.

AE signals can be analysed by correlating one feature to the others or to other parameters such as load, strain location or time. Fig. 2.3 below shows AE data displays based on data feature correlation that are commonly used in AE signal analysis.

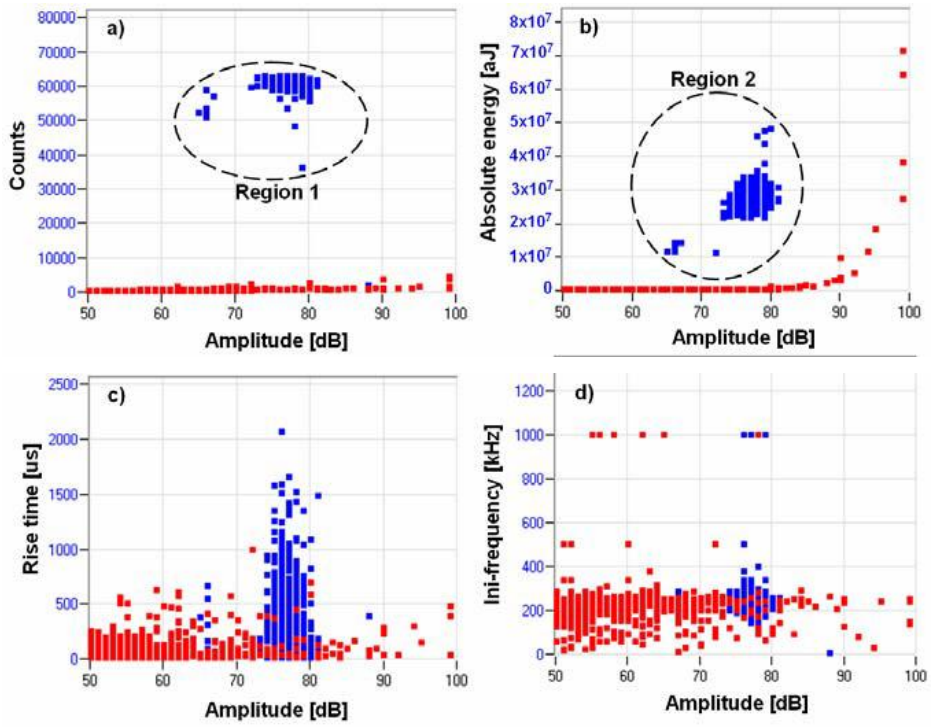

Fig. 2.3 Typical AE data display for AE signal analysis based on signal feature extraction (Baxter 2007)

A detailed explanation about AE data display was well explained by Pollock (1989) and in general AE can be classed as:

- History/Time plots
- Distribution functions to show the statistical properties of the emission
- Channel plots showing the distribution of detected emission by each channel
- Location displays that shows the position of an AE source
- Point plots showing the correlation different AE parameters and
- Diagnostic plots showing the severity of AE indications from different parts or locations of the structure

2.2.3 AE sources mechanism

AE are stress waves produced by rapid released of elastic energy in stressed materials. Emission from these sources can be categorised as either transient or continuous wave.

Continuous waves are produced by rapidly repeated processes such as machine vibrations, fluid flow and continuous friction between surfaces. The amplitude and frequency of the continuous wave fluctuates but the signal does not end (Fig. 2.4).

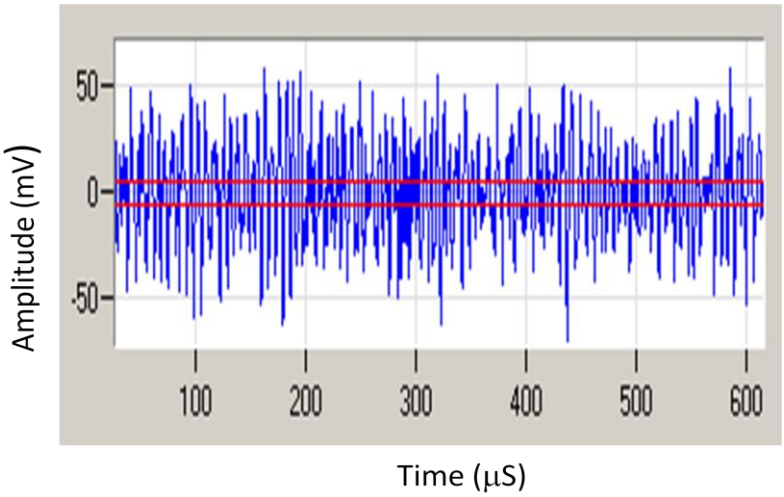

Fig. 2.4 Typical continuous AE signal

Transient waves are burst type signals generated by some abrupt and permanent change in material such as corrosion and defect related deformation processes.

They are identified by obvious start and end of the signal and it evidently different from the noise signal (Fig. 2.5).

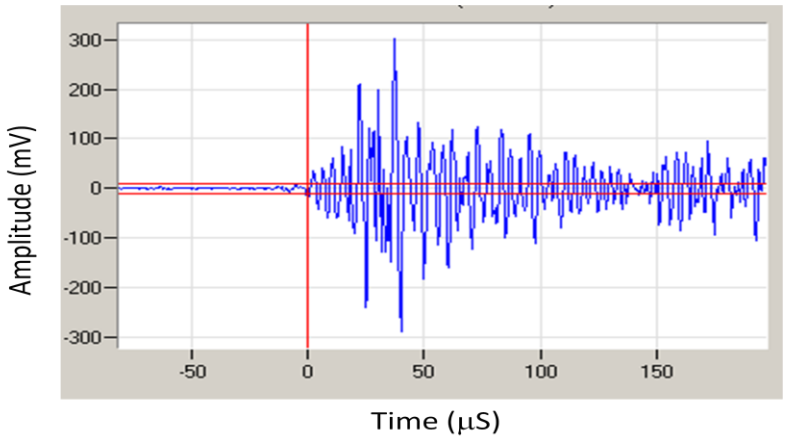

Fig. 2.5 Typical transient AE signal

The classic sources of acoustic emissions are defect related deformation processes such as crack growth and plastic deformation (Scruby, 1987). Other mechanisms that produce AE in metals include the movement and multiplication of dislocations, micro cracks formation and growth, sudden crack advances and frictional processes during crack closure and opening (Heiple, 1987).

The amount of AE energy released depends primarily on the size and speed of the local deformation process. The formation and movement of a single dislocation does produce an AE stress wave, but it is not large enough to be detected as an isolated process. However, when millions of dislocations are combined and move at the same time, the individual stress waves overlap and superimpose to give a detectable result (Heiple, 1987).

AE is a useful tool for studying material damage because it can provide detailed and immediate information. Acoustic emission analysis is most useful when used in conjunction with other techniques, such as stress-strain measurements, crack growth measurement such as Krak gauge or visual tool such as microscopy or digital image correlation. AE complements these techniques and offers additional information on the dynamics of the underlying deformation or damage processes

and the transitions from one type of deformation or damage to another (Pollock, 1989).

2.2.4 AE wave and propagation

AE signals are a transducer's response to sound waves generated in a solid medium (Miller & McIntire 2005). AE waves released at the source are essentially a stress pulse due to permanent displacement in a material as illustrated in Fig 2.6.

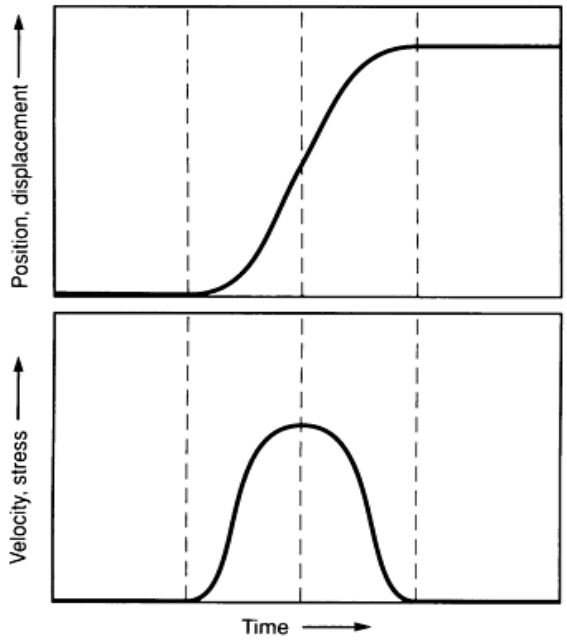

Fig. 2.6 Stress waves released at AE source (Pollock 1989)

The displacement waveform is basically a function corresponding to the permanent change associated with the source processes. The width and height of the pulse depend on the dynamic of the source processes. For example, microscopic crack growth is often completed in a few microseconds so the pulse has a correspondingly short duration.

The amplitude and energy of stress pulses vary over an enormous range from sub microscopic dislocation movements to gross crack extensions. The stress wave radiates from the sources in all directions, often having a strong directionality and dependence on the nature of the source, as shown in Fig 2.7.

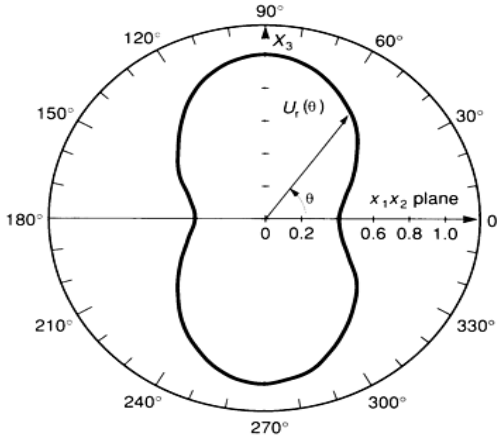

Fig. 2.7 Angular dependence of AE radiated from a growing micro-crack (Pollock, 1989)

Acoustic emission initially propagates from a point source as bulks wave. These elastic waves propagate in two basic forms, longitudinal and transverse wave as shown in Fig. 2.8 (Rindorf 1981).

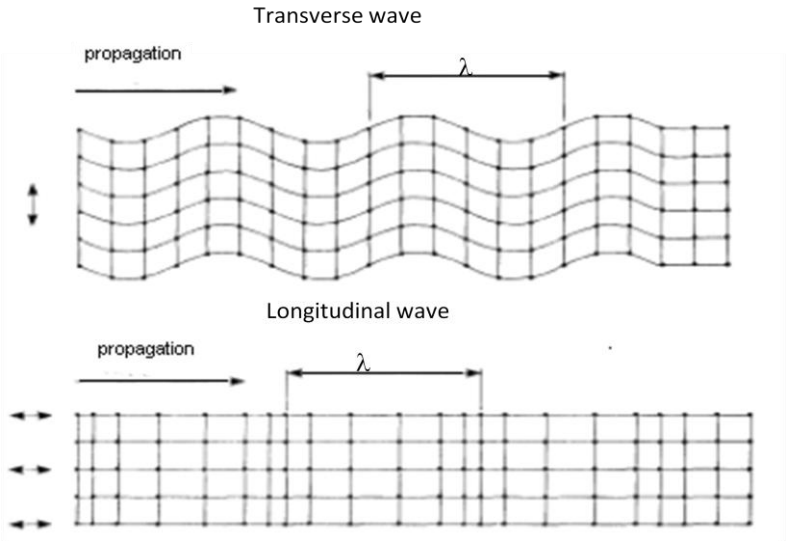

Fig. 2.8 Basic mode of wave propagation in solid (Rindorf 1981)

As longitudinal waves reach the surface of solid media, a further wave mode may exist and is known as a surface wave or Raleigh wave (Fig. 2.9).

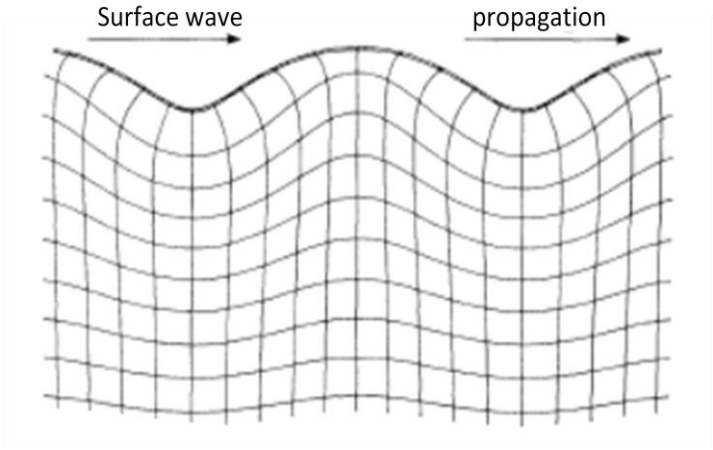

Fig. 2.9 Surface wave particle motion (Rindorf 1981)

In many acoustic emission studies, the test specimen is a plate like geometry (Aggelis et. al. 2011, Holland et. al. 2000, and Grondel et. al. 2002)**.** The wave that propagates in this type of structures are called Lamb waves and there are two modes of propagation, extensional or symmetric (S_0) and flexural or asymmetric (A_0) mode (Fig. 2.10).

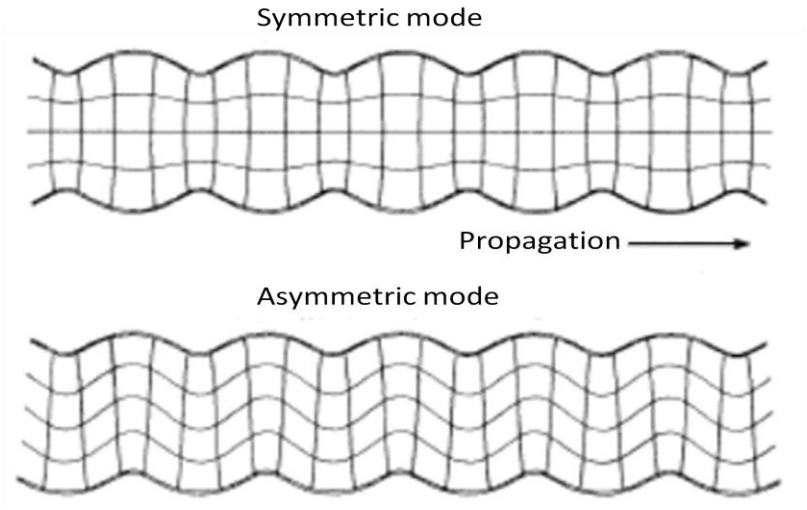

Fig. 2.10 Lamb wave (Rindorf 1981)

For the extensional mode, the larger displacement component is in the plane of the plate, while the larger displacement component in the flexural mode is perpendicular to the plane of the plate. The limits for Lamb waves to occur are that the plate thickness is much smaller than the two other dimensions and the wavelength is much larger than the plate thickness (Gorman 1991).

Nuclear piping network consist of hollow cylinders which can be considered as a plate with two free edges joined and therefore the source location analysis carried out in this study will focus on Lamb waves theory.

2.2.5 Wave attenuation

AE response is directly affected by the loss of energy as waves propagate within the medium. The loss of amplitude as wave travels through a media is known as attenuation (Miller and McIntire 2005). Attenuation occurs both in the near and far field. Near field attenuation is the loss of amplitude in close proximity to the source while the loss of amplitude further from the source is described as far field attenuation.

Attenuation has several causes and is usually related to the amplitude of the wave. The four main causes of attenuation as discussed by Pollock (1986) are; geometric spreading, internal friction, velocity dispersion and dissipation of acoustic energy into adjacent media.

Geometric spreading is the major contributor of attenuation mechanism in the near field and causes significant amplitude decreases. As the wave propagates away from the source, the energy is redistributed within the material which causes an amplitude decrease correspondingly. For a bulk wave, the amplitude decreases in proportion of 1/r where r is distance of propagation. For two dimensional wave propagation, such as Lamb waves, the amplitude of the signal decrease is in proportion to $1/r^{1/2}$ (Miller and McIntire 2005).

In the far field, attenuation may be affected by energy absorption due internal friction. Acoustic energy is converted into thermal energy within the material during internal friction. The absorption mechanism is usually frequency dependent and greater losses usually occur as AE waves propagate at a higher frequency.

Attenuation caused by dispersion usually occurs when Lamb waves propagate within a plate like structure. The frequency components of different Lamb wave modes superimposed at source spread with propagation distance due to velocity

variations. This type of attenuation can be very large for highly attenuated dispersive mode such as guided waves in ultrasonic testing.

The fourth attenuation mechanism is dissipation of acoustic energy into adjacent media. Scattering of AE signals due to internal scattering from in-homogeneities such as grains in metals can cause this type of attenuation. Other sources of this kind of attenuation are surface coating and fluids contained in vessel or piping system.

To avoid the AE signal escaping detection due to attenuation, several transducers should be placed close together to ensure that an AE event emanating from any region on the structure can be detected. The minimum spacing between two sensors can be identified empirically through simulated AE testing or through experience with similar structures.

Attenuation can be measured by placing several sensors at different distances from an AE source. Attenuation can be calculated as:

$$\gamma = 20/x \log A1/A2 \qquad (2.1)$$

Where:

γ is attenuation coefficient (decibels over distances); x is distance between detection points; A1 is amplitude of signal at point 1; and A2 is amplitude of signal at point 2. Attenuation coefficient is a function of the frequency content of the AE wave and the medium of wave propagation.

2.3 Modal analysis

The wave propagation in plate like structure is complicated because of the interaction of the wave with its two free surfaces. Complicated resonant conditions occur as the frequency changes and propagation can occurs in a series of symmetric and asymmetric modes. The way in which acoustic wave propagates in plate like structures is governed by Lamb wave theory, also known as plate wave theory (Gorman 1991).

Lamb wave propagation and velocity are very strongly dependent upon both frequency content and plate thickness. The dependency of velocity upon frequency is known as dispersion and any particular frequency can propagate a number of different velocities (Pollock 1986, Holford 2000). Multiple symmetric and asymmetric Lamb wave modes could exist together at given signal frequency. The number of coexisting wave-modes goes up as the frequency-thickness product is increased (Harker, 1988).

Conventional AE analysis techniques have mainly utilised simple signal parameters like amplitude, duration, counts and energy and the rate at which AE signals occurred. In an alternative to this conventional technique, the dispersive nature of Lamb wave can be exploited and is known as modal acoustic emission (Holford 2000).

2.3.1 Modal Acoustic Emission (MAE)

MAE uses wideband and high fidelity instrumentation to detect and capture the transient wave associated with defect growth (Chang 2006). The MAE technique involves the determination of the arrival time of S_0 (extensional) and A_0 (flexural) wave components and computing the distance of the source to sensor by measuring their temporal separation of the source waveform (Holford 2000, Pullin 2007).

A few researchers have observed flexural and extensional mode propagation in plate like structures. Gorman (1991) studied signals in aluminium and composite plates using a range of sensor types. He demonstrated the occurrence of the fundamental flexural and extensional components and observed that the two modes have significantly different frequency contents and dispersion characteristics.

Using signals obtained from the testing of carbon fibre reinforced polymer (CFRP), Surgeon and Wevers (1999) determined the difference in arrival times for symmetric and asymmetric modes. The difference in arrival times of symmetric and asymmetric modes is calculated based on simple plate wave theory and was compared with measured values of separation and the results were in good agreement.

Based on modal characteristic of the wave mode propagation in plate like structures, the velocity and the different arrival time of these modes could be used for accurate source location. Since the detection of the arrival time of different modes is not determined by a preset threshold of data acquisition, it is expected that SSMAL will produce more accurate source location (Surgeon, 1999) compared with the traditional based source location method. Ziola and Gorman (1991) suggested that accurate linear location can only be performed if the modal nature of AE signals is taken into account.

Maji and Sapathi (1995), Dunegan (1997) and Holford (1999) have demonstrated that the location of pencil lead break sources using single sensor source location can be carried out by band pass filtering. Filtering of the original signal to high frequency content and low frequency content was used to establish the arrival of S_0 and A_0 modes to estimate source to sensor distance.

Pullin (2005) used the two fundamental components of Lamb waves for estimating the artificial and fatigue crack source to sensors distance in aerospace grade steel. He showed that, in a controlled laboratory study of fatigue crack growth, it is possible to calculate the distance of a fatigue crack source from a single sensor with reasonable accuracy.

Nevertheless, this method also suffers from some drawbacks. The arrival time of A_0 and S_0 modes is often difficult to determine due to the superposition of these fundamental modes with reflections from specimen boundaries, superposition with other wave modes and also from noise signals. Furthermore, the uses of incorrect modes will contribute to a larger error in SSMAL measurement when compared with the commercial TOA method.

2.3.2 Dispersion Curve

Dispersion curves are a very useful tool in MAE. Dispersion curves are generated by plotting either phase or group velocity values against their frequency-thickness

products. The curves are displayed as a function of velocity on the vertical axis and frequency (or thickness-frequency) on the horizontal axis from the test item setup as shown in Fig. 2.11.

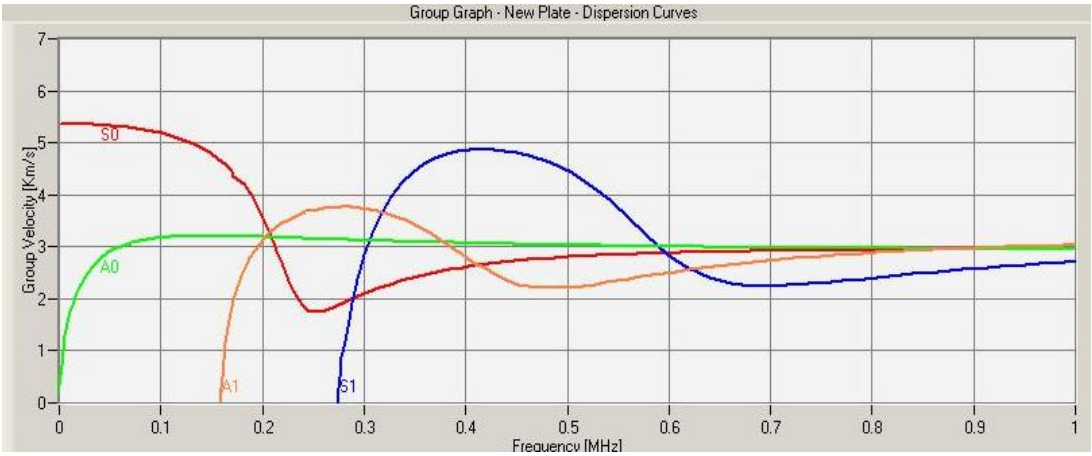

Fig. 2. 11 Typical dispersion curves for 10 mm steel plate (generated using PAC Sharewavelet software)

The dispersion curves illustrate how, for a fixed plate thickness, different frequency components of lamb waves travel at different velocities. If the wave is detected by a suitable transducer, separation of the difference frequency components can be observed and respective arrival times can be measured. The dispersion curve graph can be modified in a variety of ways to help the user visualise the wave propagation characteristics.

2.3.3 Modified dispersion curve

A modified dispersion curve is a plot of frequency of a series of Lamb wave modes against their arrival time for known sources to sensor distances for a specific plate thickness. Instead of having velocity against frequency plot as per normal dispersion curves, modified dispersion curve displayed the frequency content of the signal in vertical axis against arrival time in the horizontal axis.

This new dispersion curve can be overlaid onto the waveform signal to determine the mode of particular signal in the waveform. Since both graphs have the same horizontal time axis, the arrival time of the fundamental symmetrical and asymmetrical modes in the waveform can be determined as shown in Fig. 2.12.

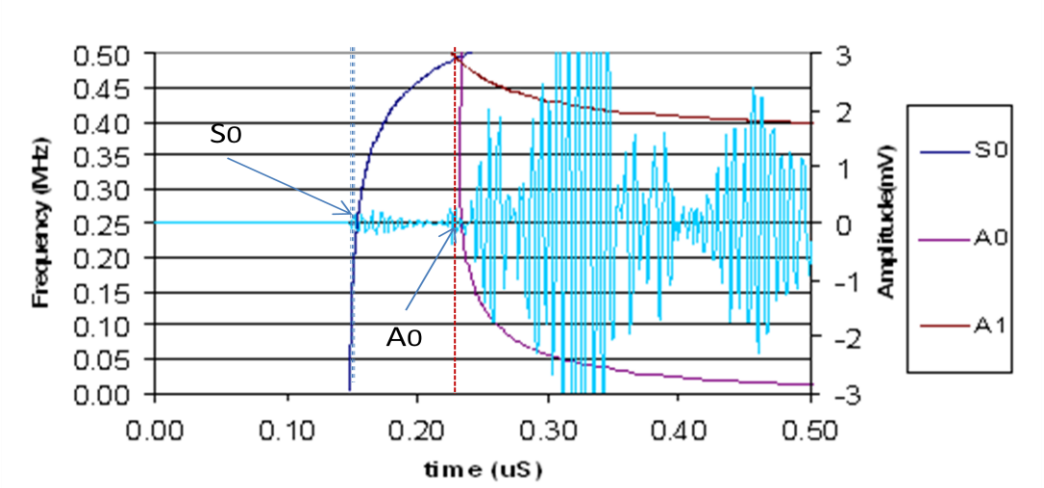

Fig. 2.12 Illustration on how a modified dispersion curve overlaid on waveform can be used to determine the arrival of Lamb wave modes

2.4 AE source location

2.4.1 Introduction

Locating the source of significant AE is often the main goal of an inspection. AE systems are capable of using multiple sensors during testing, allowing them to record a hit from a single AE event. As hits are recorded by each sensor/channel, the source can be located by knowing the velocity of the wave in the material and the difference in arrival times among the sensors, as measured by hardware circuitry or computer software. By properly spacing the sensors in this manner, it is possible to inspect an entire structure with relatively few sensors (Miller and McIntire 2005, Pollock 1989).

Most source location techniques assume that AE waves travel at a constant velocity in a material. However, various effects may alter the expected velocity of the AE waves such as reflections and multiple wave modes which can affect the accuracy of this technique. Therefore, the geometric effects of the structure being tested and the operating frequency of the AE system must be considered when determining whether a particular source location technique is feasible for a given test structure (Baxter 2007).

Good knowledge of source location is the basic requirement for further characterisation of a damage mechanism. Calculation of the AE source location is mostly based on arrival time differences of the signals recorded by different transducers. Errors in arrival time determination and elastic wave velocity measurement can crucially affect the inaccuracy of AE source location (Miller and McIntire, 2005).

2.4.2 Time of Arrival (TOA) source location

The AE event causes a micro-seismic wave that travels within the material and is detected by the transducers and the time of arrival is then determined. Usually, the AE events are located based on the time of arrival at a number of transducers, using the known distances between the transducers and the P-wave (bulk longitudinal wave) propagation velocity. This method is known as time of arrival (TOA) approach (Miller and McIntire 2005, Rindorf 1981).

Time of Arrival (TOA) source location is the most widely used method for AE source location. This method is based on the measurement of time difference between the arrivals of individual AE events at different sensors in an array and is the basis of most commercial AE software.

The sensors are arranged either in linear, triangular or rectangular arrays. In order for point location to be justified, signals must be detected by a minimum number of two sensors for linear, three for planar and four for volumetric location.

Linear location methods can be explained by considering an array of three sensors along a beam. An AE event occurring at any point in this beam will emit stress waves which propagate in both directions. The simplest method of locating this event is using zonal location.

This method examines the order in which the AE signal reaches the sensors in its array. By noting which sensor is ‘hit’ first, the zonal location can be determined. In Fig. 2.13 a), sensor 2 is hit first and therefore the source must have come from an

area defined by the midpoint between sensors 1 and 2 and the midpoint between sensors 2 and 3.

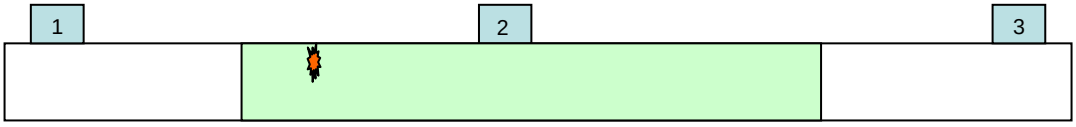

a) Zonal location examining first hit at sensor 2

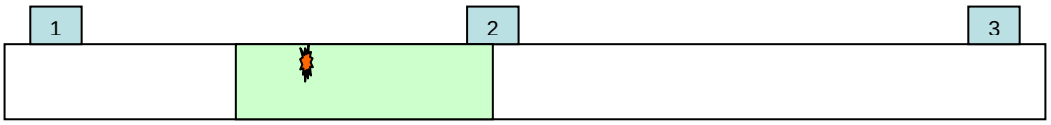

b) Zonal location examining first hit at sensor 2 and second hit at sensor 1

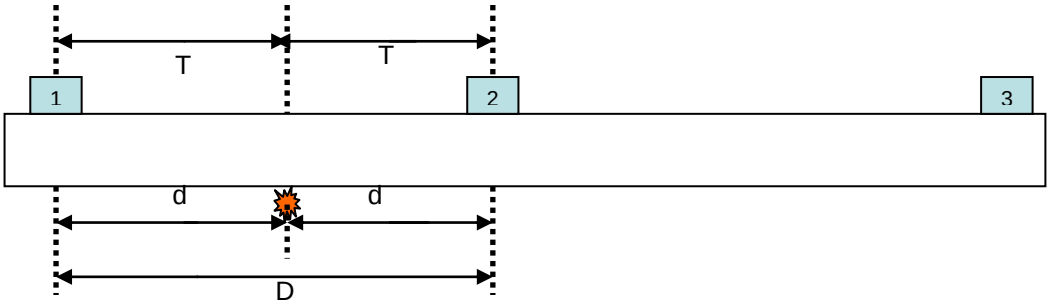

c) Location based on time delay $\Delta T = T_1 - T_2$

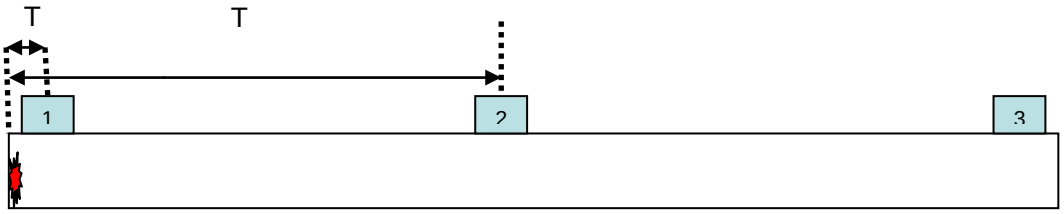

d) Location outside of the array, known because $C_{AE} * \Delta T = C_{AE}(T_1 - T_2) = D$

Fig. 2.13: Linear location using time of arrival (TOA) theory (Miller and McIntire, 1987)

This method can be made more accurate by examining not only the hit order, but the difference in time of arrival (TOA) of hit at the sensors. For example, Fig. 2.13 c) represents a hit arriving at sensor 2 followed by sensor 1. The time difference between these hits can be written as:

$$\Delta t = (d_2 - d_1)/C_{AE} \qquad (2.2)$$

where: C_{AE} = calculated wave velocity

Δt = time difference between sensors

d_1 = distance from source to first hit sensor

d_2 = distance from source to second hit sensor

This is however, commonly expressed in terms of d_1

$$d_1 = (D - C_{AE}.\ \Delta t)\ /2 \qquad (2.3)$$

where D= total distance between sensors

If the source originates from outside the array, Fig. 2.13 d), then the time difference between the two signals will become equal to the time taken for the wave to travel between the two sensors. The source will be located at the sensor at the edge of the array; in this case of the example, at sensor 1.

The same technique can be expanded for two-dimensional planar location. The TOA method relies on the arrival times of the AE signal at each of the sensors. Considering an infinite plate with two sensors separated apart with distance D, it is no longer possible to locate a point, but a hyperbola as shown in Fig. 2.14.

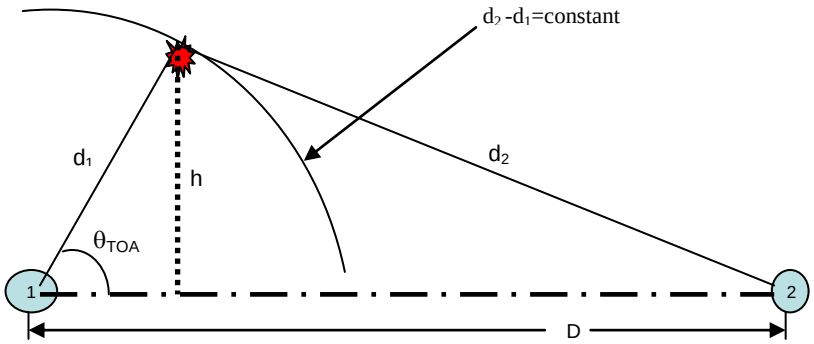

Fig. 2.14 Planar (2D) location on an infinite plate (Miller and McIntire, 1987)

The equation of this hyperbola is (Miller and McIntire, 1987):

$$\Delta t.C_{AE} = (d_2 - d_1) \qquad (2.4)$$

and $$h = d_1 \text{ Sin } \theta_{TOA} \quad (2.5)$$

$$h^2 = d_2^2 - (D - d_1 \theta_{TOA})^2 \quad (2.6)$$

then $$d_1^2 \sin^2\theta_{TOA} = d_2^2 - (D - d_1 \cos\theta_{TOA})^2 \quad (2.7)$$

$$d_1^2 = d_2^2 - D^2 - 2Dd_1 \theta_{TOA}$$

substituting $d_2 = d_1 + \Delta t.C_{AE}$ from the (2.3) gives:

$$d_1 = ½ ((D^2 - \Delta t^2 C_{AE}^2) / (2\Delta t C_{AE} + D\cos\theta_{TOA})) \quad (2.8)$$

this provides insufficient information to locate the event, but by adding a third sensor to the array as suggested by Fig. 2.15, it is possible to repeat this process for the three pairs of sensors 1-2, 2-3 and 1-3. The intersection of the three hyperbolae indicates the location of the event. By adding a fourth sensor to form a rectangular array, the accuracy can be further increased, creating six sensor pairs.

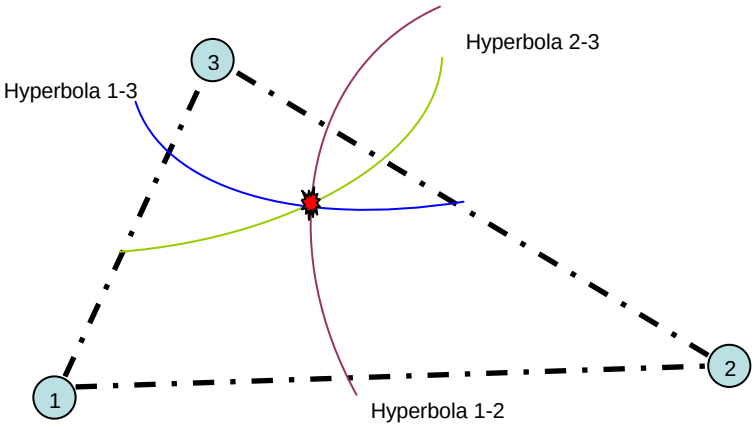

Fig. 2.15 2D location with three sensors (Miller and McIntire, 1987)

The conventional TOA for source location of AE signals based on threshold crossing is well developed. This method is very useful for approximate source location in large structures, however, the result of source location is greatly affected by the level of threshold voltage and the average value of velocity used. This method can completely fail under conditions when high background noise is present.

The sources of error are fully investigated by Rindorf (1981) and detailed explanation can be found in Miller and McIntire (2005). However, according to Holford (2000), the main sources of error associated with the TOA method are:

- Premature triggering of detection threshold by a low amplitude symmetric component – timing is usually based on the arrival of the asymmetry (flexural) component.
- Dispersion of the asymmetric mode component – wave dispersion within the structure will cause alterations in the waveform. This may cause the detection threshold triggered by a different phase of the signal.
- Different wave-paths due to inhomogeneitis in structure.

Other sources of error include inaccurate sensor location, incorrect group wave velocity and human error.

2.4.3 DeltaT location

The Delta location method as proposed by Baxter (2007) utilises an artificial source to acquire the time of arrival data at each sensor within an array. This method also utilises the time arrival of AE signal at the sensor, as with the TOA methods; however, a location is derived from a user defined map system rather than using an average velocity.

The arrival time difference (ΔT) is analysed at pairs of sensors within an array. A map is constructed displaying contour lines of equal ΔT sources for each sensor pair. Any previous, current or future AE data received from within the mapped area can be overlaid on ΔT maps to identify the source location without considering the wave path and wave speeds (Baxter 2007).

The ΔT location method involves five major steps as outlined below;

- *Determine area of interest* – The area where the crack is expected to initiate and growth is first determined.
- *Grid construction* – a grid is constructed in the area of interest on an engineering component in which future AE events will be located. The resolution of the grid should be as higher as possible for higher source

location accuracy. Sources are located with reference to the grid applied to structure rather than sensor location.

- *Obtain TOA of training data* – Pencil lead break (H-N source) is conducted at each node on the grid to obtain the time arrival data at each sensor. It is essential to have enough AE sources at each node to provide reliable result and to eliminate erroneous data. At least five sources at each node are required to provide a reliable result.
- *ΔT map calculation* – For each H-N source, the TOA time difference (ΔT) for each sensor pair are calculated. An array of three sensors has three sensor pairs 1-2, 1-3 and 2-3 while array of four sensors has six sensor pairs (1-2, 1-3, 1-4, 2-3, 2-4 and 3-4). The average ΔT for each sensor pair at each node is stored in a map. The maps can be displayed as contour plots of equal ΔT.
- *AE source location* – To locate an actual event from an AE source, ΔT for each sensor pair is calculated. A line or contour on each map corresponding to the calculated ΔT can be identified. Source locations are determined by overlying the results from each sensor pairs and identifying their convergence point. For source location using an array of four sensors, six lines from six sensor pairs will be used and these six lines are expected to intersect at one point to give the location of the source.

The ΔT location method cannot be used for complete coverage of structure but it is suggested to be used as a tool to improve source location around critical or complicated areas. This method overcomes the assumption that the wave propagates with constant velocity in the straight path which is untrue for structures with multiple thickness changes. A further advantage of the DeltaT source location method is that new areas of interest can be added during or post test and therefore active areas identified by TOA can also be more accurately assessed (Baxter, 2007). According to Baxter (2007), this method has an associated error equivalent to one grid square.

2.4.4 Waveform filtering based source location

Waveform based source location is achieved by digital filtering combined with dispersion curve reviewing. In plate like structures, sources are located by reviewing the different wave modes that propagate within a structure using the dispersion curve as shown in Fig. 2.16.

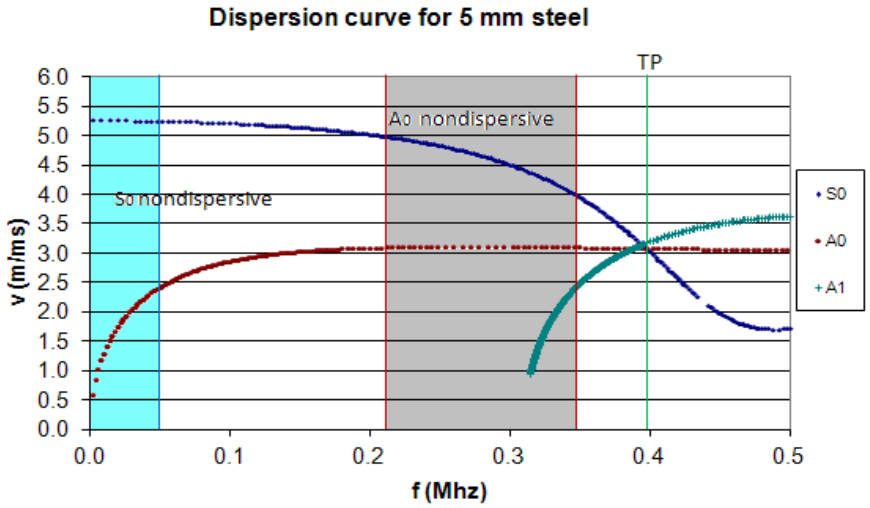

Fig. 2.16 Dispersion curve for 5mm thick steel.

This location method is based on filtering the waveform at certain frequencies ranges either using first arrival detection (S_0 mode arrival detection), arrival of A_0 mode or triple point filtering (TP).

For source location determined by first arrival detection, the velocity of the fastest wave mode (S_0 mode) is used to determine the arrival time of AE source. In this method, AE data is filtered over the non dispersive range of S_0 mode to remove other unwanted signal. When the filtered data is replayed back by the AE source location software, the detection threshold is expected to be triggered by the S_0 mode since the other mode will propagate at a much slower speed than S_0 mode.

Triple point is a term to refer to the frequency where the S_0, A_0 and A_1 modes propagate at the same speed (Fig. 2.16). Filtering the AE signal at the triple point is

expected to produce more accurate source location result since the detection threshold is expected to be triggered simultaneously by the S_0, A_0 and A_1 mode.

2.4.5 Single Sensor Modal Analysis Location (SSMAL)

Conventional AE locations technique have mainly utilised the arrival time of first threshold crossing. An alternative to this conventional technique exploits the dispersive nature of Lamb waves and is known as modal acoustic emission (MAE) (Gorman 1991, Posser 1992). For a fixed plate thickness, different frequency components of Lamb waves travel at different velocity.

Single sensor modal analysis location (SSMAL) works on the MAE theory. SSMAL utilised the time delay of the S_0 and A_0 modes of waveform signals (time domain signals) and the distance of the source from sensor is determined by the velocity of two modes and their time delay (Holford, 1999 and Pullin 2005). If the two basic components of lamb waves, S_0 and A_0, travel at different velocities C_{S0} and C_{A0}, and the time lapse (Δt) between their arrival is measured, then the source to sensor distance (D) is given by;

$$D = \Delta t \, (C_{S0}C_{A0}/ C_{S0}-C_{A0}) \quad \text{(Pullin et. al, 2007).} \qquad (2.9)$$

SSMAL method also suffers from some drawbacks. The arrival of A_0 is often difficult to determine due to the superposition of this fundamental mode with reflection signals from specimen boundaries, superposition with other wave modes and also from noise. This can cause incorrect mode arrival time determination which leads to temporal separation measurement error.

Furthermore, the use of the incorrect mode arrival time of A_0 mode will contribute to a larger error in SSMAL measurement when compared with the commercial TOA method. To overcome this drawback, a modified dispersion curve as discussed in section 2.3.4 can be used to verify the temporal separation measurement however this curve can only be produced if the source to sensor distance is known.

SSMAL location method promises an accurate source location result if the temporal separation error due to the superposition of A_0 mode with other wave components can be resolved. Temporal separation measurement error in SSMAL can be improved by deploying time-frequency analysis such as wavelet transform which can discriminate the content of AE signal.

2.5 Wavelet transform

2.5.1 Introduction AE signal analysis

The AE signal processing method is divided into time domain analysis and frequency domain analysis. Temporal separation determination of fundamental Lamb wave modes for single sensor modal analysis location (Pullin 2007) is the typical time domain analysis. Frequency spectrum analysis describes the frequency-domain characteristics of an AE signal. The Fourier Transforms (FT) spectrum analysis and spectrum estimations are typical spectrum analysis methods (Takemoto 2000).

The FT is only able to retrieve the frequency content of the signal but at the same time it loses any temporal information. This is overcome by a Short Time Fourier Transform (STFT) which calculates the FT of a part of a signal as a window and shifts the window over the entire signal. However, the STFT gives the content of a signal with a constant time and frequency resolution due to the fixed window length (Takemoto 2000). For analysing AE Lamb wave signals propagating in plate like components, this is not the desired resolution. The broadband and dispersive nature of Lamb waves need a multi resolution analysis and it is possible by using a wavelet analysis (Takemoto 2000).

Wavelet transform (WT) theory is a signal processing method which overcomes the limitation of Fourier analysis by performing time- frequency analysis at the same time. It also solves the conflict of time and frequency resolution in STFT analysis (Takemoto 2000). Detailed mathematical derivation on STFT and WT and their construction methods is well explained by Daubechies (1999).

Wavelet analysis has attracted attention in AE signal processing for its ability to analyse rapidly changing transient signal (Jeong 2000). WT analysis is suitable for processing transient AE signals because it not only describes the signal spectrum corresponding to a local time, but also describing the time-domain information within that spectrum (Serrano 1996).

2.5.2 Fundamental of wavelet transform

A WT is a time-frequency representation technique which describes a signal by using the correlation translation and expansion (rescaling) of a function called a mother wavelet. Fig. 2.17 shows how multi resolution is achieved by WT analysis when compared with STFT.

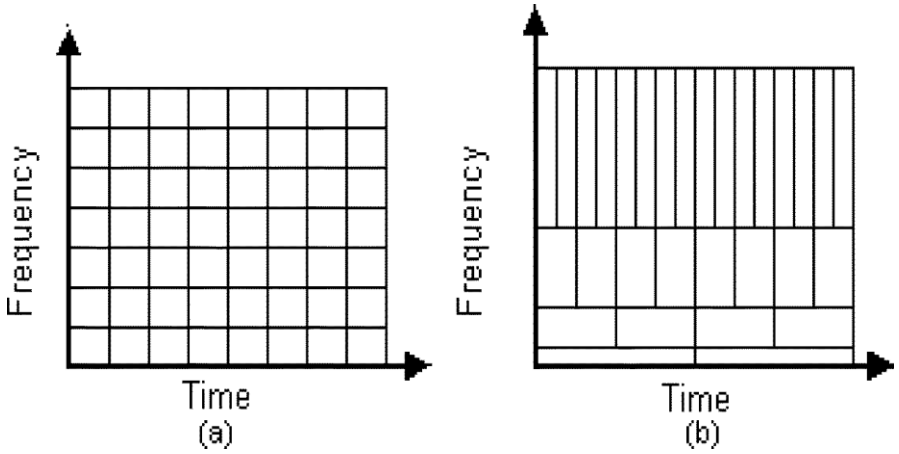

Fig. 2.17 (a) STFT with fix window and (b) WT with variable aspect window (Ganesan et. al 2003)

Temporal analysis is performed with a contracted high frequency mother wavelet, while frequency analysis is performed with dilated, low frequency of the same mother wavelet. The translation operation allows signal features to be isolated in times while the dilation operations allow identifying signal features that exist at different frequencies. In this way, the WT represents a signal as a sum of wavelets with different frequency components (Takemoto 2000, Addison 2005).

Typical time domain AE signal and its WT is shown in Fig. 2.18.

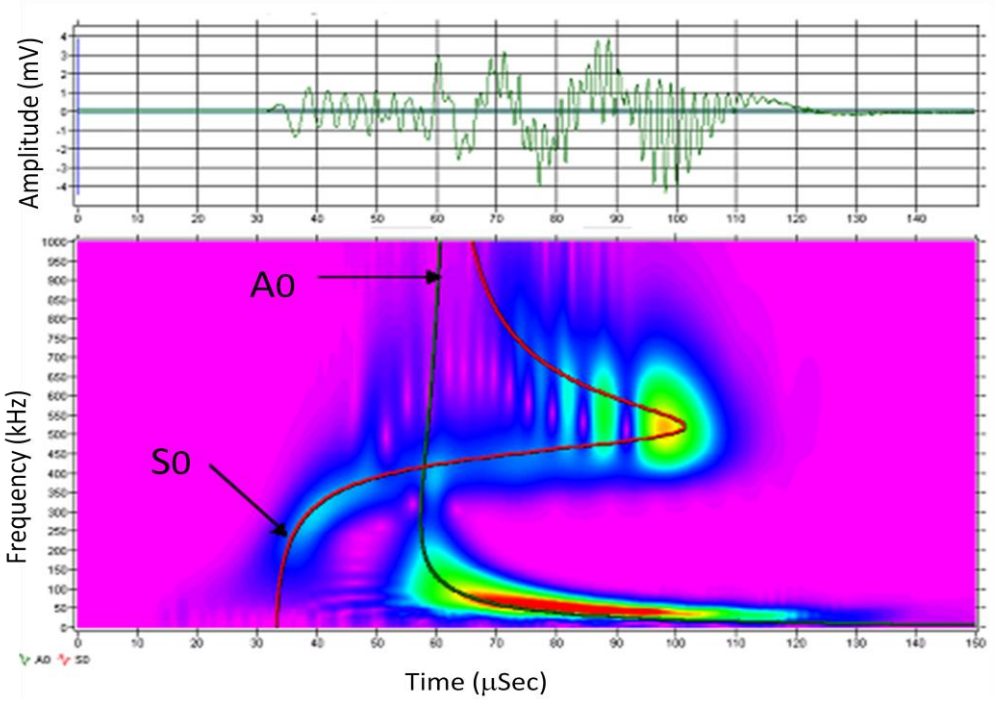

Fig. 2.18 Typical AE signal and its WT (Hamstad 2002)

WT analysis can be divided into two categories, continuous wavelet transform (CWT) and discrete wavelet transform (DWT). The continuous wavelet transform is calculated by the convolution of the signal and wavelet function (Addison 2005).

2.5.3 Source location of Lamb waves AE signals by WT

Since AE wave propagates in a thin plate is governed by Lamb waves as discussed in section 2.3, the accuracy of source location can be improved by SSMAL method as discussed in section 2.4.5. However, due to the dispersive nature of Lamb waves, inaccuracy of temporal separation measurement may lead to a source location error. WT has been applied to an AE source location based on plate wave theory (Jeong 2000, 2001 and Jingpin 2004, 2008) as an alternative for SSMAL.

H. Jeong (2000) shows that WT method can be used to improve AE source location accuracy by improving temporal separation measurement. Experiments were performed using pencil lead breaks as simulated fracture sources on the surface of an aluminium plate. Two plate modes corresponding to the S_0 and A_0 Lamb waves were identified and their group velocities were accurately measured. The study

showed that the source location measured by this approach mostly agreed with the actual locations.

Gabor wavelet has been used in the analysis of AE signals due to its good resolution in both time and frequency domain. The frequency component in the output signal has been extracted from the output of the envelope of a WT (Jeong 2001, Jingpin 2008).

H. Jeong (2000) applied the WT using Gabor wavelet to the analysis of flexural transient wave propagation in anisotropic composite laminates. He found that dispersion of the flexural mode obtained by WT analysis shows a good agreement with experimental results. Based on his analysis, the peak of WT analysis amplitude is related to the arrival time of the group velocity and the arrival time of each frequency has been successfully determined by WT analysis.

In principal, both Jeong and Jinpin used peak amplitude of AE signals to determine the arrival of fundamental mode and temporal separation. Most of the conventional TOA based AE system use first threshold crossing to determine the arrival AE signal rather than peak amplitude. It is expected that the minimum value of wavelet coefficient magnitude for each mode component could be more accurate for determining mode arrival times.

Aljets (2010) used WT to pick the arrival time of S_0 and A_0 modes and located the AE source in a large plate like structures using a local triangular sensor array. He found that, there is a possibility to wrongly pick the arrival time of the mode of interest which leads to significant location error. This error may make worse by noisy testing environment.

2.5.4 Signal denoising of AE using Discrete Wavelet Transform (DWT)

AE signals are broadband and contain environmental and electrical noises. This noise signal should be eliminated before further signal analysis is carried out and this can be done by performing DWT analysis.

The denoising of signals using the wavelet transform is done by representing the signal by a small number of coefficients. The waveform is decomposed into a series of wavelet coefficients. Each coefficient has different amplitudes at the various locations and durations. The wavelet coefficient is related to position (or time) and frequency of waveform (Zhao 2000).

Many of the wavelet coefficients generated by the WT are at a coefficient value near zero. They add very little to the composition of the waveform itself and most of them are produced by noise in the waveform. By applying a threshold process, these noise signal coefficients can be removed without affecting the integrity of the original signal. DWT is a very powerful tool for denoising and filtering certain components of AE signals when combined with the inverse DWT (Takemoto 2000).

Signal denoising using wavelet analysis has several advantages compared with conventional filtering methods. It can reduce the noise of a signal and at the same time keep the original features of the signal. Detailed signal denoising using WT can be found in Alfouri (2008) and common steps to reduce high frequency noise using wavelet denoising can be summarised as follow:

i) Discrete wavelet transform are calculated based on the best mother wavelet
ii) Wavelet coefficient threshold are applied onto the waveform to eliminate high frequency noise
iii) Waveform are reconstructed by inverse transform and normalising

2.5.5 Signal characterisation using WT analysis

WT method is not just useful for source location and signal denoising but also can be used for source identification or defect/damage characterisation. Some work has been carried out to utilise WT analysis to characterise the AE signal. Zhihao (2009) combined WT with the energy analysis to study the AE signal from the rubbing fault of a rotary machine. AE feature of the rubbing fault was successfully extracted by using this method.

Gang Qi (2000) used wavelet analysis to study the fracture behaviour on glass fibre reinforced plastic. He found that wavelet based methods could approximate residual strength better than classical AE technique.

Hamstad (2002) was used A_0/S_0 ratio based on WT analysis to distinguish different sources types all centred at the same depth below the plate surface and with the same propagation system. He found that the values of this ratio overlapped for different source types at different depths and concluded that it is not possible to uniquely identify the source type with a small set of WT -based data.

2.6 Thermal fatigue

2.6.1 Introduction to fatigue

Fatigue is the progressive, localised, and permanent structural change that occurs in a material subjected to repeated or fluctuating strains at nominal stresses that have maximum values less than (and often much less than) the static yield stress of the material (Fine and Chung 1996).

A very useful way to visualise time to failure for a specific material is with an S-N curve. The "S-N" means stress amplitude, σ_a, versus cycles to failure, with σ_a plotted on the vertical axis and the logarithm of the number of cycles to failure plotted horizontally as shown in Fig. 2.19.

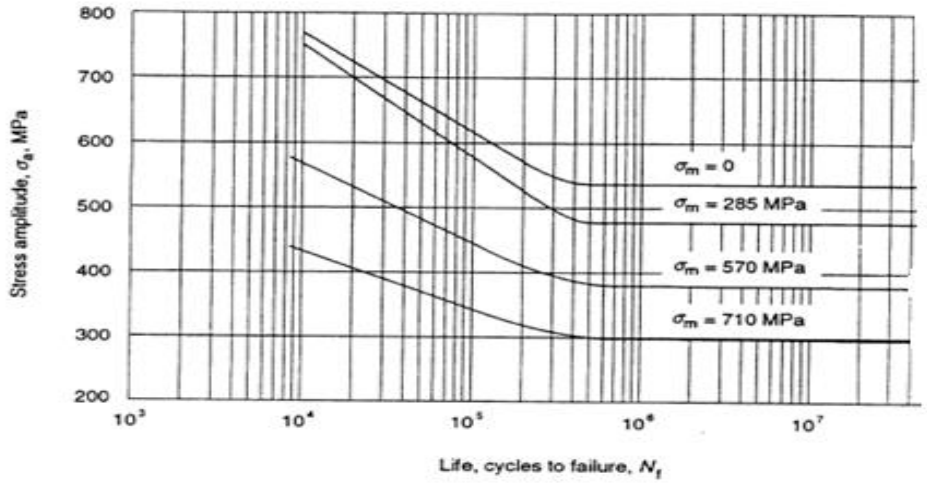

Fig 2.19 Schematic representations of the fatigue life and its dependence on stress level (BS 1993)

Fatigue may produce cracks and cause fractures after a sufficient number of cycles. According to BS (1993), failure of a material due to fatigue may be viewed on microscopic level in three steps:

i. Crack Initiation: The initial crack occurs in this stage. The crack may be caused by surface scratches caused by slip bands or dislocations intersecting the surface as a result of previous cyclic loading or work hardening.
ii. Crack Propagation: The crack continues to grow during this stage as a result of continuously applied stress range.
iii. Failure: Failure occurs when the material that has not been affected by the crack cannot withstand the applied stress range. This stage often happens very quickly.

A schematic diagram of fatigue crack growth curve is shown in Fig 2.20.

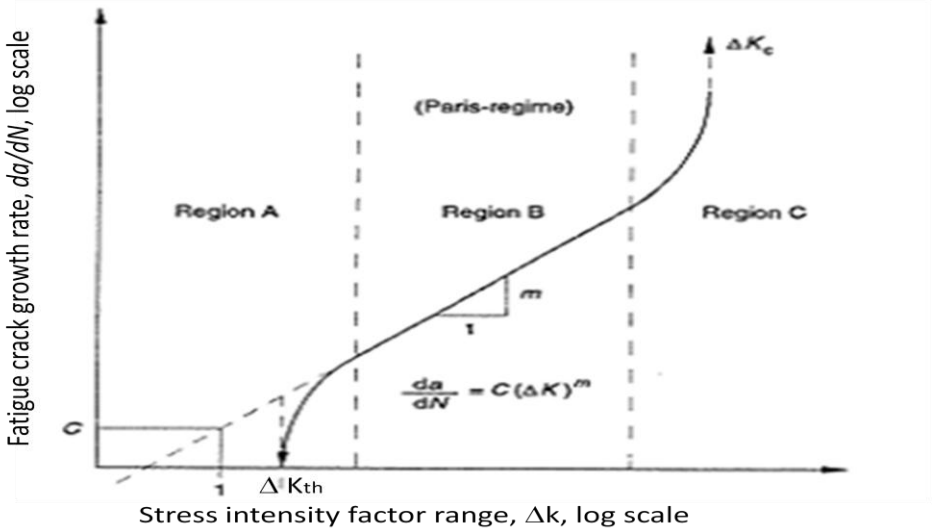

Fig. 2.20 Schematic *da/dN* versus Δ*K* curve for fatigue crack growth (BS 1993)

The rate at which a crack grows from a pre-cracking crack has considerable importance in determining the life of a material. The rate at which the crack continues to grow depends on the stress intensity range. Fatigue damage is caused by the simultaneous action of cyclic stress, tensile stress, and local plastic strain. If any one of these three is not present, a fatigue crack will not both initiate and propagate. Cyclic stress refers to the repetitive change in internal distribution of

force and it can be in form of load, pressure or temperature. Damage caused by thermal cyclic loading is called thermal fatigue.

2.6.2 Thermal fatigue in nuclear piping

Thermal fatigue cracks have been reported to occur in primary loop recirculation pipes and various other components of nuclear power plants (Hayashi, 1998). The main source of fatigue cracks in the nuclear piping system is the thermal stresses associated with plant heat-up and cool down which were not included in the original fatigue design analyses. For example, thermal fatigue cracks were initiated at a branch pipe connection between a feed water system and shut down cooling system (Hayashi, 1998).

Branch piping subject to turbulence can be considered to have three sections. At the tee junction point, hot and cold temperature waters are mixed together. The vibration at the mixing boundary will cause the temperature fluctuation on the inside surface of the pipe (EPRI 2000). Schematic turbulence penetration in nuclear piping is shown in Fig.2.21.

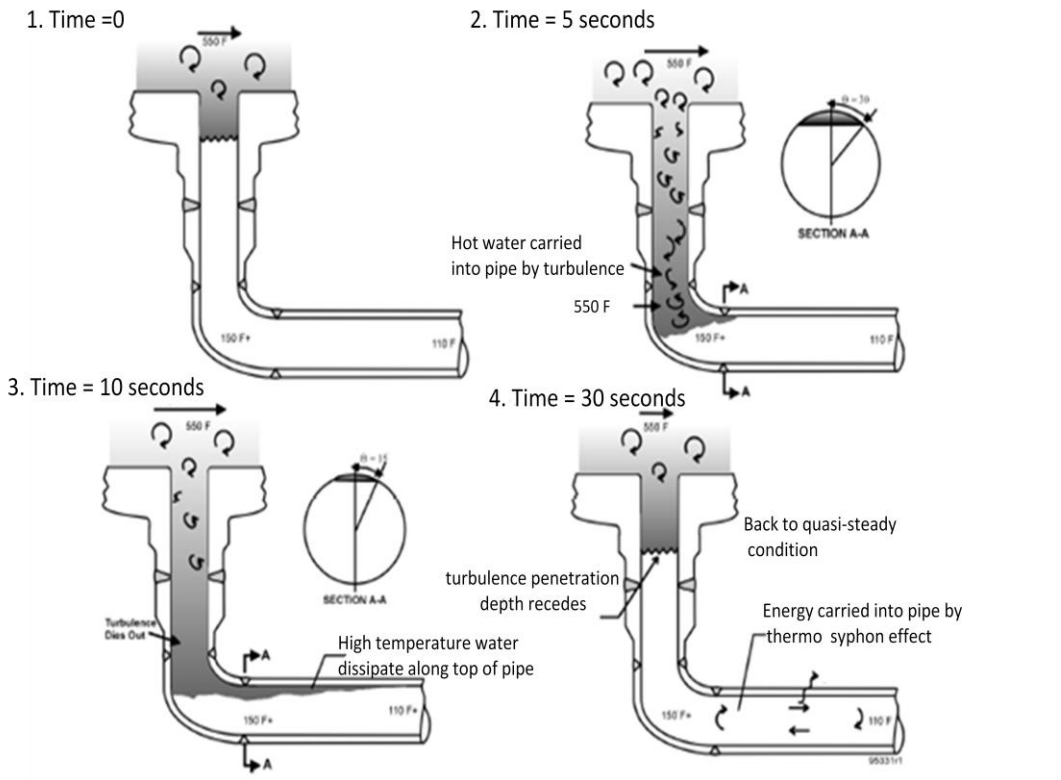

Fig. 2.21 Schematic turbulence penetration in nuclear piping (EPRI, 2000)

In the section closest to the run pipe, the entire pipe's cross section is at a hot temperature. In the second section, the run pipe temperature permeates into the branch pipe, but to a lesser extent, such that it stratifies at the top of the pipe. Combined with this are flow turbulence effects, which cause local thermal cycling at points in the pipe cross-section. In the third section of turbulence penetration, further away from the run pipe, only the effects of run pipe temperature permeating into the pipe due to natural convection effects are present. There is no flow turbulence across the cross section. However, cycling can still occur in this region, as the length of turbulence penetration may produce temperature variations over time in both the axial and radial directions.

Thermal stratification may also cause leaks in normally stagnant lines connected to the reactor coolant loop in safety injection systems, reactor coolant drain lines, a residual heat removal suction line, and an excess letdown line. In addition, stratification has caused cracking of steam generator feed water nozzles and high piping displacements in pressuriser surge lines (Bieniussa 1999).

Thermal fatigue can lead to crack formation, small leaks in piping, medium leaks in piping (when crack opening is more than 1 mm) or a total break of piping system (NEA/CSNI/R, 2005). The leak before break (LLB) concept is widely used in the nuclear industry to describe the idea that in the piping carrying the coolant of power reactor, a leak will develop before a catastrophic failure will occur (IAEA 1993).

The LLB concept is based on a fracture mechanic approach that a crack would grow through the wall of piping system, resulting in a leak, and that this postulated small 'through wall' defect in plant piping would be detected by a leakage monitoring system before the flaw could grow to critical size. Leakage exceeding a specified limit requires the plant to be shut down (IAEA 1993).

For the application of the LLB concept to take place in the nuclear power plant, leak detection methods must be added to the plant. However, no single currently available leak detection method can provide optimal detection sensitivity, location ability and measurement accuracy. Although quantitative leakage determination is

possible by using condensate flow monitors (Kupperman 1985), sump monitors and primary coolant inventory balance, these methods are not adequate for locating and measuring leak size and are not sensitive enough to meet LLB requirements (IAEA 1993)

Currently, piping structures in nuclear power plants are inspected using conventional non-destructive methods like ultrasonic testing which are carried out during power plant shut down, which are usually held every 10 years (IAEA, 2003). If cracks due to thermal fatigue occur within this period, it will be left unattended unless a proper continuous leak monitoring system is installed to monitor such failure in piping systems in nuclear power plant. This type of critical failure not just causes leaks of radioactive material into the environment but also may contribute to the catastrophic failure of the nuclear power plant.

A suitable technology to improve leak detection capability at specified sites in the nuclear power piping is the use of AE monitoring. AE offers the opportunity to monitor the thermal fatigue damage continuously and cracks can be identified at early initiation stage without intrusion on the plant operation schedule. However, current AE techniques still have difficulties with sources discrimination and flaw size measurement.

With current development in WT analysis, it may be possible that the MAE technique can detect, identify and measure the size of thermal fatigue cracks in piping systems in a more accurate manner.

2.6.3 Fatigue and AE

AE from crack growth is of interest for practical non-destructive testing applications. The formation of the stress concentrations in their vicinity, cracks and other defects will emit stress waves when load is increased, while an unflawed part in material will remain silent. It is useful to distinguish between AE signals from the plastic zone at the crack tip and AE signals from the movement of the crack itself. If the size of the plastic zone is very big, the signal released from this mechanism will not represent the actual location of the crack tip. Growth of the

plastic zone typically produces many emissions of low amplitude (Khan 1982, Talebzadeh 2001).

AE from the crack front movement depends on the nature of the crack growth process. Microscopically, rapid mechanisms such as brittle inter-granular fracture and trans-granular cleavage are detectable when the crack front is advancing one grain at sub-critical stress levels. Slow, continuous crack growth mechanism such as micro-void coalescence and active path corrosion are not detectable in themselves but they may be detectable through associated plastic zone growth (Miller, 1987).

AE monitoring, together with fracture mechanics methods, have been used to study cleavage crack growth in laboratory specimens of several alloy steels. Experimental results indicate that, during the onset of rapid unstable crack growth, spontaneous acoustic events are emitted. The fractographic studies on the fractured surface have demonstrated that a large number of energetic signals result from local brittle fracture at the crack tip. It was found that the stress intensity factor corresponding to the first trans-granular or inter-granular cleavage crack extension provides predictive information regarding the final unstable failure (Khan, 1982).

Roberts & Talebzadeh (2002, 2003) used AE to monitor fatigue crack propagation in steel and welded steel specimens for T-section girders. The study showed that AE count rates have a reasonable correlation with crack propagation rate and suggests that AE monitoring can be used to predict the remaining life of fatigue damaged structures.

Crack closure also emits AE. Singh et al (2007) was correlating Elber's crack closure result with AE data by showing that the primary cause of the generation of AE is considered to be crack opening and closure associated with friction between two fatigue crack surfaces. Chang (2009) used AE to study fatigue crack closure in aluminium alloy during unloading and suggested that the AE technique could be used to measure the crack closure level especially for short cracks.

The AE technique also has also been used to study the creep fatigue deformation. Han & Oh (2006) correlate the AE count rate with this deformation parameter and suggest that it could be used as an effective tool to evaluate this kind of fatigue.

For locating the crack growth in nuclear piping, it is very important to properly characterise the AE signal released from the crack growth area and differentiated it from other sources mechanism. Baxter (2006) used AE feature data to characterise active AE signals emanating from fatigue crack growth area in aircraft grade material under a four point bending test. He found that, AE feature data extraction and filtering techniques were useful to characterise AE signals from fatigue crack growth and other areas which produced active AE events.

2.7 Conclusions

Fatigue crack growth emits acoustic energy and one of the advantages of acoustic emission (AE) testing is its ability to locate this kind of defect by using an array of sensors at a distance from the source. The cost saving of deploying an AE inspection method can be achieved by reducing the time to perform the follow up test due to the localisation of the damage source and the downtime associated with plant shut down. Further cost saving can be achieved if defects can be sized as well as located.

Accurate AE source location is very important for nuclear piping structural integrity monitoring. The conventional TOA for source location of AE signals based on threshold crossing is well developed and is very useful for approximate source location in large structure. However, the result of source location is greatly affected by the level of threshold voltage and the average value of velocity measured. This method can completely fail under condition when high background noise is present.

DeltaT location method has been developed to overcome the in accuracy of TOA location method especially for testing the complex structure. DeltaT method works on the same principle as the TOA method utilising the time arrival of the signal at the sensor.

This method has been shown to be more accurate than TOA because velocity and geometry errors are minimised. Effects from boundary reflections and mode conversions are also accounted for in DeltaT location algorithm. This method is found suitable for structural health monitoring of structures with non uniform geometry such as in aircraft landing gear.

The main disadvantages of the DeltaT location methods are; the map should be constructed before the actual test for a specific location (i.e., the AE data from outside the map area cannot be analysed by this technique) and the analysis is only valid if the location of the sensor arrays does not change.

Single sensor modal analysis location (SSMAL) works on the MAE theory. This method is based on the dispersive characteristic of Lamb waves that propagate in plate like structure. SSMAL is expected to produce better location results compared with TOA methods since the timing error due to the arrival delay between first hit arrival and first threshold crossing is minimised. However, due to dispersion characteristic of Lamb wave, superposition of the A_0 mode arrival with other higher order asymmetry components will lead to source location inaccuracy.

MAE location method promises an accurate source location result if the temporal separation error due to the superposition of A_0 mode from other wave components can be resolved. Temporal separation measurement error in SSMAL can be improved by deploying time-frequency analysis which can discriminate the content of AE signal instead of depending on the time domain waveform analysis for temporal separation measurement.

The availability of an additional representation, in term of time frequency analysis of acoustic wave propagating in the dispersive media, by WT analysis the discrimination of various frequency ranges of AE signals which, when used in conjunction with modal analysis, can improve location accuracy.

WT for AE signal analysis can be divided into two parts, continuous WT analysis and discrete waveform analysis. The discrete WT decomposes the signal into wavelet coefficients from which the signal can be reconstructed again.

The reconstructed waveform can be used to calculate more accurate source location by deploying wavelet coefficient value. WT analysis can be used for multi-resolution analysis of local frequency content of an AE signal. It can be used for signal compression, signal denoising, feature extraction and source location.

In this study, the AE feature data will be used to characterise crack growth data from steel plates and pipes under four point bending and the AE signal released from crack growth will be differentiated from other sources mechanisms. The waveform of this signal will be analysed using WT analysis. The accuracy of WT analysis will be compared with other methods such as TOA and DeltaT and also waveform filtering method. This study is also carried out to seek the feasibility of using AE for measuring crack length due to thermal fatigue.

CHAPTER 3: EXPERIMENTAL EQUIPMENT, PROCEDURE AND TECHNIQUES

This chapter describes specific AE equipment, software and techniques and other systems utilised throughout this research. Experimental work detailing the calibration and validation of location techniques is also presented.

3.1 AE instrumentation and software

3.1.1 Data acquisition and storage

The two Acoustic Emission systems, DiSP and MISTRAS, used in this study are manufactured by Physical Acoustics Corporation.

The DiSP Acoustic Emission system utilizes parallel 32 bit digital signal processor (DiSP) technology and uses **P**eripheral **C**omputer **I**nterface- **D**igital **S**ignal **P**rocessor (PCI-DSP) boards. Each board carries 4 channels with data transfer speeds up to 20 Mb/sec assuring a wide bandwith for multi-channel AE data acquisition and waveform processing (PAC 2005) as shown in Fig. 3.1.

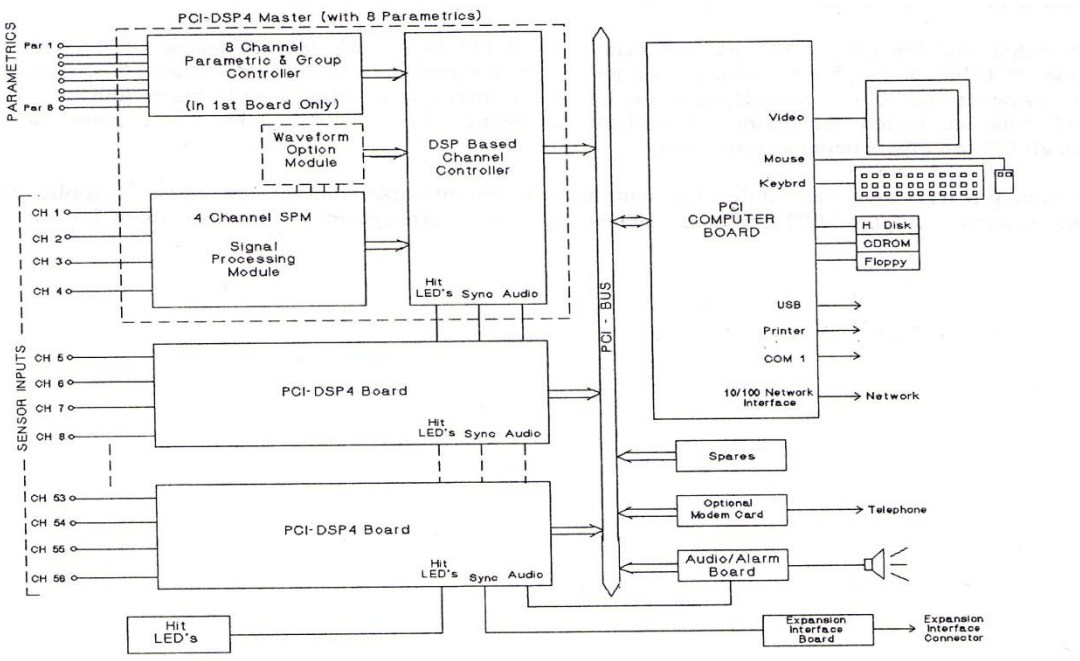

Fig. 3.1 PCI/ DISP System Block Diagram (PAC 2005)

The MISTRAS system (Massively Instrumented Sensor Technology for Received Acoustic Signals) is a fully digital, multichannel computerised system that performs AE signal waveform acquisition and feature extraction and stores, displays and analyses the acquisition data in real time (Fig. 3.2).

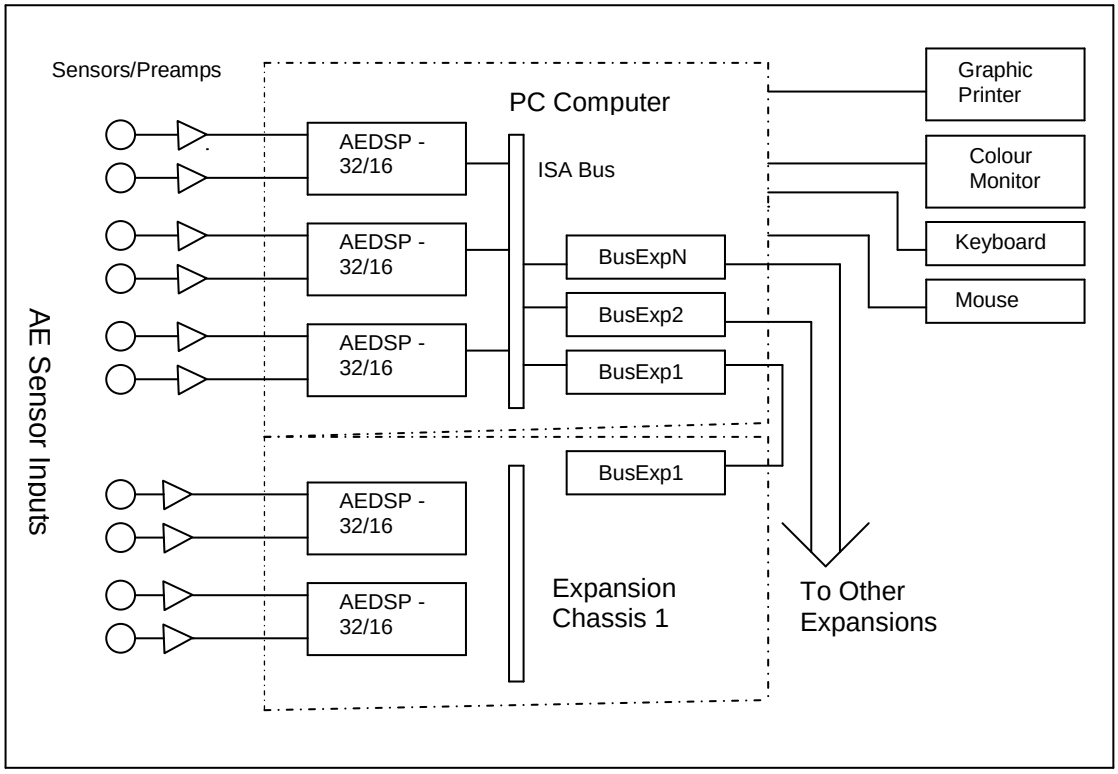

Fig. 3.2 MISTRAS system block diagram (PAC 1995)

The main component of the MISTRAS is the AEDSP (Acoustic Emission Digital Signal Processor) board. Each board provides two AE channels and is plugged into the Industrial Standard Architecture (ISA) slots of a Personal Computer (PC).

3.1.2 AE sensors

The most important factor for success in AE testing is the selection of the correct AE sensor. The main considerations behind sensor choice are sensitivity, operating frequency and bandwidth.

A transducer is a device that produces a measureable voltage signal proportional to the physical parameter it is monitoring. When stress wavefronts arrive at the

specimen surface, small displacements will occur. AE sensors are used to detect this mechanical movement and convert it into an electrical signal.

Generally, AE sensors are categorised into two types; resonant and wideband. Resonant sensors are more sensitive to AE sources at particular frequencies, where the piezoelectric materials of these sensors oscillate at greater amplitude than the other frequency as shown in Fig. 3.3. By matching the expected frequency of AE events with a resonant transducer, a greater contrast between the actual AE signal and the noise can be achieved that can improve the signal-to-noise ratio significantly.

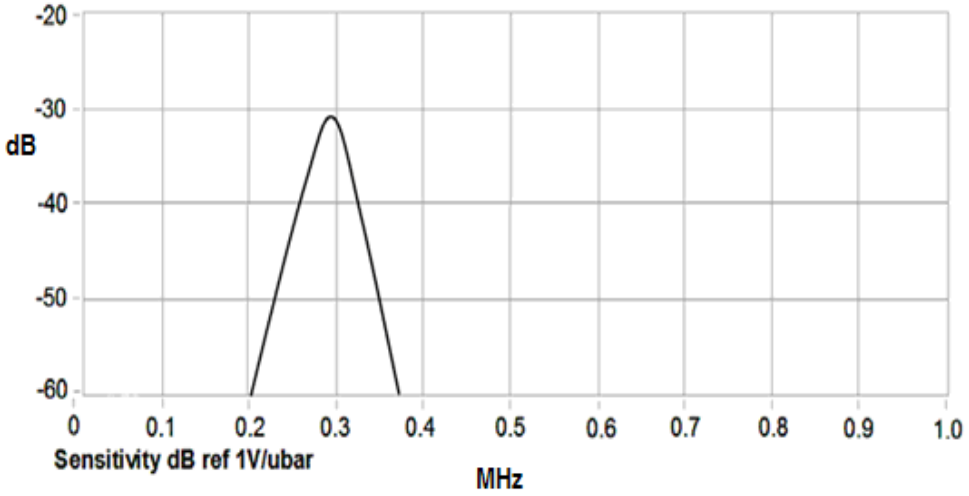

Fig. 3.3 Theoretical frequency response of resonant sensor with resonant frequency of 300 kHz (Baxter 2007)

Wideband sensors work across a much larger frequency range than that of resonant sensor. Usually, wideband sensors have a relatively flat frequency response across their working range as shown in Fig. 3.4. The wideband sensor is very important in research applications, especially when frequency analysis of the signal is required for determination of the predominant frequency source for noise discrimination. Furthermore, in high fidelity applications such as modal acoustic emission (MAE) analysis, various AE wavemode components can be detected using a wideband sensor, providing more information about the AE source and the distance of an AE event from the sensors.

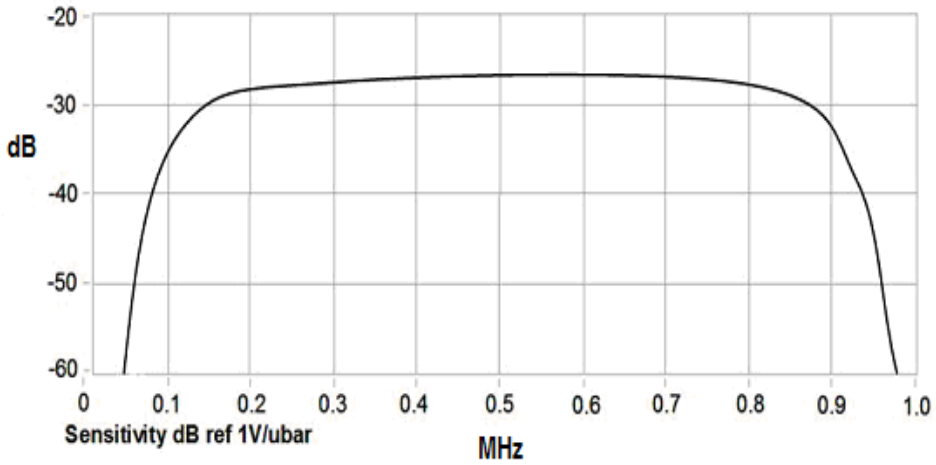

Fig. 3.4 Theoretical frequency response of wideband sensor (Baxter 2007)

The key element in an AE sensor is a piezoelectric transducer. When a mechanical strain is applied in a piezoelectric material, a measurable potential difference is produced across the transducer. This phenomenon is reversible, i.e., by application of a potential difference across the transducer; a mechanical vibration can be induced in the piezoelectric crystal. For linear piezoelectricity, there is a linear relation between mechanical vibration and potential difference allowing direct measurement of distortion from the output voltage. The piezoelectric material is usually made from ceramic material such as zirconate titanate (Miller & McIntire, 2005).

The transducer is housed in a suitable enclosure with a wear plate and connector. The sensor is excited by the stress waves hitting its face, and it transmits an electrical signal to a nearby preamplifier and then onto the main signal processing equipment. A schematic diagram of a typical AE sensor is shown in Fig. 3.5.

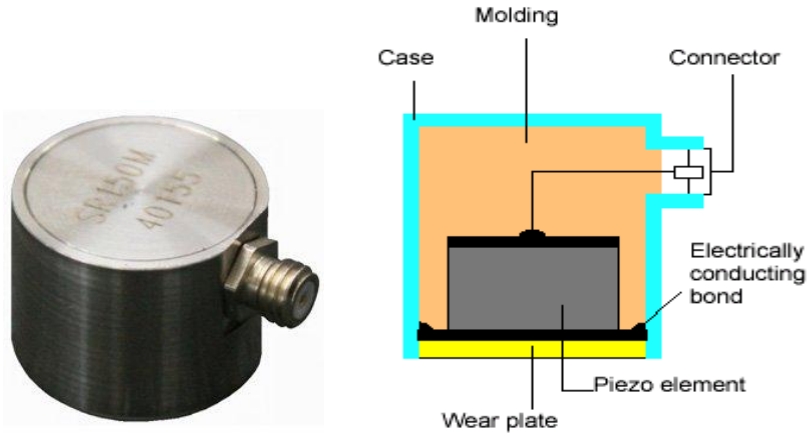

Fig. 3.5 Typical AE sensor and it schematic diagram (Vallen 2002)

Several AE sensors were used in this investigation. WDI, D9202B and WD sensor are wideband sensor while R15D, R15I AST and R15I are resonant sensor. Their working frequency, resonant frequency and dimension are shown in Table 3.1. A typical calibration certificate for each type is shown in Fig. 3.6

Table 3.1 Specifications of AE sensors used in throughout this work (according to manufacturers rating using NIST transient surface wave calibration to ASTM E1106-86)

Sensor Type	Dimension Diameter x HT (mm)	Operating Frequency Range (kHz)	Resonant Frequency (kHz)
WDI	29 x 30	100-1000	650
WD	18 x 17	100-1000	650
R15I AST	29 x 31	70-200	150
R15D	18 x 17	50-200	150
R15	18 x17	50-200	150
D9202B	18 x 17	400-1000	450

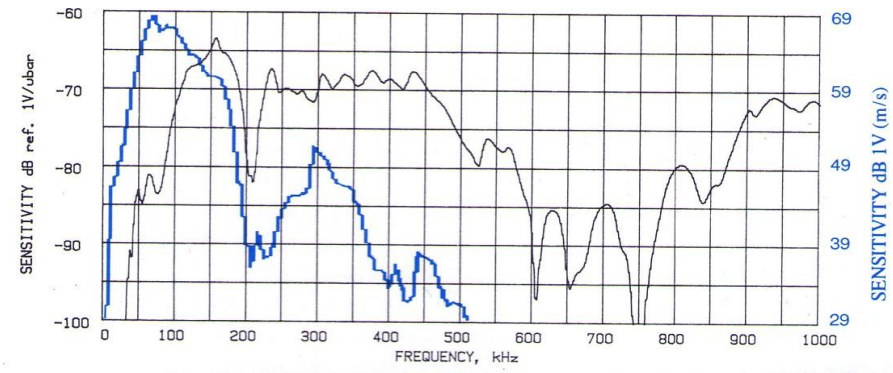

R15D Sensor calibration certificate

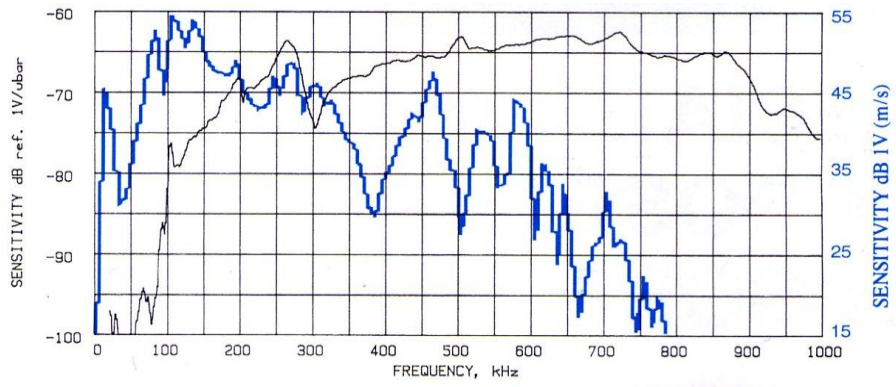

WD Sensor calibration certificate

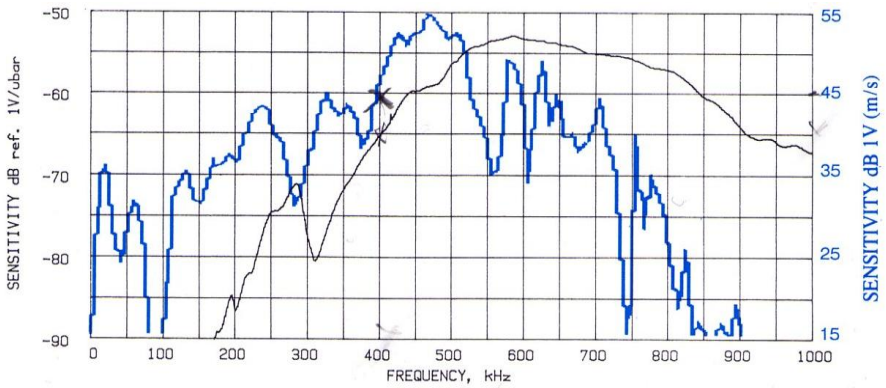

D9202B Sensor calibration certificate

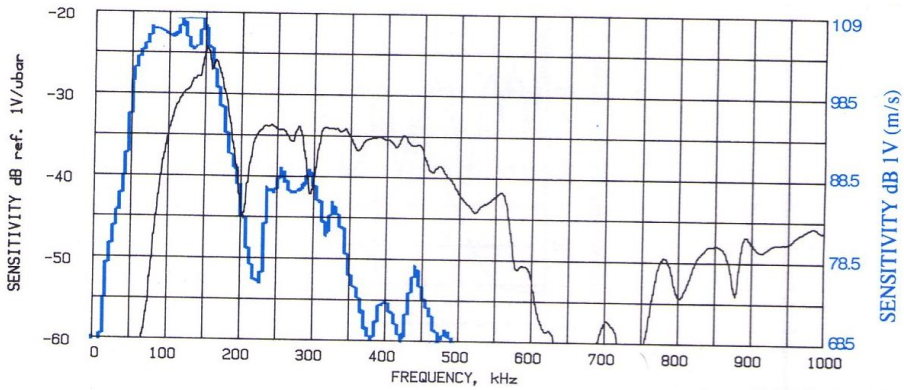

R151 Sensor calibration certificate

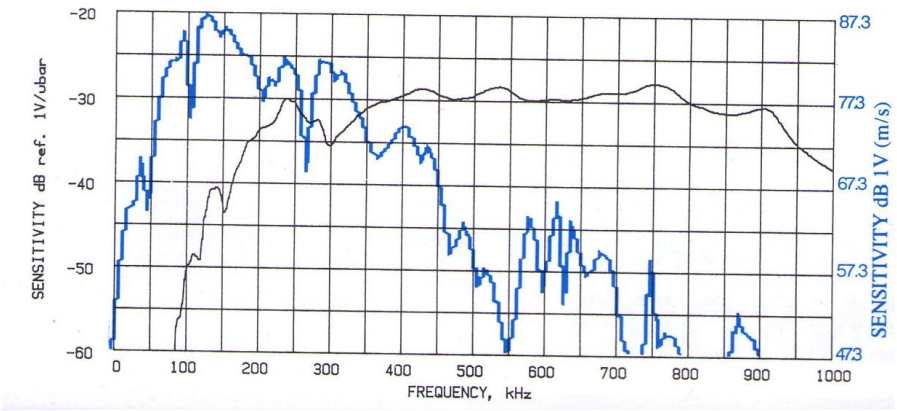

WDI Sensor calibration certificate

Fig. 3.6 Typical calibration certificates for all sensors used in this investigation.

However, all data used for wavelet transform analysis in this study was obtained from WD Broadband sensors.

3.1.3 AE preamplifier

The small voltage generated by the piezoelectric element in the sensor is amplified to a more useable voltage before this signal is transmitted to the measurement circuitry. This is accomplished with a preamplifier, which is placed close to the sensor to minimize the pickup of electromagnetic interference (PAC 2005). Some sensors have preamplifiers built in, these are called integral sensors.

The preamplifier has a wide dynamic range and can drive the signal along a length of cable. The main instrumentation can then be placed hundreds of metres from the structure under test if necessary. The pre-amplifier typically provides a gain of 40 dB and includes a high-pass or band-pass filter to eliminate the mechanical and background noise.

For non-integral sensors, the preamplifier is usually placed close to the sensor to provide optimum sensor coupling, suitable gain and excellent cable drive capability. PAC 2/4/6 preamplifiers were used throughout this study (Fig. 3.7).

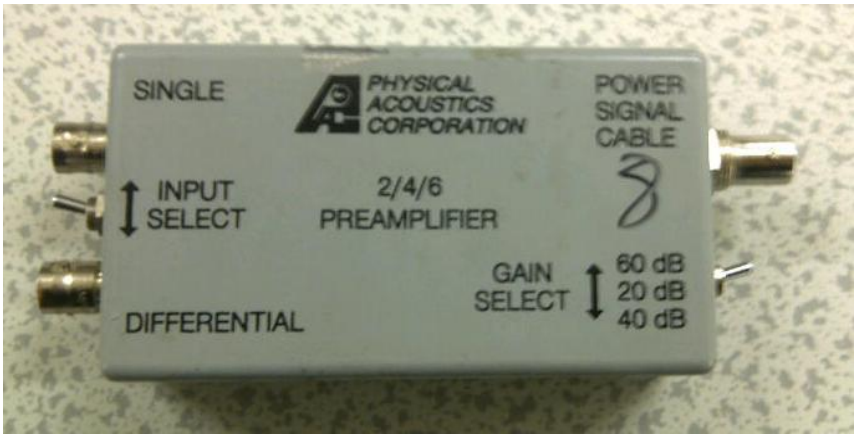

Fig. 3.7 PAC's 2/4/6 preamplifier

In integral sensors, the preamplifier is completely enclosed in the same case as the piezoelectric transducer and is coated to minimise radiofrequency and electromagnetic interference. R15I and WDI sensors are examples of integral sensors where a low noise FET input 40dB preamplifier is enclosed inside standard high sensitivity R15 and WD sensor (PAC 2005).

The availability of integral sensors makes the permanent installation that is necessary in an industrial application is possible. Fig. 3.8 shows the block diagram for an industry standard R15I sensor.

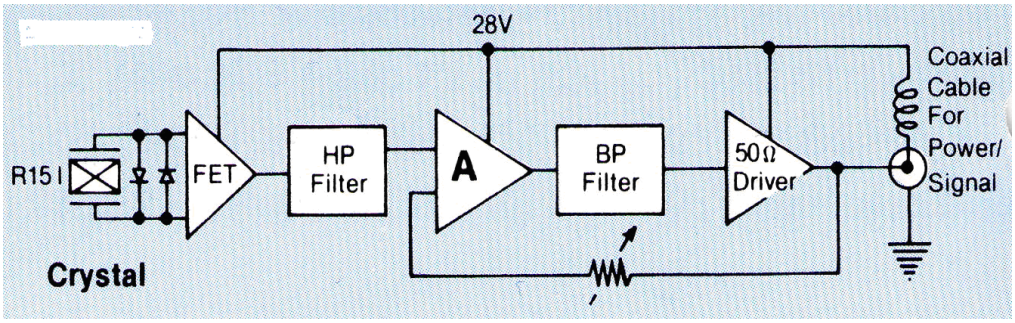

Fig. 3.8 Block diagram for the industry standard R15I sensor (PAC 2005).

3.1.4 Hsu-Nielsen source

After the sensor is installed and connected to the monitoring equipment, system sensitivity (performance) is checked before monitoring begins. Work by Hsu and Breckenridge (1979) using Hsu-Nielsen (H-N) pencil source has led to an affordable, cost effective method for sensitivity assessment. This involves the

breaking of pencil lead near the sensor to verify the response from an acoustic signal (ASTM E976, 1994). This test is carried out to ensure that a transducer has been properly coupled to the structure or specimen prior to test.

The H-N pencil lead must be grade 2H with 0.3 mm or 0.5 mm diameter and be broken at angle of 30^{o}. This angle is obtained with the use of a 'Nielson shoe' that attaches to the end of the retractable pencil (Fig. 3. 9). When properly performed, the lead breaks deliver a reproducible signal that closely matches "a point impulse loading" source.

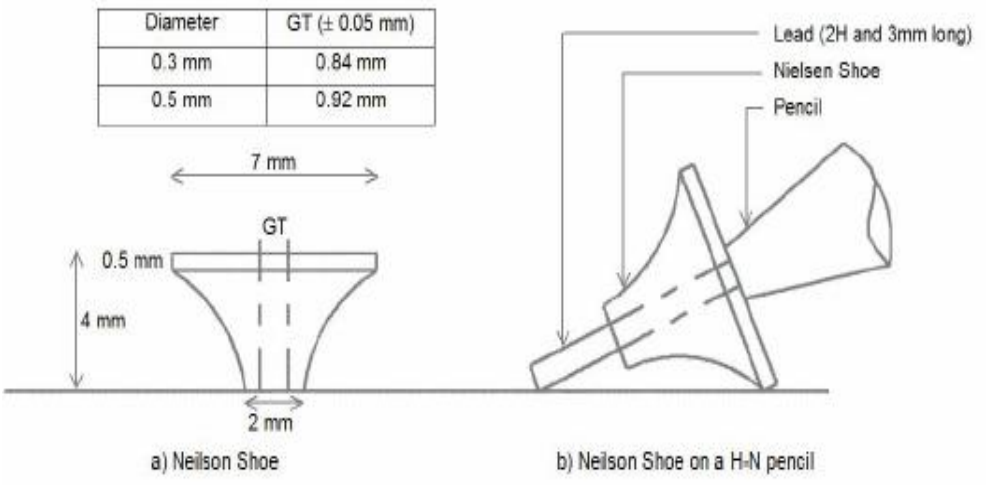

Fig.3.9: The H-N source method and guide ring (Rindorf, 1981)

The recommended procedure for pencil lead break is as follows (ASTM 1994);

a) The lead feed button on the pencil is pressed repeatedly until the lead protrudes.
b) The end of the lead is levelled with the end of the guide tube by pressing the tip of the pencil perpendicularly towards an even surface while the feed button is pressed down.
c) The button is pressed few times to cause the lead to protrude about 3 mm
d) The pencil is guided obliquely towards the test object until the guide ring rest on the surface.
e) The pencil is pivoted about the point of contact towards a steeper position to cause the lead to break.

The H-N source will provide a hit with amplitude of 98 to 100 dB adjacent to AE transducer, mounted on a specimen surface.

3.1.5 Couplant

When a sensor is simply placed on the surface of the test object, only a very weak signal is produced at the sensor. However, if a thin layer of couplant is placed between test object and sensor, a much larger signal is obtained. A couplant is any material which aids the transmission of an acoustic wave between the test object and sensor.

A couplant material is primarily used to remove any air gap at the interface of sensor and test specimen due to the microstructure of two contacting surfaces. Air gap at this interface will cause loss of energy transmission because the acoustic impedance of air is much lower than that of test object and sensor surface. Therefore, placement of a couplant material with higher acoustic impedance will replace the air in the gap between two surfaces and increase the transmission of energy.

Correct coupling of AE sensor to the surface of the test object is very important for obtaining good energy transmission. Duration of test, long term stability of the couplant, the frequency of sensors removal, environmental condition, and type of wave to be detected should be put into consideration in selecting the right couplant for AE test. According to ASTM guidelines (ASTM 1997), a selected couplant should;

a) Suit the test environment
b) Incur no damage to the structure or transducer
c) Be suitable for the type of motion detected.

There are various types of couplant used for AE testing such as liquid, gel, grease and adhesive couplant. Liquid couplant generally can offer good longitudinal wave transmission compared with other types of couplant. They are easy to use and easy to remove the air gap between sensor-specimen interfaces. However, they provide lower acoustic impedance compared with other type of couplant and tend to drip

due to low viscosity. Therefore, they are not suitable for any vertical mounting application as this encourages loss of the couplant layer with time.

Grease based couplants have much higher viscosity than gels or liquids and therefore are more suitable for rougher surface application. Brown grease is predominantly used in this investigation. This type of couplant allows lateral sensor movement to encourage displacement of trapped air (Theobald et. al 2008). Furthermore, if well clamped, grease offers better long-term stability than gels and liquids and generally does not damage the surface. However, due to high viscosity of grease couplant, application of force on the sensor is required to remove all the trapped air, a mounting fixture is used to meet this purpose.

Adhesive agent can also be used as a couplant. If applied on a clean flat surface, an adhesive agent can provide better transmission for both longitudinal and shear wave if correctly applied. This type of couplant is ideal for the applications that need absolute coupling and sensor stability such as DeltaT source location. The most common adhesive agents used in AE testing are cyanoacrylate and silicon rubber compound.

Silicone rubber compound has also been used in this work because it can be applied as a fluid to achieved a thin layer, bubble free couplant and at the same time provide a permanent bond on the structure under test. This thin layer can provide excellent sound transmission which is comparable with greased based couplant but with a relatively strong bond (Theobald et. al. 2008). Furthermore, silicone rubber compound also works very well on rough surfaces and has good resistance to bond failure if surface movement might occur during the test and therefore is suitable for vertical mounting application. This type of bond enables easier sensor removal after use with lower risk of sensor damage compared with cyanoacrylate bond.

3.1.6 Sensor mounting

Sensor mounting fixtures are necessary to hold the sensor in a fixed position when the non-adhesive couplant is used. Typically, when the sensor is coupled to the test piece, it is secured with tape or a magnetic hold-down device (together with either a

spring or a screw thread). In some applications, when the surface temperature of structure is high or the access is limited, the AE sensor may be mounted on a waveguide.

Mounting fixtures also provide constant pressure for optimising the transmission of energy from the test object to the sensor when high viscosity couplant is used. However, precautionary measures should be taken so that no electrical contact between the sensor case and specimens occurs in the presence of these mechanical mounting fixtures.

In this study, both brown grease and an adhesive bond, and magnetic hold down devices have been used to couple the sensors to the specimen surfaces. The magnetic hold down device (Fig. 3.10) can keep the sensor on the ferromagnetic specimens for the whole duration of test. Furthermore, it can provide a constant pressure for optimum coupling between pipe specimen surface and sensor when brown grease is used as a couplant.

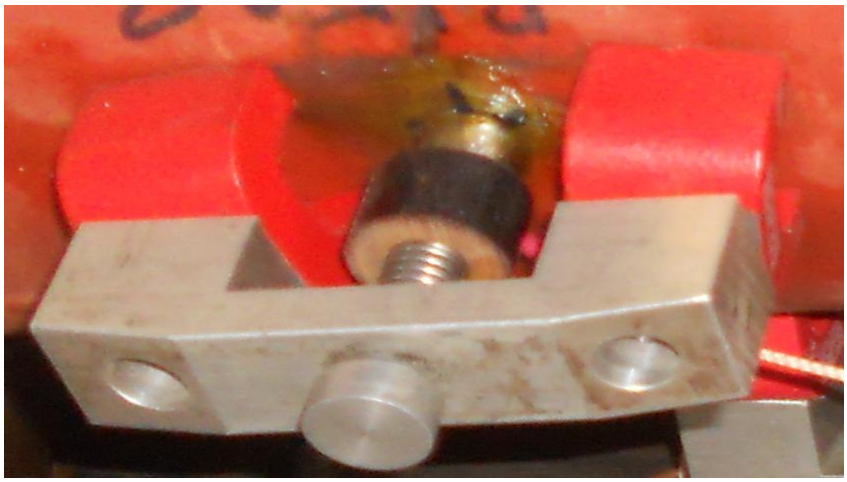

Fig. 3.10 Magnetic hold down with spring used to secure the sensor position on the pipe surface

Bonding agent (adhesive couplant) can also be used for physically mounting the sensor to the test object. This type of mounting is ideal for application where the sensor will not be removed from the test object and, for measurement where the coupling or sensor position stability is required.

The coupling is then tested with H-N source and checked periodically to ensure that it has not changed.

3.2 Data replay and analysis

AEwin for MISTRAS E 1.30 was used to replay and display stored AE data throughout this study. This 32 bit Windows program is able to replay and analyse previously collected AE files and is fully compatible with PAC standard data files.

3.2.1 Graphical representation

AE data is most commonly viewed in graphical format, comparing two or more data features. The AEwin software used throughout this research allows the user to replay data with a wide range of graph selections. The different types of graph used to report the finding of AE tests are discussed below.

Time-history plots display user-selected AE features or other parameters such as load against time, showing general trends over the test period. The graph can be displayed as cumulative plot or rate based plot of AE hits or events against time. It is possible to identify the point at which a source mechanism became active using time history plots (Fig. 3.11).

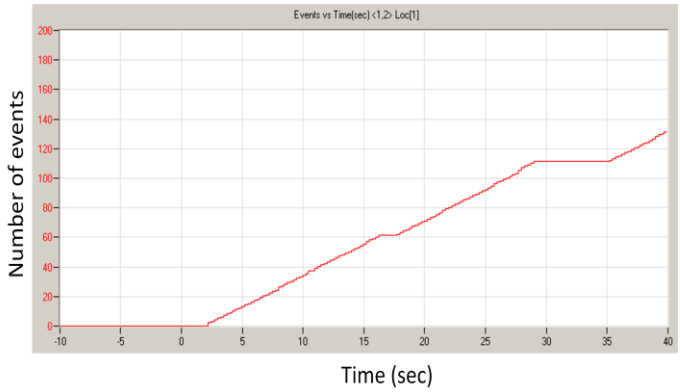

Fig. 3.11 Typical time history plot of cumulative AE events

Location plots are used to display the location of an AE event within a sensor array. Two type of array used in this research are linear and planar arrays (Fig. 3.12 and 3.13).

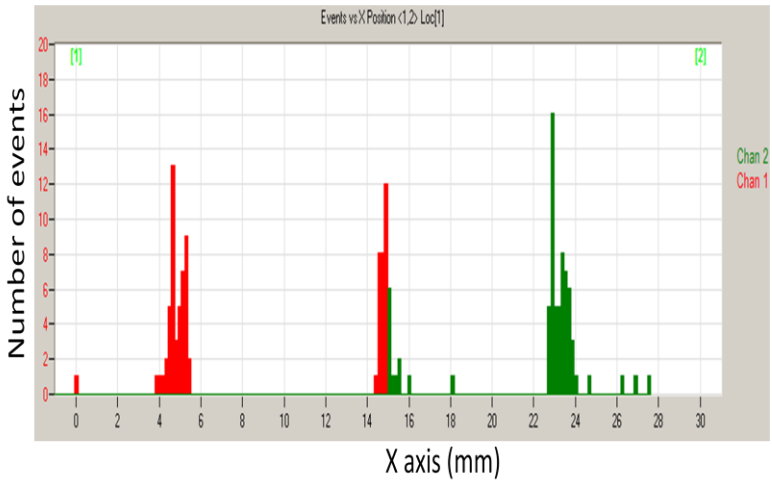

Fig. 3.12 Typical location plot under linear sensors array

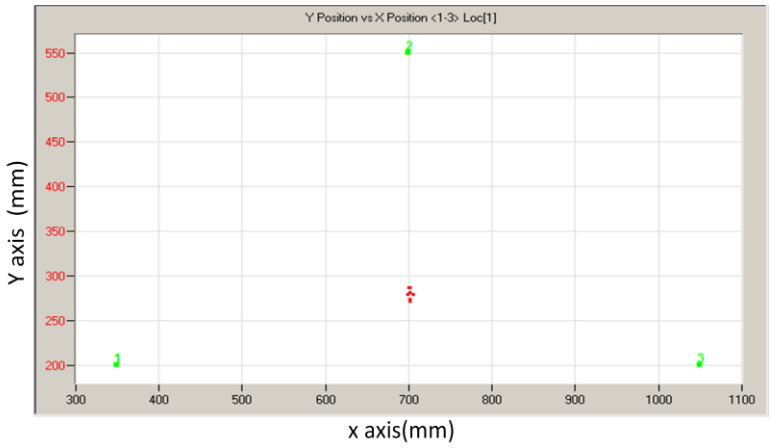

Fig. 3.13 Typical planar location using an array of three sensors

Circle intersection plot represents the location of AE source detected by several sensors under certain array calculated by WT modal location technique (Fig. 3.14).

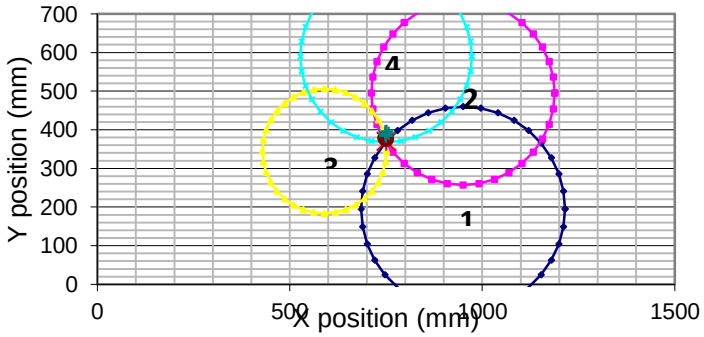

Fig. 3.14 Typical circle intersection plot

Correlation plots are used to compare the relationship between different AE feature data collected during test. The features of AE data such as duration, rise time and absolute energy are compared against amplitude or location. Colour scatter plots are used to identify the particularly active areas (Fig. 3.15).

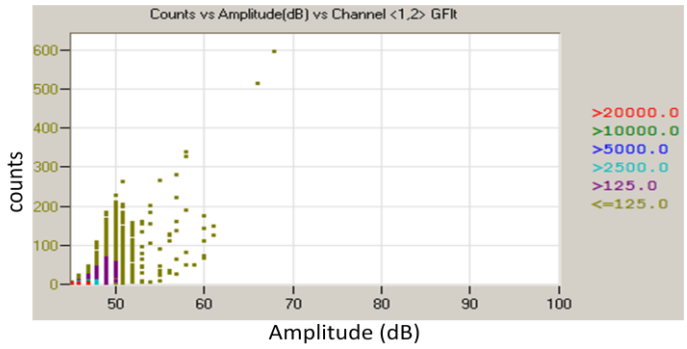

Fig. 3.15 Typical correlation plot

AE waveform plot is a time domain representation of AE signal similar to a trace captured on an oscilloscope. The vertical deflection represents the amplitude of the signal in volts, and the elapsed time from the trigger point is present in the horizontal scale. An example of an AE waveform display in time domain is shown in Fig. 3.16.

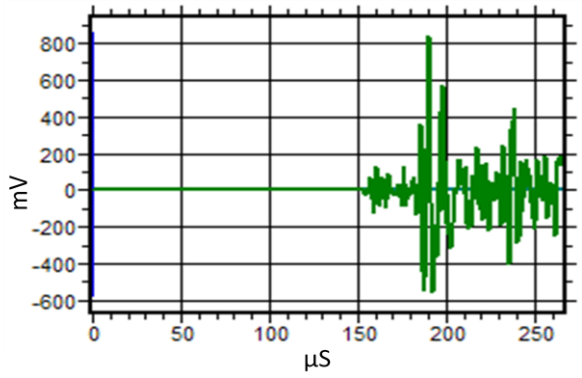

Fig. 3.16 Typical AE waveform plot display

The MISTRAS (PAC) system measures the signal amplitude relative to a 1 µV signal at the transducer; the amplitude in dB is then given according to Equation 3.1.

$$A = 20 \log_{10} (V_s/V_{ref}) \qquad (3.1)$$

3.2.2 WT analysis

The AGU-Vallen wavelet software package was used for wavelet transform modal location (WTML) analysis. AGU-Vallen wavelet software from Vallen System GmbH (2009) is a tool to calculate the WT on individual waveform data sets out transient (*.tra) data file. The package consist of three programs; wavelet, wave importer and Vallen dispersion.

Vallen dispersion is a program used to calculate the ***dispersion curves*** of the AE Lamb wave in plate-like structures. This program calculates the wave velocity of every possible mode of plate wave propagating within certain plate thicknesses against their frequency content based on Lamb wave theory. Fig. 3.17 shows a typical dispersion curve calculated by this software.

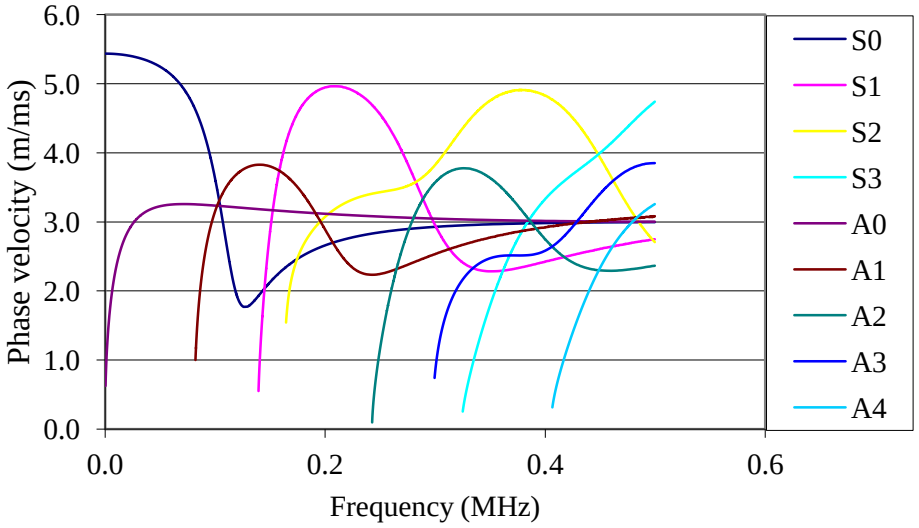

Fig. 3.17 Typical dispersion curve for 20 mm thick steel

These curves are used for determination of the velocity of Lamb wave components for calculation and validation of location calculated by wavelet transform modal location method (detail explanation is in chapter 4).

Wave importer is a program used to convert the ASCII data recorded by PAC acoustic emission system to Vallen transient (*.tra) data format. The wavelet program is used to transform this time domain waveform signal into a time-frequency diagram of the wavelet using continuous wavelet transform (CWT).

A ***Wavelet diagram*** is a time-frequency domain representation of the transformed AE signals. This plot enables time and frequency, and the amplitude of the AE waveform to be viewed simultaneously. In two dimensions wavelet display, the vertical axis represents the frequency range of the signal in kHz, the horizontal axis represents the time domain of the signal while the wavelet coefficient of the signal is presented by a colour contour. Fig. 3.18 shows a typical WT display.

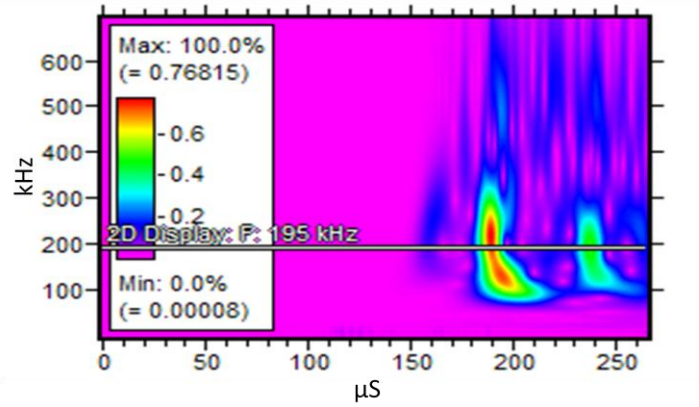

Fig. 3.18 Typical display of a wavelet diagram calculated by wavelet software

The strength of the signal at any particular frequency is represented by a ***wavelet coefficient plot*** as shown in Fig. 3.19. The vertical axis represents the wavelet coefficient value and the horizontal axis represents the time domain of the analysed wavelet.

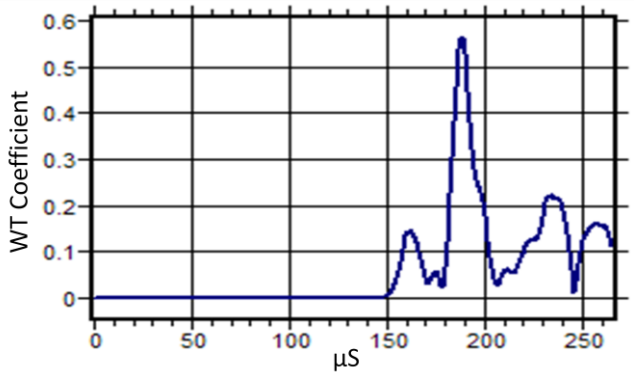

Fig. 3.19 Typical wavelet coefficient plot again time domain at 195 kHz

Fig. 3.20 shows a waveform display overlaid by a dispersion curve used for WT source location validation process.

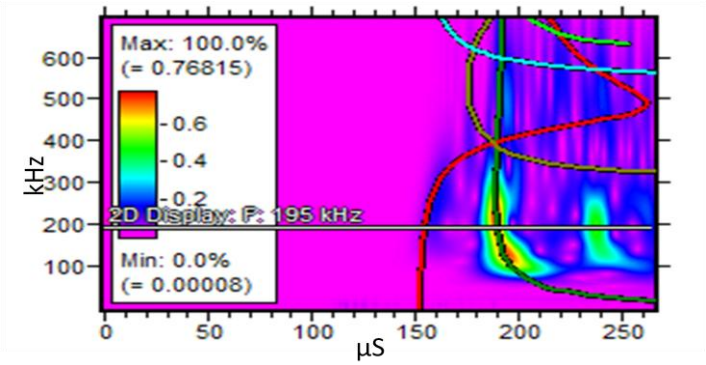

Fig. 3.20 Modified dispersion curve overlaid onto wavelet for WT source location validation.

PACshare wavelet software is used to perform waveform denoising using discrete wavelet transform (DWT) analysis. Many of the wavelet coefficients that are generated by the DWT are at a coefficient value near zero. Most of these near zero values are a result of noise. Fig 3.21 represents a typical example of a noisy waveform before denoising.

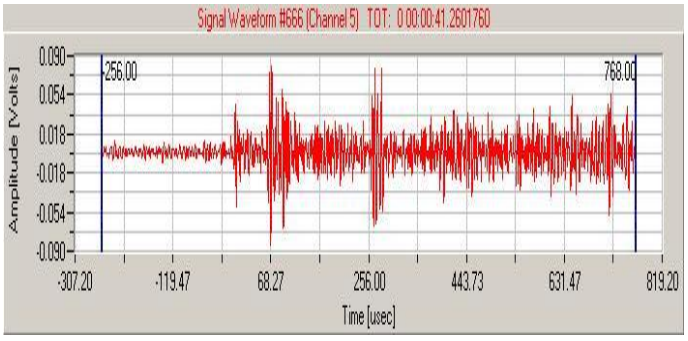

Fig. 3.21 Typical display of noisy waveform signal before WT denoising

By applying a wavelet coefficient thresholding using PAC wavelet software, this noise can be successfully eliminated. Fig. 3.22 represent a ‘clean’ waveform which was reconstructed after removing the near zero coefficients using WT denoising

approach. Note that the major signal components remain completely unaffected but that the arrival times are much clearer.

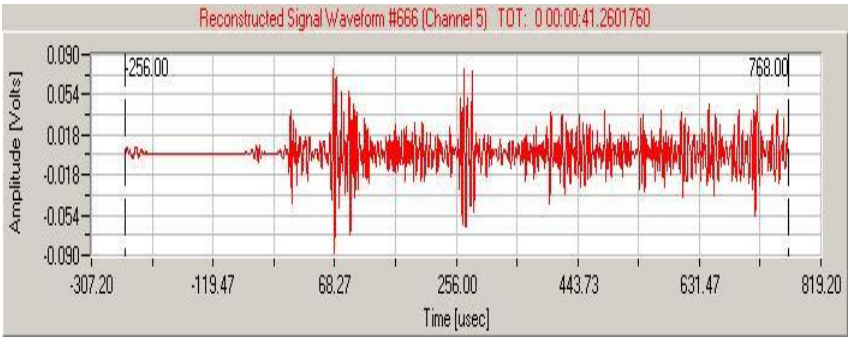

Fig. 3.22 Display of a reconstructed waveform signal after wavelet denoising

3.3 Fatigue loading and crack monitoring

3.3.1 Loading machine

A cyclic load was applied to all specimens using a Dartec 500 kN dynamic testing machine. The testing machine includes a test frame, a hydraulic actuator and a 40 lit/min pump, a load cell and a Dartec 9500 control unit.

3.3.2 Linear variable differential transducer (LVDT)

The LVDT is a common type of electromechanical device that produces an electrical output proportional to mechanical displacement of a separate moveable core. It consists of a primary coil and two secondary coils symmetrically positioned on cylindrical former. The free moving electromagnetic core positioned in the coil assembly provides a path for the magnetic flux linking the coil. A schematic representative of the LVDT construction is given in Fig. 3.23.

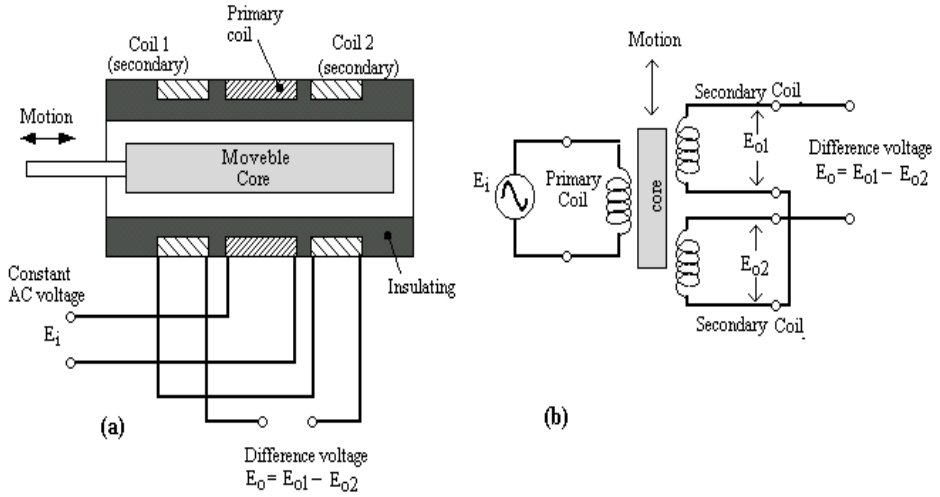

Fig. 3.23 A schematic representative LVDT construction (de Souza, 2008)

An LVDT can convert the rectilinear motion of an object to which it is coupled mechanically into a corresponding electrical signal. An LVDT was attached to the test system, to monitor the linear displacement applied to the specimen throughout the test.

3.3.3 Crack gauge

Krak gage® is a registered trade mark of the crack gauge system used for measuring the crack length in fatigue tests throughout this work. The gauge is a bondable, thin, electrically insulated metal foil from a constantan alloy. The gauge backing is a flexible epoxy-phenolic matrix providing the desired insulation and bonding surface area (Liaw et al, 1985).

This gauge works on the "Indirect potential method" principle as shown in Fig. 3.24. A potential drop is caused by the cracking of the test specimen, when a constant direct current with sufficient value passes through the foil material. With the use of suitable foil material, foil backing and adhesive material (insulator), a crack will simultaneously propagate in the thin foil as it does in the test specimens.

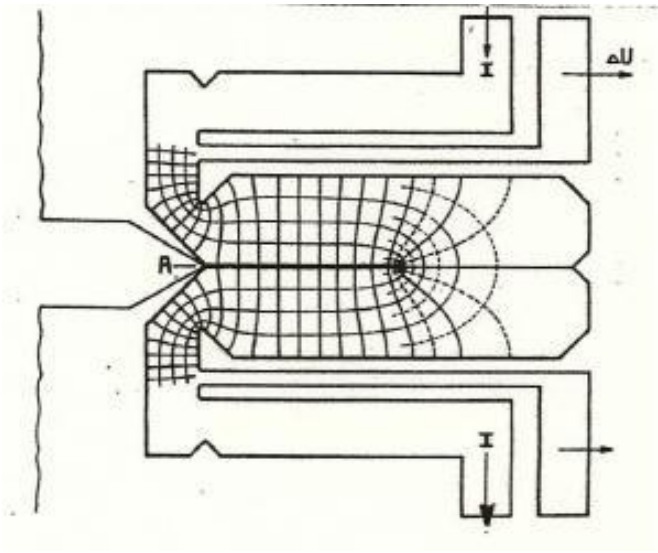

Fig. 3.24 Crack gauge "indirect potential method" to measure crack length (Hatrun, 2009).

The gauge provides a directly proportional and linear relationship between the output voltage and the crack length. Fig. 3.25 below shows a typical calibration curve of a 20 mm crack gauge, showing the linear relationship between the crack length and the output voltage. However, the actual calibration curve depends on the value of the excited current and signal readout circuit.

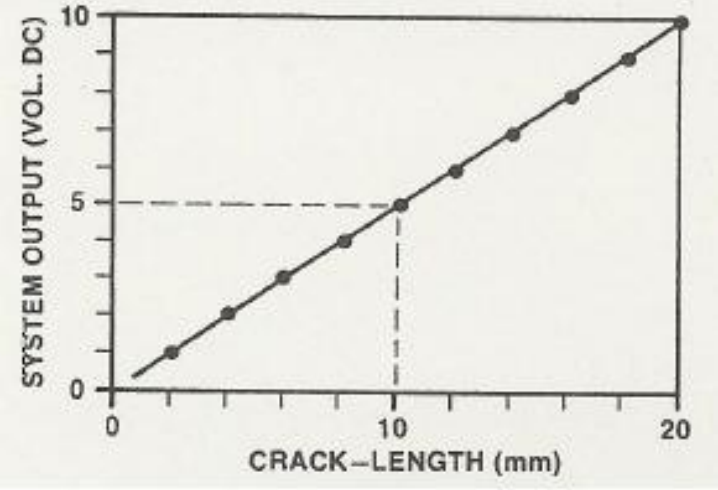

Fig. 3.25 Calibration Curve of a 20 mm Krak-gage® (Hatrun 2009).

According to Baxter (2007), crack length can be measured from the output voltage of the gauge by using the following relationship; $L_k = a_k V_k + b_k$, where L_k is the

crack length, V_k is the measured voltage across the gauge while a_k and b_k are the gain and offset required to convert the measured voltage into a crack length.

The main advantages of using Krak-gage® as crack length measurement tool are as follows:

- It is independent of specimen size, conductivity and material composition because the potential different is measured across the gauge itself instead of the specimen
- It is small in size and of low mass for easier attachment to the test item and adaptable to large specimens or large structural testing
- It is easy to interface to conventional instrumentation such as data logger, control circuit (current supply and voltage readout) and data storage.
- It produces high potential and infinite resolution of continuous DC output (volts) with a very low input current (mA)
- It produces high linearity between potential output and the crack length.
- It has an uniform calibration constant for all gauges size and independent of specimen geometry
- It permits automation of testing

3.4 Experimental techniques

3.4.1 AE sensors mounting and sensitivity verification

The correct mounting of sensors to the test object is one of the most important parts of AE testing. An essential requirement for sensor mounting is a sufficient acoustic coupling between the sensor face and the structure surface. The sensor and specimen surface must be clean and smooth for maximum couplant adhesion. Only a thin layer of suitable couplant should be applied so it can fill gaps caused by surface roughness and eliminates air gaps to ensure good acoustic transmission.

The following describes the methods used to mount and calibrate transducers during all AE investigation.

a) The specimen surface for sensor mounting is cleaned to remove all irregularities to ensure maximum area contact between sensor and surface. This is for optimising the AE transfer coupling. This usually takes the form of light sanding for normal surfaces. For paint coated specimen, filing is used to remove the paint from the surface.

b) A couplant is applied to ensure the optimum transmission of AE signal between specimen and sensor. Brown grease is predominantly used in this investigation especially for the test carried out on the non flat surface such as on pipe specimen whereas silicone rubber compound is also used for flat surface specimens.

c) The sensor is placed on the structure surface and rotated slightly to ensure an adequate layer of couplant covers the surface of the sensor. The sensor is secured by a magnetic clamp for the whole test duration, which ensures that a constant pressure is applied between the sensor and the test specimen.

d) A cable is attached to the sensor and to the corresponding channel at the rear of the AE data acquisition system. The cable is secured to ensure that no strain occurs in the cable during monitoring.

e) The sensitivity of the mounted sensor is verified using an artificial source (H-N source). Pencil lead fracture is performed adjacent to the sensor and the AE signal is recorded. A well mounted sensor should record a signal with amplitude of 98-100 dB. If a sensors response is below 98dB, the sensor has to be remounted and rechecked again. If the response is still low, the cabling is checked by performing a pencil lead break on the face of the sensor. The cable should be replaced if the signal response is less than 100dB. If the signal response still does not meet those criteria after cable replacement, then the sensor should be replaced.

3.4.2 Wave velocity determination

For time of arrival (TOA) and single sensor modal analysis location (SSMAL) source location techniques, the wave velocity in the structure must be known. For the carbon steel and mild steel, the velocity of longitudinal wave propagate in these structure is 5900 m/s (Krautkramer, 1975). This velocity is used to calculate the velocity of various Lamb wave components that propagate in both mild steel and carbon steel.

An AE signal in a plate is composed of two principal modes; S_0 and A_0 as discussed in chapter 2. The theoretical velocity of these modes is calculated using dispersion curve software from Vallen. For modal source location determination, the principal mode velocity at their non-dispersive range has been used and determined from the theoretical dispersion curve.

3.4.3 Crack length measurement

Automated crack length measurements provide the possibility to link AE data to the crack length. Crack gauge was used for crack length measurement throughout this study. It was bonded to specimen using solid epoxy adhesive. A constant electrical current (25 mA) is passed through the foil to excite the low resistance Krak-gage® at outer gage terminal as shown in Fig. 3.26.

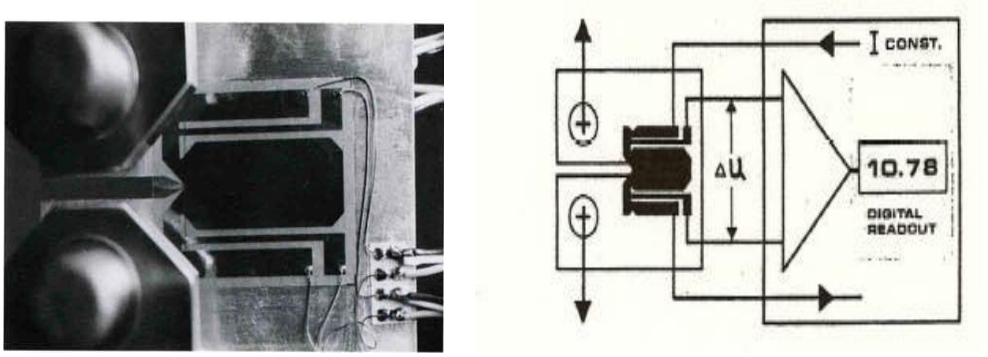

Fig. 3.26 Typical crack gauge attached to notched specimen (Hatrun, 2009)

A propagating crack produces a large change in resistance of the gauge and results in high d-c output, typically in mV range, which is proportional to the crack length. The output voltage of the gage is further amplified and the resulting voltage is then

measured using a circuit, the output of which is fed to the data logger to enable digital data to be stored into computer.

3.4.4 Dye penetrant inspection

Dye penetrant is a non-destructive method used to aid visual inspection by enabling cracks that have broken to the surface to be readily seen. Dye penetrant testing works on capillary action where dye liquid with low surface tension penetrates inside the crack. Red dye penetrant is used in this work to ensure the indications produce a good contrast with a white developer.

Dye penetrant testing is carried out in accordance with ASTM E 165-95 (2001) which involve six major steps; pre-cleaning, penetrant application, removal excess penetrant, application of developer, inspection and post cleaning.

i. Pre cleaning

The surface of the specimen is first cleaned by wiping with tissues damped with solvent material. This step is carried out to remove any dirt or any loose scale that may prevent the penetrant from penetrating the crack or may cause false indication.

ii. Application of penetrant

Once the surface is cleaned, the red dye is then applied to the clean surface of the specimen under test. The red dye is left to remain on the specimen surface for about an hour. This time is called “dwell time” which provides enough duration for the penetrant material to soak deep into the fatigue crack and at the same time allows the excess penetrant to drain out from the surface of the part under test.

iii. Removal of excess penetrant

Excess penetrant is removed from the surface after an hour of penetrant application by wiping with clean cloth damped with solvent material. This will remove any trace of excess penetrant material on the specimen surface to avoid false indication while at the same time leaving penetrant inside the crack.

iv. Application of developer

A white developer is applied onto the specimen surface, this draws penetrant from cracks out onto the surface to form the visible indication. This action is known as "bleed out". Any areas that bleed-out reveal the location and orientation of crack on the surface.

v. Inspection

Inspection of the test surface is carried out one hour after developer application. This duration is known as developing time, the time required to allow penetrant inside the crack to blot out onto surface of specimen to form a visible indication. The length can be measured and the image (picture) captured.

vi. Post cleaning

The test surface is cleaned after the test and recording of defects using the solvent remover.

The dye penetrant test is used throughout this work to locate the fatigue crack growth because of the following;

- it is a low cost inspection method
- test is easy to carry out and does not involve complicated instrumentation
- the inspection can be carry out in shorter time and
- Results are visible.

3.4.5 DeltaT source location

DeltaT source location is an AE location method based on the different time arrival at a pair of sensors. It requires a time contour map of the specimen to be constructed and this provides expected time arrivals regardless of specimen thickness and geometry. The source location is accomplished by comparing the actual AE data from the test with the time contour map.

Delta T analysis involves five important step as follows;

i. Determine the area of interest
ii. Construct a calibration grid
iii. Obtain training data

iv. Calculate DeltaT map

v. Compare actual data with contour map

Before DeltaT analysis is carried out, the area of interest on in the structure under test should be first identified. A grid is then constructed around this area. The grid area should be sufficient to cover the final location of the defect/damage and the direction of fatigue crack growth. Training data for DeltaT map was obtained by conducting an H-N source at each node (5 sources per node) of the grid.

A time contour map (which is independent of velocity) is constructed over the area of interest by analysis of the arrival time delay at pairs of sensors from particular source locations. Noesis software from PAC and DeltaT software developed by Baxter et al (2007) has been used for this analysis. The contour map is saved as data file and gives information of the time delay between pairs sensor at each nodes. Any crack signal will be processed with DeltaT software (by calculating the time different at each sensors pairs for any detected events) and then is compared with contour map.

3.4.6 Triple point filtering analysis

Triple point waveform filtering based source location is achieved by performing narrow band filtering at the frequency at which S_0, A_0 and A_1 modes propagate at same velocity. This analysis is carried out to improve the accuracy of TOA source location by eliminating the timing triggering error.

3.5 Summary

This chapter described the equipment used for AE data acquisition, data replay and data analysis. Two Acoustic Emission systems, DiSP and MISTRAS, manufactured by Physical Acoustic Emission were used in laboratory testing. Wide band WD sensors with working frequency range of 100-1000 kHz were used to detect the Lamb waves.

AEwin for Mistras E 1.30 was used for replay and displayed the stored data throughout this study. This software was also used for data feature extraction for

characterisation of damage mechanism, data filtering, TOA source location and triple point waveform filtering source location.

The software utilised for WT analysis was also described. The AGU-Vallen wavelet software package was used for continuous WT analysis. PACshare wavelet software from Physical Acoustic Corporation is used to perform waveform denoising using discrete wavelet transform (DWT) analysis.

Other equipment for monitoring the crack growth in steel plate was also well explained. Crack gauge and liquid penetrant testing has been used to monitor the crack length during the fatigue test.

CHAPTER 4: DEVEPLOPMENT AND VERIFICATION OF NOVEL WAVELET TRANSFORM ANALYSIS AND MODAL LOCATION (WTML) METHODOLOGY FOR ACCURATE SOURCE LOCATION AND CRACK SIZING

4.1 Introduction

The AE technique has been used to monitor the integrity of the seam weld of reheat steam piping in nuclear piping system (IAEA, 2003) and fossil fuel power plant (Rodgers et al, 1996). Fatigue cracks have been successfully located at the critical area on fossil power plant piping systems; however other non-destructive testing (NDT) has been used to evaluate the defect size.

This chapter aims to develop a new AE source location methodology using wavelet transform analysis (WT), to compare the accuracy of the new proposed method with time of arrival (TOA) and DeltaT methods, and to seek the possibility of developing an AE crack length measurement procedure based on WT analysis and modal location theory.

4.2 AE source location technique ; principles and limitations

Source location is an important feature of AE structural integrity monitoring and accurate source location requires the application of a series of very important processes, including; accurate detection and processing of AE signals, event detection and grouping of AE signals to form an accurate event record, extraction of critical timing features and assignment of their correct propagation velocity, and application of the appropriate location algorithm.

4.2.1 Time of arrival (TOA)

Time of arrival (TOA) source location is the most widely used location method and this is the basis used in most of the commercial AE software. However, other

methods such as single sensor modal analysis method (SSMAL) (Pullin 2005), DeltaT method (Baxter 2007) and Waveform filtering methods (Miller and McIntire 2005) can also be used. A detailed explanation of source location is presented in chapter 2.

TOA method is based on time arrival of an AE event at sensors within an array. In this method, the velocity of wave propagation in the medium is assumed to be constant and in a direct path. However, due to the noise from the environment, most of the available commercial AE system use first threshold crossing for measuring this flight time of the AE signal instead of first hit arrival. Triggering error and time delay between the first hit arrivals and first threshold crossing will produce an error in the TOA measurement which may lead to source location inaccuracy. Other causes of source location inaccuracy include inaccurate sensor location, incorrect group wave velocity and human error.

4.2.2 DeltaT

The DeltaT method still uses the time of arrival of the signal at the sensor. However, in the DeltaT method, source location is derived from a user-defined arrival contour map rather than using a constant wave velocity. The method is described in detail in chapter 2.

This method was shown to be more accurate than the TOA technique because velocity and geometry errors are minimised and the effects of boundary reflections and mode conversion are accounted for. This method is suitable for structural health monitoring of structures with non uniform geometry such as in aircraft landing gear (Baxter, 2007).

This method does have its drawbacks however; the map must be constructed before the actual test for a specific location. The AE signal detected by the system is compared with the constructed map and therefore the AE data from outside the map area cannot be analysed. On top of that, the analysis is only valid if the location of the sensor arrays does not change. Furthermore, since the arrival time for this location method is also determined by first threshold crossing, time of arrival error

due to delay between first hit arrival and first threshold crossing may also lead to source location inaccuracy.

4.2.3 Single Sensor Modal Analysis Location (SSMAL)

Conventional AE location techniques have mainly utilised the time arrival at first threshold crossing. An alternative to this conventional technique exploits the dispersive nature of Lamb waves and is known as modal acoustic emission (MAE) and the method is described in detail in Chapter 2.

SSMAL is expected to produce better location results compared with TOA method since the timing error due the arrival delay between first hit arrival and first threshold crossing is minimised. However, due to dispersion characteristic of Lamb wave, superposition of A_0 mode arrival with other higher order Asymmetry components will lead to source location inaccuracy due to temporal separation measurement error.

Temporal separation measurement error in SSMAL can be improved by deploying time-frequency analysis which can discriminate the content of AE signal instead of depending on time domain waveform analysis. To the author's knowledge, this has not been achieved to date by any other researcher.

4.3 SSMAL with Modified Dispersion Curve

4.3.1 Introduction

According to Lamb wave theory, when acoustic waves propagate within plate-like structures, their movements are limited by the boundary of the plate. The propagation of Lamb waves in plate-like structures is characterised by the wave modes velocity dispersion with frequency content and can be illustrated using dispersion curves. There are several symmetric and asymmetric AE modes that will propagate with difference velocities. The temporal separation between the fundamental symmetric (S_0) and asymmetric (A_0) mode has been used in SSMAL for more accurate source location (Pullin 2005). In order to obtained the correct

temporal separation between S_0 and A_0 mode for accurate SSMAL, the arrival of A_0 mode should be discriminated from other wave mode that propagate at the velocity that is close to A_0 mode velocity. Modified dispersion curves can be used to determine the time arrival of these two modes.

The modified dispersion curve used in this study is a plot of the frequency of a series of Lamb wave modes against their arrival time for known source-to-sensor distances for a specific plate thickness. Instead of plotting velocity against frequency (as in the normal dispersion curve), modified dispersion curves display the frequency content of the signal in vertical axis against arrival time in the horizontal axis. This modified dispersion curve is then overlaid onto the waveform signal for evaluating the temporal separation between S_0 and A_0 modes.

Since both modified dispersion graph and waveform signal have the same horizontal time axis, the arrival time of the fundamental symmetry and asymmetry modes in the waveform can be determined by evaluating the arrival time of the corresponding wave mode in this new (modified) dispersion curve.

4.3.2 Objective of the study

This study has been completed to

i. Investigate the effect of plate thickness on dispersion curves.
ii. Investigate the use of modified dispersion curves to discriminate the arrival of different asymmetric mode for more accurate SSMAL.

4.3.3 Experimental procedure

A 20 mm thick ASTM 516 gr 70 steel plate measuring 80 mm x 2m and a 4 mm thick mild steel plate measuring 500 mm x 1500 mm are used in this study. The re use of plates with different thickness is to study the effect of thickness on the Lamb wave velocity dispersion. The theoretical dispersion curve for both plates was calculated using Vallen Dispersion software.

For modified dispersion curves analysis, H-N sources at four known source to sensor locations on the 20 mm thick ASTM were used in this work. Dispersion

curves were modified for four different source locations, by changing the value of the velocity horizontal axis to the time of wave mode arrival so that the new dispersion curve will show how the velocities of the wave modes disperse with time of propagation.

These new dispersion curves were then superimposed onto the waveform signal to show the arrival time of significant wave modes (S_0, A_0, A_1 or A_2). The arrival time of the symmetric and asymmetric modes of these new dispersion curves was shifted so that the arrival time of the fastest S_0 mode is coincides with the arrival time of S_0 mode in the wave form signal.

For the 20 mm thick steel plate, four WD sensors were mounted to the specimens as shown in Fig. 4.1 and held in position using a magnetic clamp. Brown grease was used as an acoustic couplant.

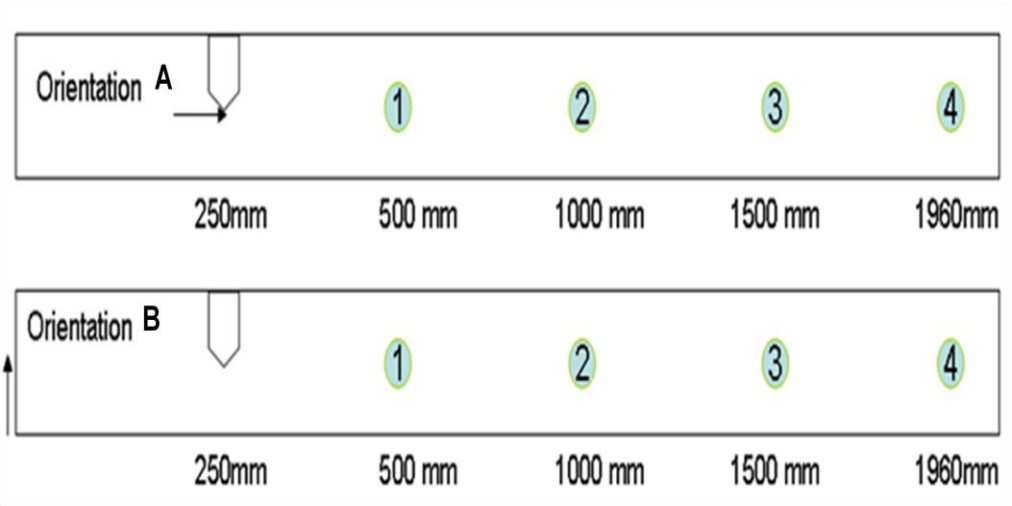

Fig. 4.1 Pencil leads breakage orientation

The sensitivity of the mounted sensor was evaluated using H-N source technique (Hsu, 1979). H-N source were completed in orientation A which is in-plane with sensor mounting and B which is normal to the sensor mounting plane. Ten H-N sources was conducted in each orientation and were recorded using AEwin software.

4.3.4 Dispersion curve analysis

Fig. 4.2 below shows the theoretical dispersion curve for a 20 mm steel plate. The curve displays how the wave velocities disperse with frequency content of wave mode.

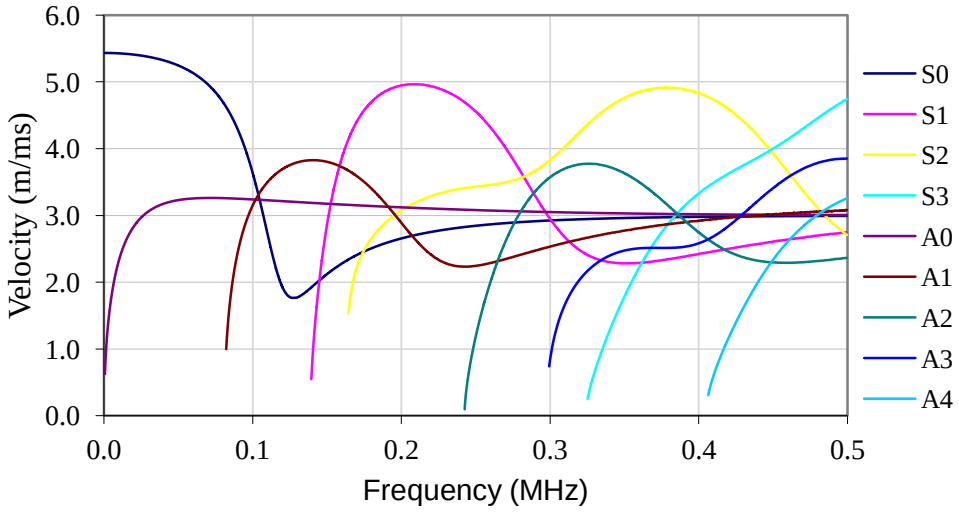

Fig. 4.2 Theoretical Dispersion Curve for 20 mm steel

At 100 kHz, three wave modes (S_0, A_0 and A_1) propagate at the same velocity and this is known as triple point. If several modes propagate in this steel plate and their frequency content is close to this value, it is very difficult to separate the S_0, A_0 and A_1 modes. This velocity can be used for more accurate TOA location result because the detection triggering error is minimised.

When the frequency content of the acoustic wave is larger than 100 kHz, modes other than the fundamental Lamb wave modes (S_0 and A_0) will be present and these complicate SSMAL. This is because two wave modes may propagate at the same velocity for certain frequency, for example, S_0 and A_1 mode propagate at velocity of 2549 m/s when their frequency content is 199 kHz. At this frequency, these two modes will overlap each other, resulting in zero temporal separation. This phenomenon then will lead to the failure of the application of SSMAL. Fig. 4.3 shows the theoretical dispersion curve for 4 steel mm plate.

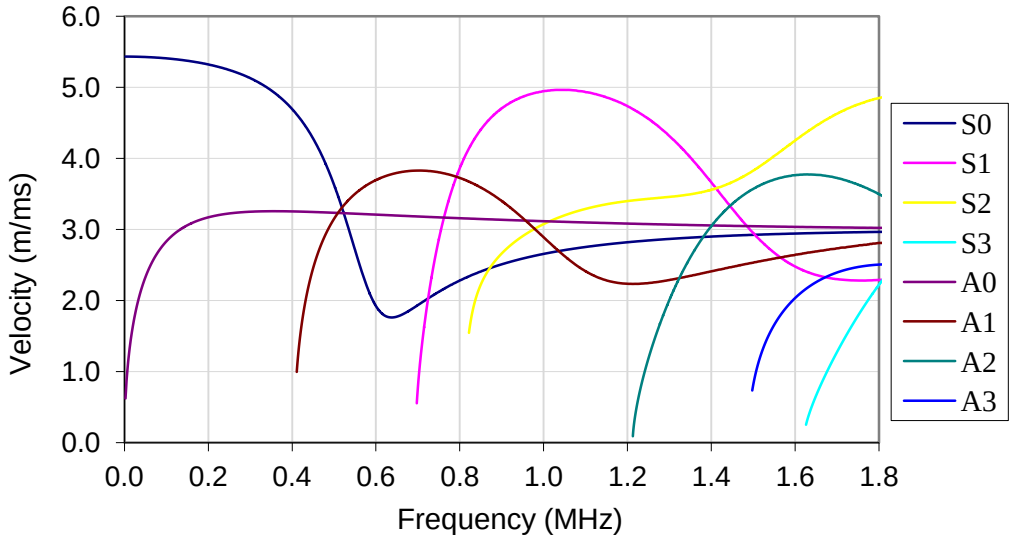

Fig. 4.3 Theoretical dispersion curve for 4mm steel plate

For 4 mm steel, the triple point occurs at 525 kHz where the S_0, A_0 and A_1 modes travel at 3353 m/s. For frequencies less than 500 kHz, the A_0 mode and S_0 mode can be clearly separated. In any material, the triple point for thicker plate will occur at relatively lower frequency than the thinner one. If the frequency content of the interested AE mode of interest for thicker plate is close to this triple point then the application of SSMAL may produce a large measurement error.

4.3.5 Preliminary SSMAL

Tables 4.1 to 4.3 show the results for source location measurement using waveform data from H-N source in 20 mm steel plate specimen. The measurement is based on the assumption that the first arrival low amplitude signal is the S_0 mode followed by subsequent high amplitude A_0 mode as suggested by Pullin et al (2005). The temporal separation of these two modes was obtained from the waveform signal and the source to sensor distance, R, is calculated using SSMAL as given by Equation 4.1.

$$R = \Delta T \, (C_{S0}C_{A0}/C_{S0}-C_{A0}) \qquad \text{(eq. 4.1)}$$

where C_{S0} is velocity of S_0 mode, C_{A0} is velocity of A_0 mode and ΔT is temporal separation. The S_0 and A_0 velocities used in this calculation were determined from

the theoretical dispersion curve and their values are 5273 m/s and 3109 m/s respectively.

Table 4.1 Source to sensors distance for H-N source in orientation A (in-plane source)

	sensor1		sensor2		sensor3		sensor4	
	ΔT1(μs)	R1(mm)	ΔT2(μs)	R2(mm)	ΔT2(μs)	R3(mm)	ΔT4(μs)	R4(mm)
1	26	189.51	62	451.91	108	787.20	162	1180.81
2	23	167.64	62	451.91	108	787.20	162	1180.81
3	25	182.22	62	451.91	108	787.20	161	1173.52
4	26	189.51	62	451.91	108	787.20	162	1180.81
5	26	189.51	62	451.91	108	787.20	162	1180.81
6	29	211.38	62	451.91	108	787.20	163	1188.10
7	29	211.38	62	451.91	108	787.20	162	1180.81
8	29	211.38	62	451.91	108	787.20	162	1180.81
9	29	211.38	62	451.91	108	787.20	163	1188.10
Average	27	195.99	62	451.91	108	787.20	162	1181.62

Table 4.2 Source to sensors distance for H-N source in orientation B (out of plane source)

	sensor1		sensor2		sensor3		sensor4	
	ΔT1(μs)	R1(mm)	ΔT2(μs)	R2(mm)	ΔT2(μs)	R3(mm)	ΔT4(μs)	R4(mm)
1	90	656.00	159	1158.94	217	1581.70	303	2208.54
2	90	656.00	170	1239.12	230	1676.45	306	2230.41
3	91	663.29	176	1282.85	240	1749.34	307	2237.70
4	91	663.29	159	1158.94	218	1588.99	322	2347.03
6	91	663.29	176	1282.85	189	1377.61	307	2237.70
7	91	663.29	179	1304.72	190	1384.90	306	2230.41
8	92	670.58	170	1239.12	224	1632.72	307	2237.70
9	90	656.00	170	1239.12	242	1763.92	308	2244.99
10	101	736.18	171	1246.41	243	1771.21	307	2237.70
Average	92	669.12	168	1224.54	218	1589.71	308	2245.72

It is found that the SSMAL using fundamental symmetric and asymmetric wave mode is inaccurate for in plane source as shown in Table 4.1. The source location errors for H-N source in plane to sensor mounting are about 20% to 52 % of the measured distance as shown in Table 4.3.

Table 4.3 Source location measurement errors for two different orientations.

	R1(mm)			R2(mm)			R3(mm)			R4(mm)		
	Actual	Measured	Err (%)	Actual	Measured	Err (%)	Act.ual	Measured	Err (%)	Act.ual	Measured	Err (%)
A	250.0	196.0	21.6	750.0	452.0	39.7	1250.0	787.2	37.0	1710.0	1181.6	30.1
B	500.0	669.1	33.8	1000.0	1224.5	22.5	1500.0	1589.7	5.9	1960	2245.7	14.6

Different percentage errors for the different source to sensor distance possibly arise due to the error in A_0 mode arrival time determination. If other modes propagate close to the velocity of A_0 mode, superposition may occur and this will lead to A_0 mode arrival time measurement inaccuracy. For sources of emission close to the sensor, the reflection of S_0 mode from the specimen boundary may also produce the same effect. Therefore, better discrimination between arrival of reflection of S_0 and A_0 mode is required to improve location inaccuracy.

4.3.6 Modified dispersion curve and analysis

For a known source to sensor distances, the velocity axis of the dispersion curve has been transformed to the time axis for further wave dispersion analysis. The theoretical arrival time of this modified dispersion curve is then compared with the arrival time of first arrival of the symmetric and asymmetric modes in the waveform signal for H-N sources in plane of the sensor mounting and normal to the sensor mounting, this can be seen in Fig. 4.4 for an H-N source at 250mm from sensor.

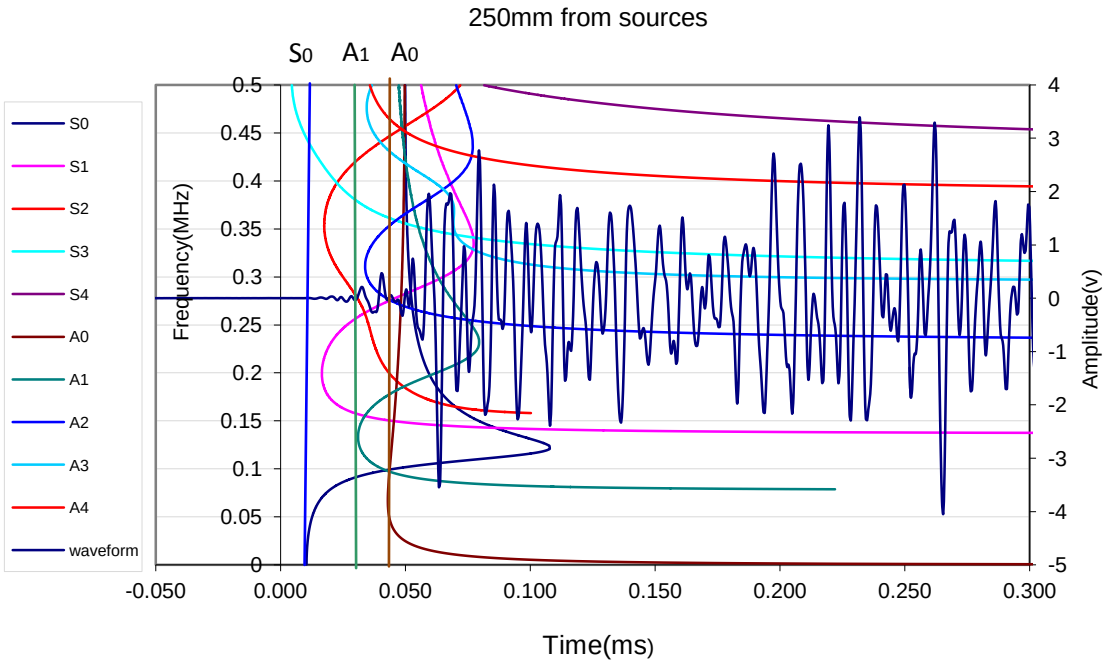

Fig. 4.4 Overlay of theoretical modified dispersion curve and waveform S_0 mode arrival time for 250mm source to sensor distance

The theoretical arrival time of S_0 mode, indicated by the S_0 line, from the dispersion curve has been shifted until it was overlaid with the arrival time of the fastest mode of the waveform signal which is presumed to be the S_0 mode. The A_1 line indicates the arrival time of the fastest A_1 mode signal and the A_2 line indicates the arrival time of the fastest A_2 mode signal.

It is also shown in this figure that for a source located 250 mm from the sensor, the arrival time of A_1 mode is quite close to the arrival time of A_2 mode. The arrival time of the first high amplitude signal is not clearly observed but it appears to coincide with the arrival time of the fastest theoretical A_1 mode. This suggests that, the arrival of A_0 mode is not easily determined by just viewing the waveform signal. Furthermore, the velocity of any propagation mode is frequency dependant and if high intensity of A_0 signal is released at a higher frequency, there is possibility that the A_0 mode is wrongly picked and will lead to temporal measurement error.

Fig. 4.5 below shows the overlaid modified dispersion curve on the waveform signal of the H-N source at 750mm from sensor.

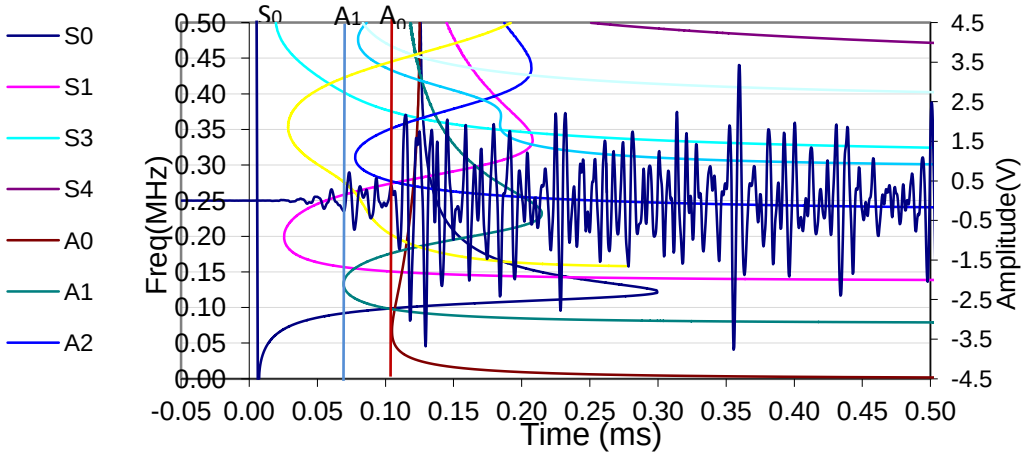

Fig. 4.5 Overlay of theoretical modified dispersion curve on the waveform signal for 750mm source to sensor distance

It is clearly shown that for a source located 750 mm from the sensor, the arrival time of A_1 mode is quite close to the arrival time of A_2 mode. The arrival time of the first high amplitude signal is not clearly observed but it is appears to coincide with the arrival time of the fastest theoretical A_0 mode.

Fig. 4.6 below shows the modified dispersion curve for the H-N source at 1250mm from sensor.

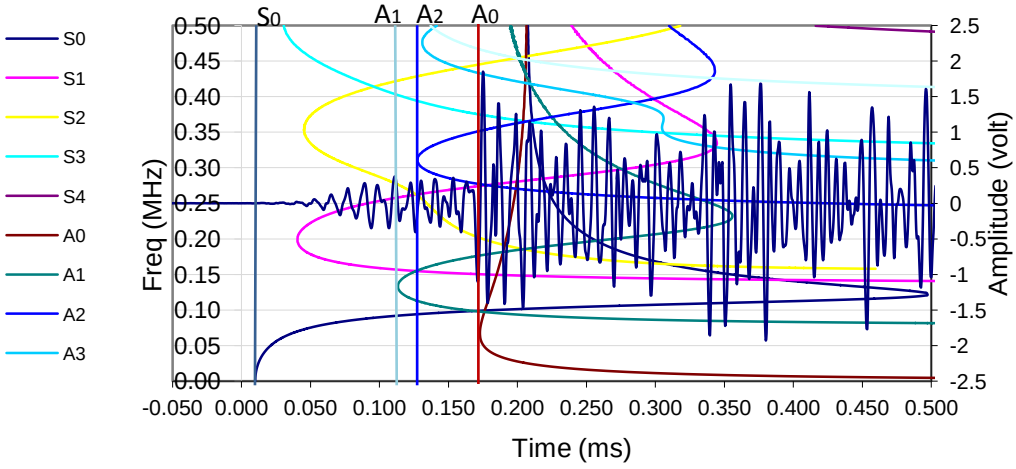

Fig. 4.6 Overlay of theoretical modified dispersion curve and waveform signal for 1250mm source to sensor distance

In Figs. 4.4, 4.5 and 4.6, the S_0 mode is clearly shown in the waveform, indicated by the arrival of the fastest low amplitude signal followed by a high amplitude

signal presumed to be from the asymmetric mode. However, the arrival of A_0 mode is not easily determined because it was superimposed with higher order asymmetric components. This means that, determination of A_0 arrival by just viewing the waveform signal is quite difficult, almost impossible. It also found that, at larger source-to-sensor distances, the separation between A_0 and other higher order asymmetric mode become clearer. The separation between those modes is important for accurate A_0 arrival determination (picking) for more accurate modal location measurement.

The modified dispersion curve is found very useful to determine the arrival of A_0 mode for accurate temporal separation measurement for modal location calculation, however this curve cannot be utilised if the distance between sources to sensors is unknown. Therefore, a new method is needed in order to accurately determine the temporal separation between S_0 and A_0 modes and the dispersion curve can be used to verify the accuracy of temporal separation measurement.

4.3.7 Summary of findings from modified dispersion curve work

Dispersion curve analysis for Lamb wave propagation in 20 mm plate and 4 mm plate demonstrate that the triple point of Lamb wave propagation in steel plate is thickness dependent. The thicker the specimen the lower the frequency at which the triple point occurs.

The triple point for 20 mm thick steel is around 100 kHz where S_0, A_0 and A_1 mode propagate at the velocity of 3163 m/s. At frequency of 40 kHz to 80 kHz the A_0 mode is almost non-dispersive.

For 4 mm steel, the triple point occurs at around 525 kHz where S_0, A_0 and A_1 mode travel at 3353 m/s. For plate-like structural steel with 4 mm thickness, A_0 and S_0 mode could be used for SSMAL since there is no other propagation mode having frequency content less than 400 kHz and the arrival time of both modes can be easily separated.

The success of SSMAL is dependent on the accuracy of temporal separation. For known source-to-sensor distances, the modified dispersion curve can be used to

determine the arrival of A_0 mode for accurate temporal separation measurement. However, this curve cannot be utilised if the distance between sources and sensors is unknown.

The larger the source-to-sensor distances the clearer the separation between A_0 and other higher order symmetric mode. The separation between those modes is important for accurate A_0 arrival determination (picking) for accurate modal location measurement.

A new method is needed to accurately determine the temporal separation between S_0 and A_0 modes and the dispersion curve can be used to verify the accuracy of temporal separation measurement. If a suitable method is developed for recognising and picking the first arrival of A_0 mode, modal location can be utilised for accurate thermal fatigue source location and crack size measurement in nuclear piping system.

The modal location method promises an accurate source location result if the temporal separation error due to the superposition of A_0 mode with other wave components can be resolved. Temporal separation measurement error in SSMAL can be improved by deploying time-frequency analysis which can discriminate the content of the AE signal instead of depending on time domain waveform analysis for temporal separation measurement.

4.4 Proposed wavelet transform analysis and modal location (WTML) methodology

4.4.1 Introduction

The wavelet is a very short, time base signal, usually an oscillating signal with one or several cycles. This wavelet is used as a basis for decomposition of the waveform into multiple component parts called coefficients, based on location and scale.

WT provides two dimensional coefficients, frequency and time. The strength of each coefficient provides insight into the percentage of correlation of that particular wavelet to the waveform. The coefficient value gives a third dimension of the data, an amplitude or strength associated with them. WT analysis can be divided into two categories, continuous wavelet transforms and discrete wavelet transforms.

With the wavelet approach, the frequency content and the time localisation of the waveform signal can be viewed simultaneously. WT analysis can also be used to discriminate various frequency ranges of AE signals and can be presented in the time domain signal.

4.4.2 WTML approach

Due to the ability to view the frequency content and the time localisation of the waveform signal simultaneously, it is proposed that WT can be deployed for more accurate source location and crack length measurement and improve SSMAL by providing more accurate temporal separation measurements. WT assisted by a modified dispersion curve could be used to distinguish the arrival A_0 from the arrival of other components and noise signals. The temporal separation between those two modes can be accurately measured using wavelet coefficient against time. This temporal separation measurement can then be utilised in the SSMAL calculation. WTML source location technique is expected to produce more accurate source-to-sensor location compared with other location method. The modified dispersion curve also can be used to validate the WTML location calculation.

This novel approach is called Wavelet Transform analysis and Modal Location (WTML) method, and it utilises the wavelet coefficient plot against time from WT analysis to accurately measure the temporal separation between A_0 and S_0 modes. In WTML method, temporal separation is measured from first minimum value of wavelet coefficient of those wavemode components rather than using peak value as used by other researchers (Jeong 2000, Takemoto 2000, Hamstad 2002, Jinpin 2004, Alex 2010).

It is expected that this temporal separation measurement approach will give more accurate result since the first minimum wavelet coefficient represents the actual first arrival wavemode component while the maximum coefficient represents the peak to peak temporal separation. This temporal separation measurement is then utilised in the SSMAL calculation and it is expected that WTML approach will produce more accurate source to sensor location results compared with other location methods. Furthermore, WTML method utilises the modified dispersion curve to validate the location calculation accuracy.

The WTML method developed and used in this study involves four main steps; Waveform acquisition and processing, Source to sensors distance calculation, Verification of source to sensor distance measurement and Location of events.

1. Waveform acquisition and processing

The AE waveform from AE source is acquired. This waveform is then transformed into wavelet. This transform will produce the wavelet of the waveform and the plot of wavelet coefficient strength against time.

2. Source to sensors distance calculation.

The SSMAL equation (Pullin 2005) is used to calculate the source to sensors distance. However, temporal separation is determined using WT analysis instead of using the time domain waveform signal. The following are the steps for source to sensors distance calculation.

a) Calculate theoretical dispersion curve (velocity against frequency) for material under investigation. The theoretical velocity of fundamental symmetric (cS_0) and asymmetric (cA_0) modes from this dispersion curve need to be determined.

b) Measure the temporal separation between S_0 and A_0 component from wavelet coefficient plot for every sensor.

c) Calculate source to sensor distance using the SSMAL equation.

3. Verification of source to sensor measurement

This verification is performed by calculating a new dispersion curve, frequency against time, for material under test using the calculated source to sensors distance from step 2 a) above. This modified dispersion curve is then overlaid onto the transformed wavelet from step 1. The position (time) of S_0 and A_0 modes is then evaluated against the wavelet, wavelet coefficient plot and waveform plot.

4. Location of Events.

The circle intersection technique has been used for determining the source location. For verified source to sensor location from previous step, a circle is plotted around every sensor and the verified source to sensor distance is the radius of the circles. The intersection of every circle has been used as the source location.

4.5 Wavelet Transform Analysis and Modal Location (WTML) of artificial sources in a steel plate

4.5.1 Experimental setup and validation procedure

MISTRAS WD sensors (working frequency range of 100-1000 kHz) were used throughout this work. The sensors were mounted on a steel plate and held in position with magnetic clamps. The plate was manufactured from mild steel with dimension of 5 mm thick, 790 mm long and 300mm width. Two sharp notches with length of 50 mm were introduced onto both edges of the specimen as shown in Fig. 4.7 to represent the edge of a crack. Four sensors were mounted onto the plate surface. A four channel MISTRAS AEwin DiSP data acquisition system was used for AE waveform acquisition. Detected events were pre-amplified by a 40 dB preamplifier. The acquired waveforms were stored on the computer for further analysis.

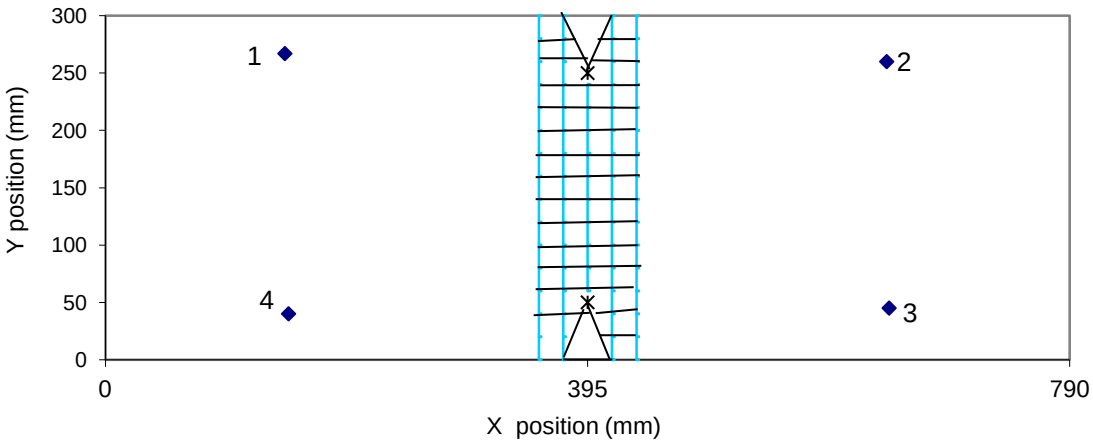

Fig. 4.7 Location of sensors and grid arrangement on the plate surface

For DeltaT location, an area of 80mm by 300mm was selected on the plate surface. A grid density of 20mm was constructed around the notches, creating 82 nodes. Five Hsu-Nielson (H-N) sources were conducted on each node. Fig. 4.7 shows the location of the sensors, notch location and the grid arrangement for the DeltaT location. H-N data on every node and notch was processed using the DeltaT software developed by Baxter (2007) for DeltaT mapping. To assess the performance of the described technique, H-N sources were conducted on each notch.

4.5.2 Results and discussion

Fig. 4.8 shows a typical result of wavelet transform of a detected waveform from H-N source at the notch tip processed by Vallen wave importer and wavelet transform software (Vallen 2009).

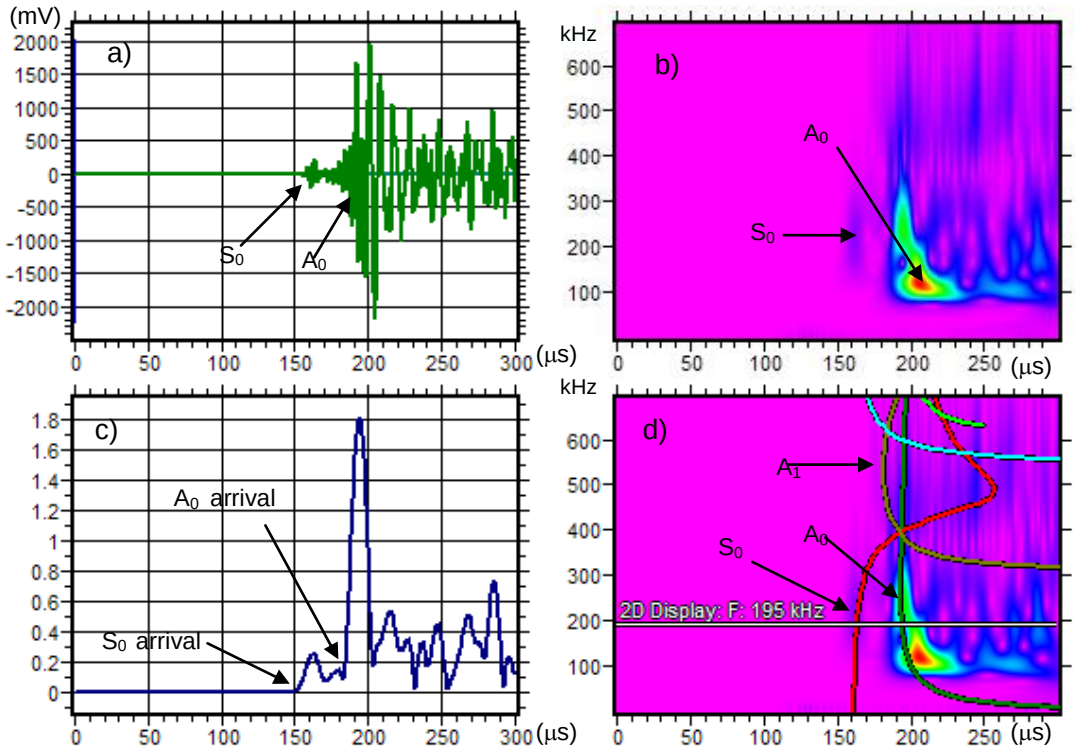

Fig. 4.8 Typical wavelet transforms analysis result

Fig. 4.8 a) shows a typical transient AE waveform signal produced by H-N source. It is clearly shown in this figure that the first detected signal is the low amplitude S_0 component followed by high amplitude A_0 component that propagates at a slower velocity than the S_0 component. The arrival of faster S_0 component can be easily determined from this waveform; however the arrival of A_0 component is overlapped with other low amplitude signal components which appear between the S_0 and A_0 modes.

Fig. 4.8 b) shows the wavelet of the waveform signal. The vertical axis shows the frequency content (in kHz) of the signal while the horizontal axis represent the time of the signal (in seconds). The colour contour represents the strength of the signal.

Fig. 4.8 c) shows a wavelet coefficient plot against time for the transformed wavelet from the above waveform. It is clearly shown in this figure that the A_1 component can be easily distinguished from A_0 by wavelet frequency-time analysis approach. Therefore, the accurate arrival of A_0 component can be accurately

determined and the temporal separation error due to superposition of A_0 mode with other waveform component (which is A_1 mode in this case) can be removed.

Fig. 4.8 d) shows how the modified dispersion curve, which is calculated based on the WTML, is overlaid on the wavelet signal. It is clearly shown that the modified dispersion curve of S_0 and A_0 modes based on this calculation is perfectly matched with wavelet transform analysis result. This result suggests that accurate location is obtained using WTML method by improving coefficient temporal separation measurement. Temporal measurement error in SSMAL is highly improved by WT location methodology.

Fig. 4.9 shows the typical location of AE event from H-N source analysed by the WTML method showing the calculated radius of source to sensor distance based on Eq. 1 as described in section 4.2.3

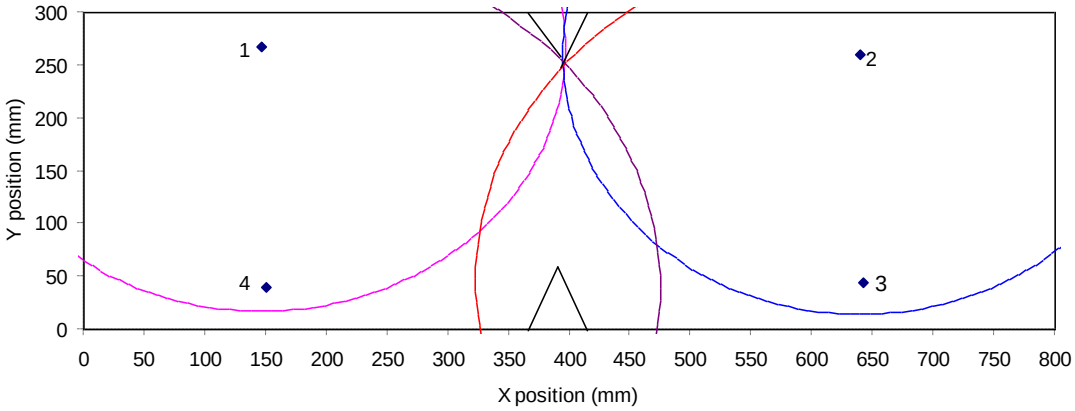

Fig. 4.9 Typical WTML location result shown by circle intersection at upper notch tip

Four circles represent the distance of H-N source from sensors 1, 2, 3 and 4 calculated by WTML methodology. The WTML source location result is achieved by using the intersection of these four circles. It is clearly shown that all circles intersect at almost a single point suggesting that the source to sensor distance using this new location method is very accurate.

Fig. 4.10 shows a comparison of the typical location of AE events from H-N sources analysed by TOA and triple point filtering under planar location setup, DeltaT and WTML methods.

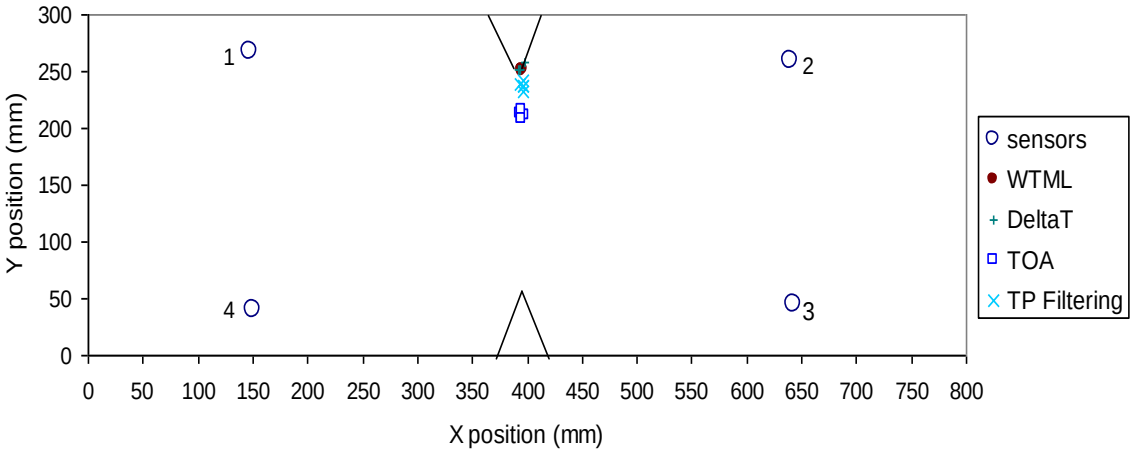

Fig 4.10 H-N source at notch tip located by TOA, TP Filtering, DeltaT and WTML methods

Fig. 4.11 presents a close up of the notch area and clearly shows that the TOA location result produces relatively the biggest location error compared with the other location methods.

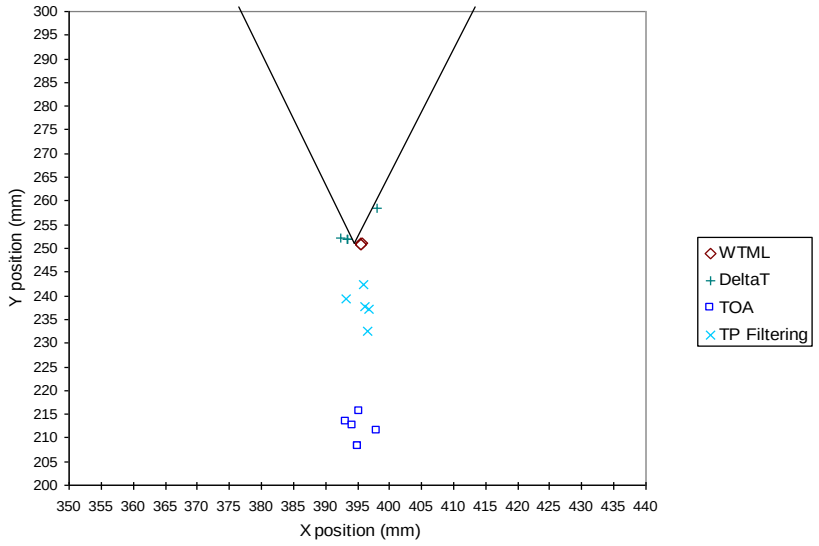

Fig. 4.11 Close-up of H-N source location result in Fig. 4.10

The possible sources of error in TOA source location are; premature triggering, inaccurate arrival time measurement or dispersion of flexural mode component as suggested by Holford (2000). The root mean square errors of location determined by different location methods and their standard deviation are shown in Table 4.4.

Table 4.4 RMS of location error calculated using TOA, TP filtering, DeltaT and WTML and their standard deviation

	Source location error (mm)								
Sensors	Actual distance (mm)	TOA		TP Filtering		DeltaT		WTML	
		RMS	STD	RMS	STD	RMS	STD	RMS	STD
1	248.58	5.25	1.23	2.34	1.59	2.17	2.10	0.56	0.04
2	245.20	5.06	0.95	1.16	1.29	2.20	2.29	0.66	0.05
3	320.99	22.79	2.08	8.56	2.81	2.84	0.46	0.12	0.05
4	322.68	24.00	1.85	7.44	2.10	3.52	3.58	1.07	0.08

It is clearly shown that the TP filtering yields more accurate source location compared with TOA source location method. The reason for the improved source location result achieved by triple point filtering method is because the three fastest components (S_0, A_0 and A_1) trigger the system detection threshold simultaneously. TP filtering will improve the location error by eliminating false threshold triggering caused by premature triggering and inaccurate arrival time measurement, usually experienced by TOA source location. Due to those reasons, triple point filtering can be considered as a more reliable source location method than TOA.

However, the triple point filtering method also has some drawbacks. It is clearly shown in Fig. 4.11 and Table 4.4 that the accuracy of triple point filtering location method is much lower than DeltaT and WTML method. The possible reason for measurement error of triple point filtering method is attenuation. The triple point occurs at a higher frequency; therefore the AE signal is more highly attenuated at

this point. Furthermore, since this method is also works on first threshold triggering principle, the attenuation will delay the detection triggering time. Time delay between the first arrival and first threshold crossing contributes to the source location measurement error.

Furthermore, the location result as presented in Fig. 4.11 also shows that the source to sensor distance determined by WTML method is more accurate than TOA and triple point filtering methods. The possible reason for higher accuracy achieved by WTML method is that the calculation of temporal separation does not involve the time delay from first arrival and first threshold crossing. The capabilities of WT analysis for presenting the AE signal in the time frequency domain also improved the location measurement error of SSML method by clearly discriminating the arrival of A_0 from other wave components.

The accuracy of WTML location result is also comparable with DeltaT method as shown in Table 4.4. However, WTML can be considered as an easier and more reliable method as sensors can be moved unlike when using DeltaT. There is also no need for a grid and H-N source for training data for initial location mapping. Furthermore, the standard deviation of WTML is better than the DeltaT method which suggests that this method provides a more precise result compared with other source location approaches.

4.5.3 Summary of findings from experimental work using artificial sources on a flat plate

It is found that the WTML methodology yields more accurate source location measurements than TOA and triple point filtering methods because the source location calculation does not involve a time delay from first arrival and first threshold crossing of AE triggering system. The WTML method improves the location error by eliminating false threshold detection by premature triggering and accurate arrival time measurement usually experienced by TOA source location.

The accuracy of the WTML methodology is better than the SSMAL. The WTML method improves the temporal separation measurement error by eliminating inaccurate arrival time measurement of A_0 mode by discriminating other wavemode component by utilising time frequency analysis of wavelet transform.

The source location accuracy achieved by the WTML is comparable with DeltaT location method. However, WTML could be considered as more reliable and easier source location methodology than DeltaT since no test grid and H-N source for training data is needed. Therefore, this method could be considered as the best candidate for source location methodology to be utilised for the fatigue crack length measurement in nuclear power plant piping system.

The next section of this chapter aims to validate the method in steel pipe geometry.

4.6 Wavelet Transform Modal Location (WTML) of Artificial Sources in A Steel Pipe Section

4.6.1 Experimental Setup and Validation Procedure

WD sensors (working frequency of 100-1000 kHz) were again mounted on the specimen and held in position with magnetic clamps with brown grease as the acoustic couplant. A 40 dB threshold was used throughout all tests. The TOA source location was conducted using commercial Physical Acoustic AE win software under planar location setup.

The pipe was manufactured from mild steel. The pipe dimension is 5mm thick, 1500mm long and 220mm outer diameter. A blunted notch with dimension of 50 mm long was introduced onto the pipe specimen. Four sensors were mounted onto the pipe surface, as shown in Fig. 4.12, and connected to AEwin DiSP data acquisition system.

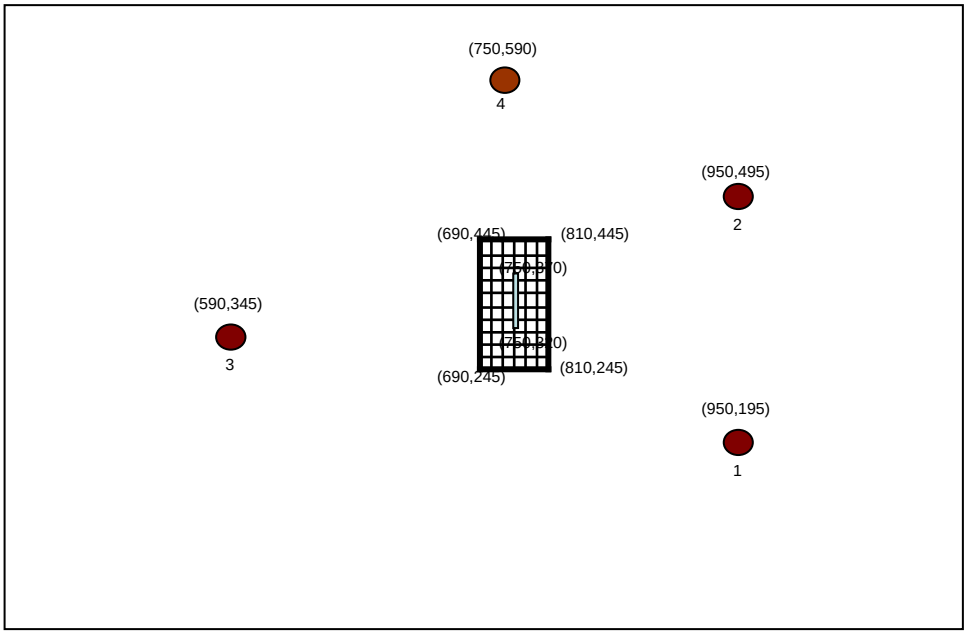

Fig. 4.12 Sensors and grid location on the unwrapped pipe surface

For DeltaT location, an area of 120 mm by 200 mm was selected on the pipe surface. A grid density of 20 mm was constructed around the notch, creating 66 nodes. Five PLB were conducted on each node. H-N data on every node was processed using the DeltaT software developed by Baxter (2007) for DeltaT mapping.

For WT modal location analysis, all of the captured waveforms were transformed into wavelet using Vallen wavelet software. Temporal separation between S_0 and A_0 mode of each waveform were determined from their wavelet coefficient plot.

Dispersion curves for 5mm thick steel were calculated using Vallen dispersion software and the velocities of S_0 (C_{S0}) and A_0 (C_{A0}) were determined from this calculated dispersion curve. Source to sensor distances were calculated using SSMAL equation (Pullin, 2005).

This distance was then used to calculate the new dispersion curve (time against frequency). This modified dispersion curve is then overlaid onto the transformed wavelet to verify the measured source to sensor distance. The WT modal location is determined by circle intersection technique. This location is then compared with DeltaT, TOA and actual location.

4.6.2 Results and Discussion

Fig. 4.13 shows a typical waveform signal from H-N source.

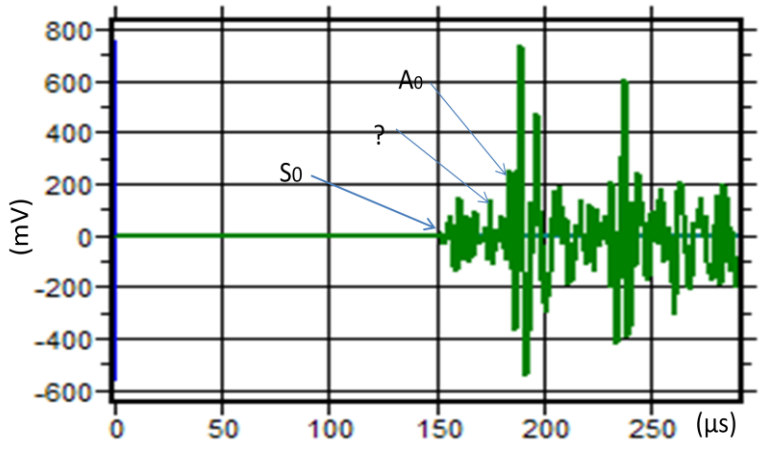

Fig. 4.13 Typical waveform signal from H-N sources

It is clearly shown in this waveform that the first detected signal is the faster S_0 component followed by high amplitude A_0 component. The arrival of S_0 component can be easily determined from this waveform, however the arrival of A_0 component is overlapped with other low amplitude signal which is appear between S_0 and A_0 components.

Fig. 4.14 shows the wavelet of the waveform signal. The vertical axis shows the frequency content (in kHz) of the signal while the horizontal axis represents time localisation of the signal (in seconds). The colour contour represents the strength of the signal.

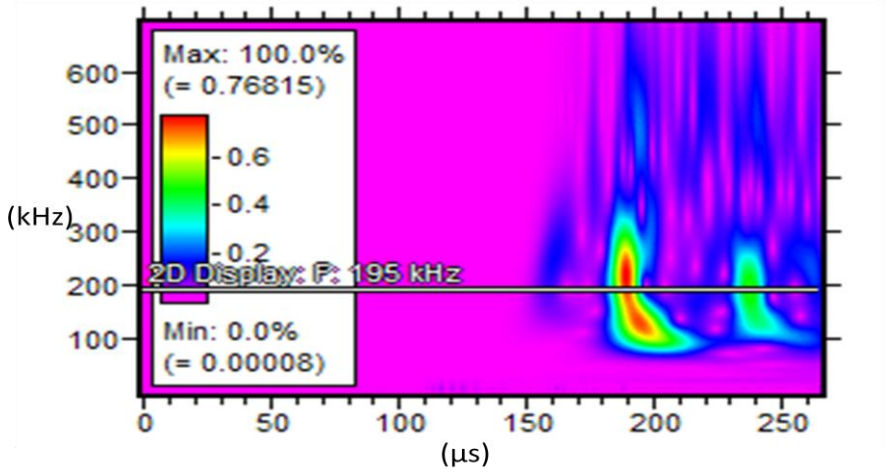

Fig. 4.14 Wavelet signal of the analysed waveform

Fig. 4.15 shows a wavelet coefficient plot against time for the transformed wavelet from the above waveform.

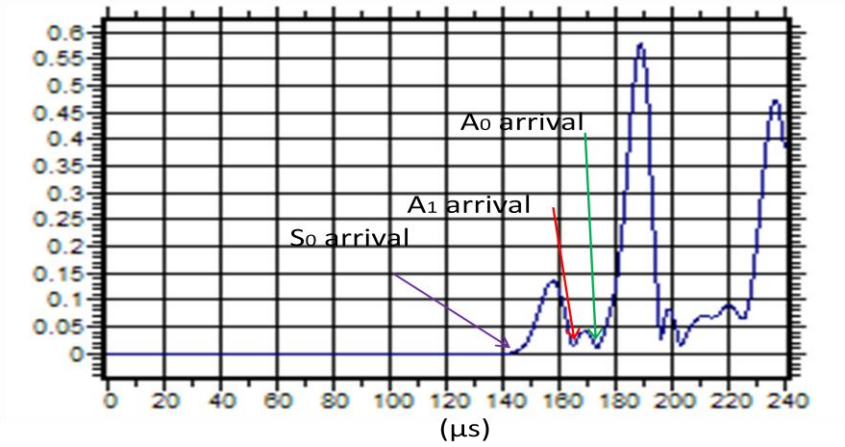

Fig. 4.15 Wavelet coefficient of the above wavelet analyse at 195 kHz

It is also shown that the low amplitude signal that is presumed to be the A_1 mode occurs between the primary modes which contribute to the error of SSMAL. Furthermore, it is clearly shown that this A_1 component can be easily distinguished from A_0 by wavelet frequency-time analysis approach. Moreover, temporal separation error due to superposition of A_0 mode with other waveform component also can be removed by analysing wavelet coefficient plot against time. In addition to wavelet coefficient plot, modified dispersion curve which is calculated based on the WT modal location can be used to verify the above explanation (Fig. 4.16).

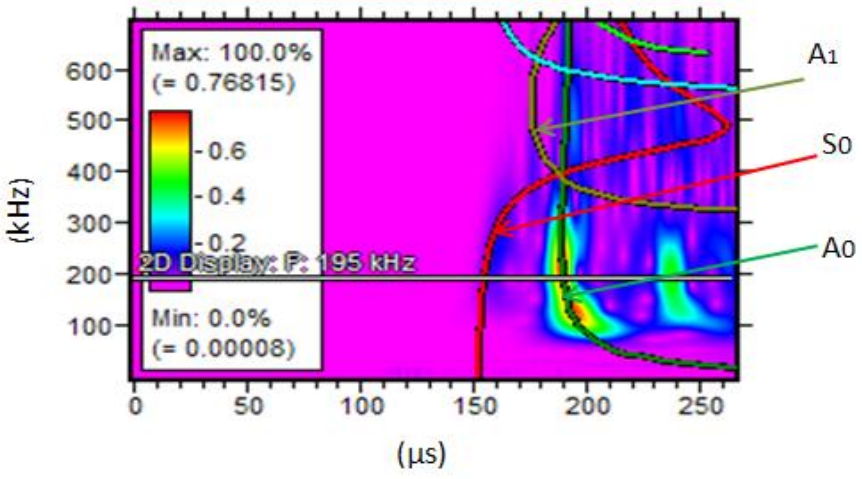

Fig. 4.16 Wavelet signal overlaid by modified dispersion curve

It is clearly shown that the modified dispersion curve of S_0 and A_0 modes is perfectly matched with wavelet transform result. The result suggests that accurate WT modal location can be obtained using WT location method by improving coefficient temporal separation measurement. Due to this argument, temporal measurement error in SSMAL can be highly improved by WT location methodology.

Fig. 4.17 shows the WT modal location result by using circle intersection technique.

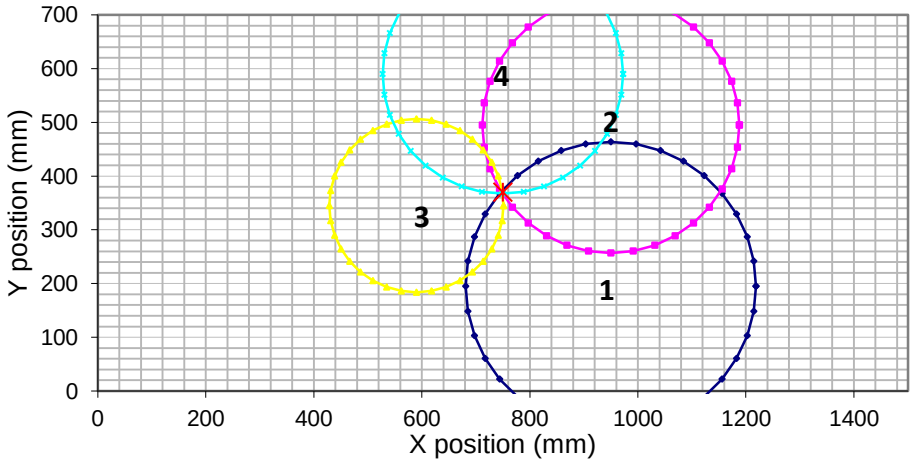

Fig. 4.17 Typical WTML Location result shown by circle intersection

Four circles represent the distance of H-N source from four WD sensors calculated by WTML modal location methodology. The WTML circles intersect at almost a single point suggesting that source to sensor distance using the new develop location method is very accurate. The location obtained with TOA and DeltaT methodologies and WT location is then compared with actual PLB location as shown in Fig. 4.18.

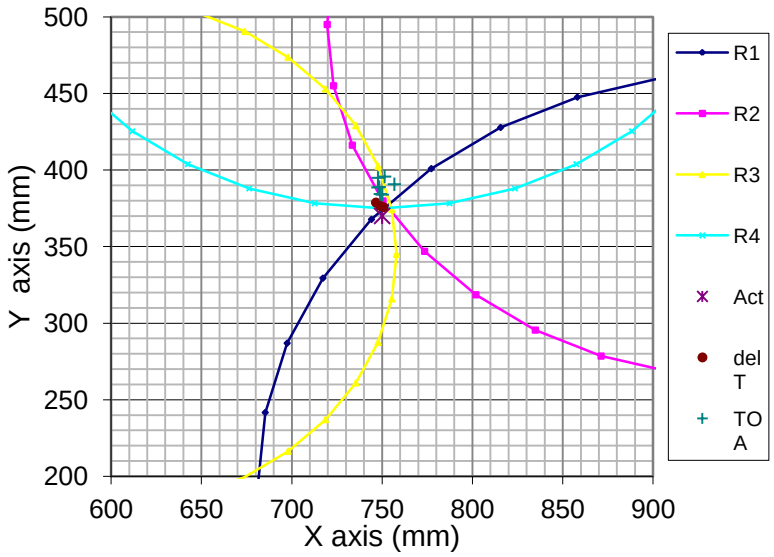

Fig. 4.18 Typical WTML result at lower notch tip compared with TOA and DeltaT locations, and actual location of H-N sources.

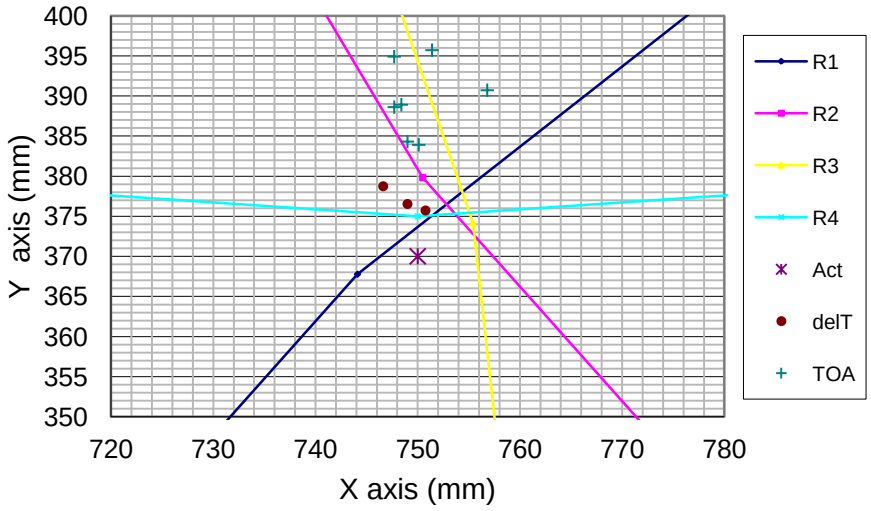

Fig. 4.19 Close up of above WTML location result

The location result as presented in Fig.4.19 shows that the source to sensor distance determined by WTML method produced is more accurate than TOA methods. The possible reason for higher accuracy achieved by WTML method is that the calculation of temporal separation does not involve the time delay from first arrival and first threshold crossing. Table 4.5 shows location error analysis of AE event from PLB sources determined by WTML, TOA and DeltaT methodologies compared with actual PLB location.

Table 4.5: Location error of TOA, Delta and WTML and their standard deviation

	Source to sensor distance error (mm)						
Sensor	Actual (mm)	TOA		DeltaT		WTML	
		RMS	STD	RMS	STD	RMS	STD
1	265.75	14.22	4	5.33	2.08	1.34	1.39
2	235.85	11.53	4.09	2.88	0.87	1.02	0.83
3	161.94	6.24	3.87	1.34	1.43	1.13	1.12
4	220.00	21.28	4.65	6.72	1.22	1.18	1.13

It is clearly shown in the table that the accuracy of WTML location result is also better than other AE location methods with DeltaT method. The accuracy of source to sensor distance using WTML giving a very consistent location result with highest accuracy error about 1.34 mm. The WTML location also yields very precise location with consistent standard deviation (STD) value around 1 mm (the highest STD value is 1.39 mm for source located by sensor 1).

4.6.3 Summary of finding from experimental work using artificial sources in a pipe geometry

- It is possible to utilise WTML to accurately locate the artificial AE sources in steel pipe geometry. The source to sensor distance errors (RMS) calculated using WTML method is very consistent with the highest RMS value of 1.34 mm (sensor 1) and the lowers RMS value of 1.02 mm (sensor 2). The accuracy of WTML location method is found much better than TOA and DeltaT method.
- The WTML location result in pipe geometry is more precise than other AE location methods. The highest STD values is 1.39 (sensor 1) and the lowest STD value is 0.83 (sensor 2)
- The accuracy of WTML for locating the artificial source in pipe geometry is less accurate than in plate geometry. The reason for lesser accuracy may due to the path different between the inner and outer part of the pipe geometry. However, the accuracy of WTML location in pipe geometry is considered much better than TOA location method.

4.7 Conclusions and future work

- WTML method was successfully developed for more accurate AE source location in this study.
- WTML methodology produced more accurate source location than TOA since calculation does not involve time delay from first arrival and first threshold crossing
- WTML methodology produced more accurate source location than SSMAL since the temporal separation can be more accurately measured
- WTML produced more reliable and easier source location methodology than DeltaT since a grid and H-N source for training data is not required
- This method could be considered as the best candidate for source location methodology to be utilised for the fatigue crack length measurement in nuclear power plant piping system
- Further work aims to validate the workability of this method for detection of actual crack growth in cracked plate and pipe

CHAPTER 5: ACOUSTIC EMISSION CRACK LENGTH MEASUREMENT IN STEEL PLATE AND PIPE USING A WAVELET TRANSFORMS ANALYSIS AND MODAL LOCATION THEORY

5.1 Introduction

This chapter discusses a fatigue crack growth study carried out on a mild steel pipe and plate specimen in order to provide better understanding of the characteristics of AE signals from fatigue under cyclic loading and to validate the workability of WTML method to accurately locating such damage

5.2 AE from fatigue crack in steel pipe

This chapter discusses a fatigue crack growth study carried out on a mild steel pipe test specimen in order to provide better understanding of the characteristics and propagation of AE signals from fatigue fracture in such structures.

5.2.1 Specimen geometry

The pipe specimen with dimension of 5 mm thick, 1500 mm long and 220 mm outer diameter was manufactured from mild steel. A blunted notch (50 mm long) was introduced onto the test specimen. The pipe geometry is shown in Fig. 5.1.

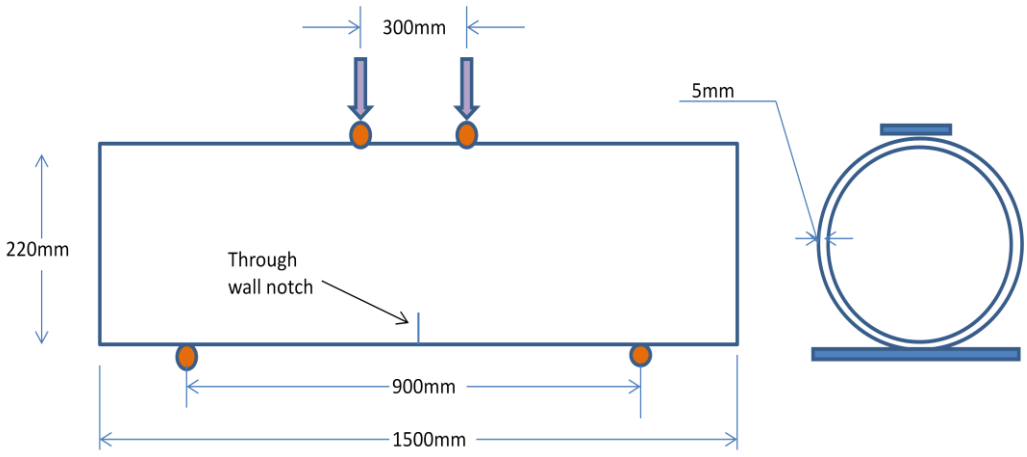

Fig. 5.1 Specimen geometry and loading arrangement

5.2.2 Experimental procedure and signal analysis

The pipe specimen was installed into the test rig under four point bend test set up as shown in Fig. 5.2.

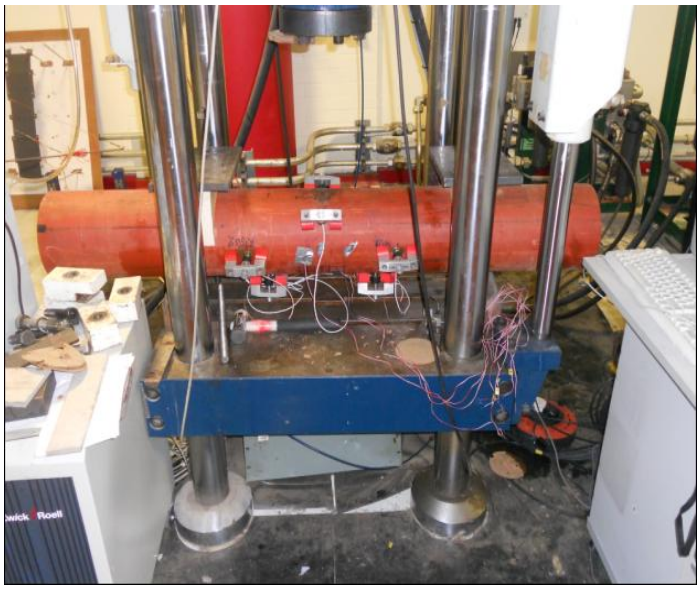

Fig. 5.2 Position of pipe specimen on the test rig

The specimen was loaded using a 500 kN dynamic actuator and a Dartec 9500 control unit. Load was applied using a sinusoidal waveform. Initially, first 6200 cycles were completed at 1 Hz, subsequently 2 Hz was used. 8 AE sensors were attached on the pipe and their arrangement are shown in Fig. 5.3.

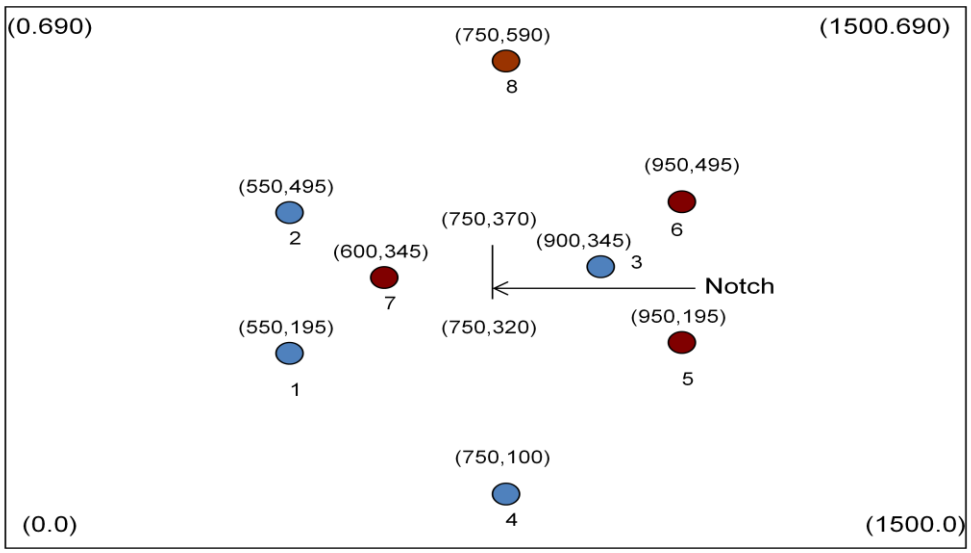

Fig. 5.3 AE sensors arrangement for four points bend fatigue test shown on an "unfolded" steel pipe.

All sensors were mounted via an acoustic couplant layer of brown grease and held in position with a magnetic clamp. Sensor response was verified using the H-N source technique (ASTM 1994).

AE activity was recorded throughout the test using a 24 channel DiSP AE system from Physical Acoustic Corporations. A 50 dB threshold was used on all sensors. AE waveforms were recorded at certain time intervals during the test for further analysis. Not all waves were recorded as waveform data due to data storage. AE activity at the crack tip was monitored under planar location setup for both R15 and WD Sensors.

Linear location setup/display was also used to locate the position of fatigue crack. The AE data feature extraction method has been used to filter out any unwanted signals.

Continuous wavelet transform (CWT) analysis for AE waveform signals emitted from the crack, detected by TOA planar location, was carried out using Vallen wavelet software. Temporal separation between S_0 and A_0 components was measured based on wavelet coefficient analysis, by viewing the temporal information within waveform signal, wavelet diagram and wavelet coefficient plot.

Source to sensor location were calculated based on modal location theory; however, the temporal separation is determined by the CWT analysis instead of analysing waveform temporal information. Calculated source to sensor distance were verified using the modified dispersion curve overlay method and source location was determined by the circle intersection technique. This location was then compared with TOA planar location result.

For noisy AE signals, signal denoising based on wavelet coefficient thresholding was carried out by the discrete wavelet transform (DWT) analysis using PACshare wavelet software. A denoised waveform was reconstructed using inverse discrete

wavelet transform (IDWT) facility incorporated in PACshare wavelet software. Temporal separation has been measured from the reconstructed waveform and source to sensor location was calculated using the standard SSMAL approach. Circle intersection was used to locate the crack signal and the results were compared with TOA location.

5.2.3 Results and Discussion

i) AE source clarification

The response to the H-N sources of the WD broadband sensors was above 98 dB, demonstrating that all sensors were mounted correctly.

ii) AE from fatigue crack growth

TOA planar location result shows that most of AE signals from fatigue test were released from the top of the specimen rather than from the notched area as shown in Fig. 5.4

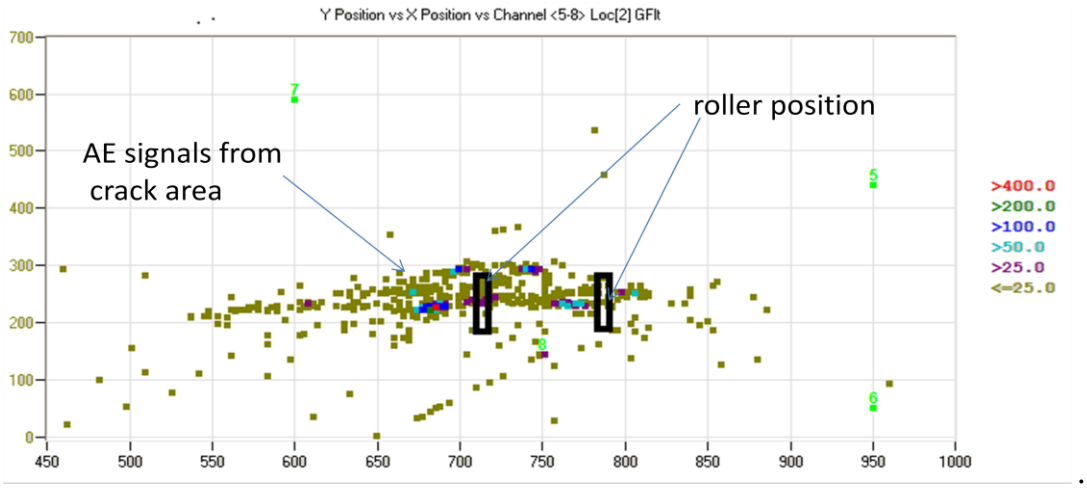

Fig. 5.4 TOA planar location result

Visual inspection and dye penetrant test shows that a longitudinal crack was present on the top of specimen and no crack indication was found at the notched tip area. The possible reason for the crack initiating away from the notched area is that the stress intensity at the loading area was much higher than the notch tip area. The load was concentrated at a very small area on the pipe specimen at the point contact between loading roller and pipe surface.

Analysis was carried out on the AE signals detected during the whole four point bend fatigue test. The cumulative AE event was plotted against the test duration to review the trend of AE events released. Fig. 5.5 shows the trend of AE events.

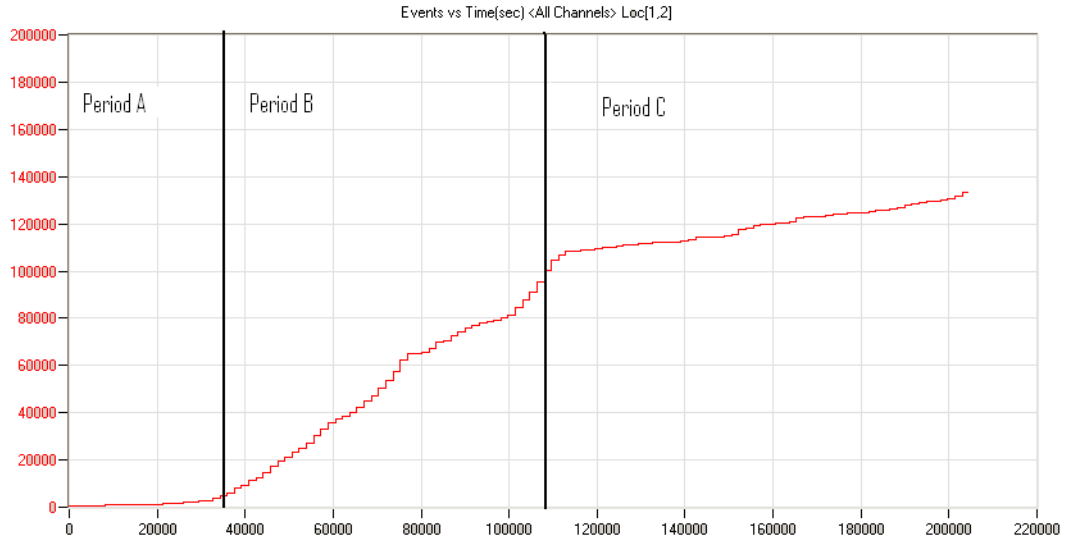

Fig.5.5 Trend of event rate for 4 point bend fatigue test

In order to gain a depth understanding on AE source mechanism, data at 60200-60400 cycles (where the abrupt change of AE event rate and high amplitude signal is released) was analysed. Linear location between sensors 8 and 5 was carried out to analyse the relation between accumulative amplitude, energy and events with respect to X-position. Fig. 5.6 shows the plot of accumulative AE amplitude against X-position between sensor 5 and 8 under linear location setup.

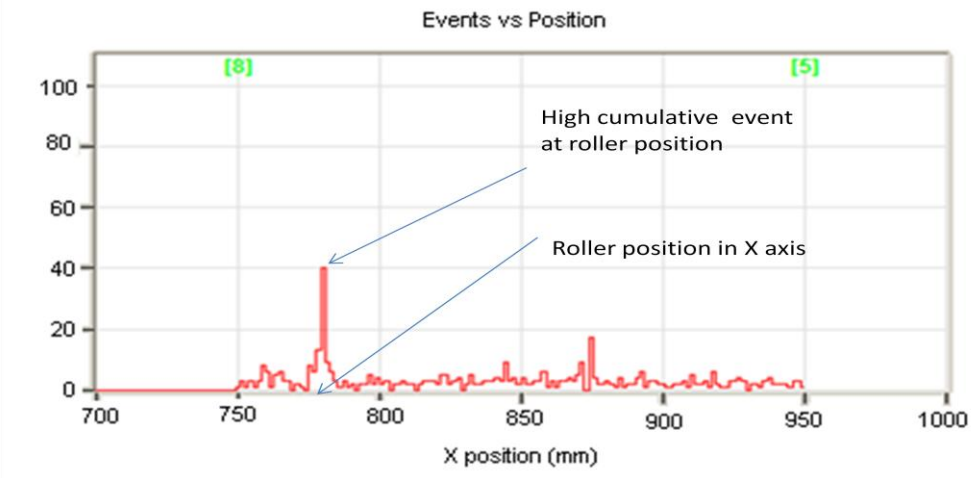

X position (mm)

Fig. 5.6 Plot of cumulative AE event under linear location against X-position

It was clearly shows that high cumulative AE signals were detected at location 780 mm in X position (about 30 mm away from sensor 8). This high peak may due to a large number of high amplitude signals were released at this location.

Amplitude density plot against X location as presented in Fig. 5.7 clearly shows that a large number of high amplitude signals (larger than 80 dB) were released at location 780 mm in X position.

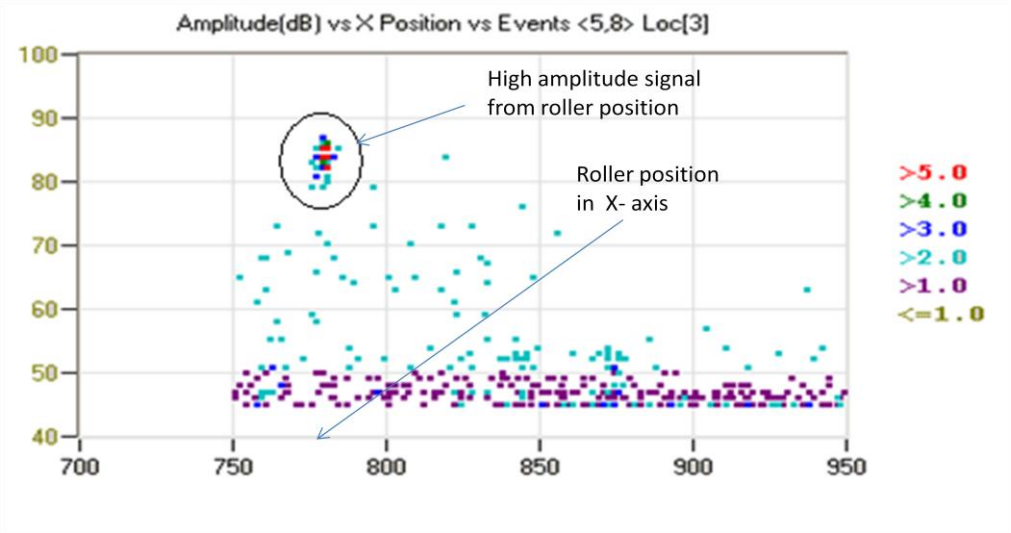

Fig. 5.7 Amplitude density plot against X location

Fig 5.8 shows linear location plot of cumulative energy detected by sensor 5 and 8 under linear location setup.

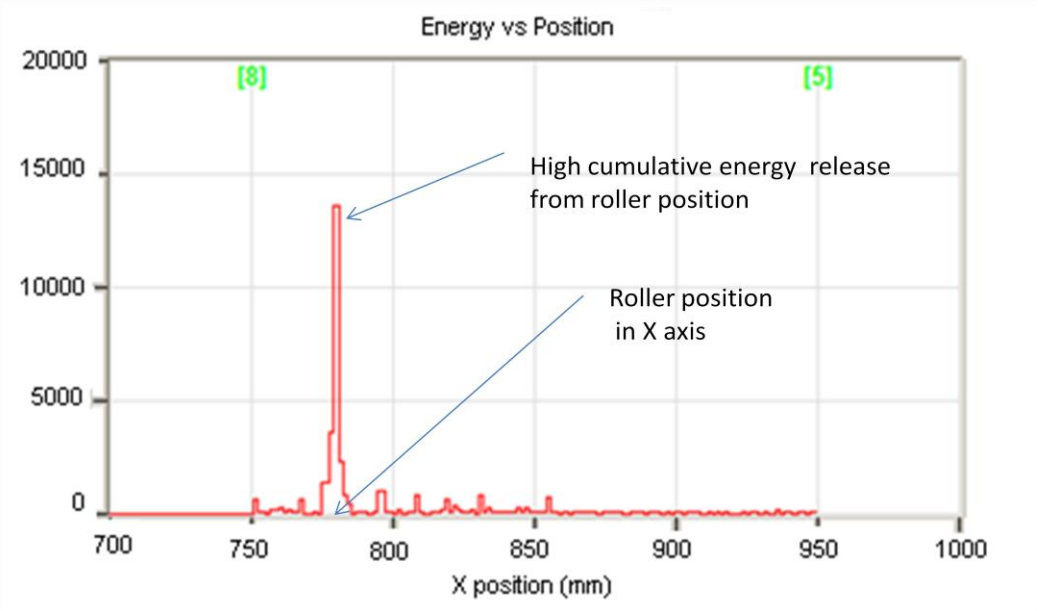

Fig. 5.8 Plot of AE signals energy against x position under linear location setup

It is clearly show that high peak cumulative AE energy were detected at the same location with the high peak AE amplitude plot in Fig. 6.6 and 6.8 i.e., at 780 mm in X position. High cumulative amplitude and energy signals at this location suggest that fatigue crack growth and related mechanism may occur at this location. Fig 5.8 shows the cumulative event plotted against X position under planar location setup between channel 5 and 8. It is clearly show in this figure that larger number AE events (about 40) were detected at location of 780 mm in respect of X position compared with the rest of the location (less than 40).

Fig. 5.9 shows the location of high amplitude events overlaid with the schematic of the pipe.

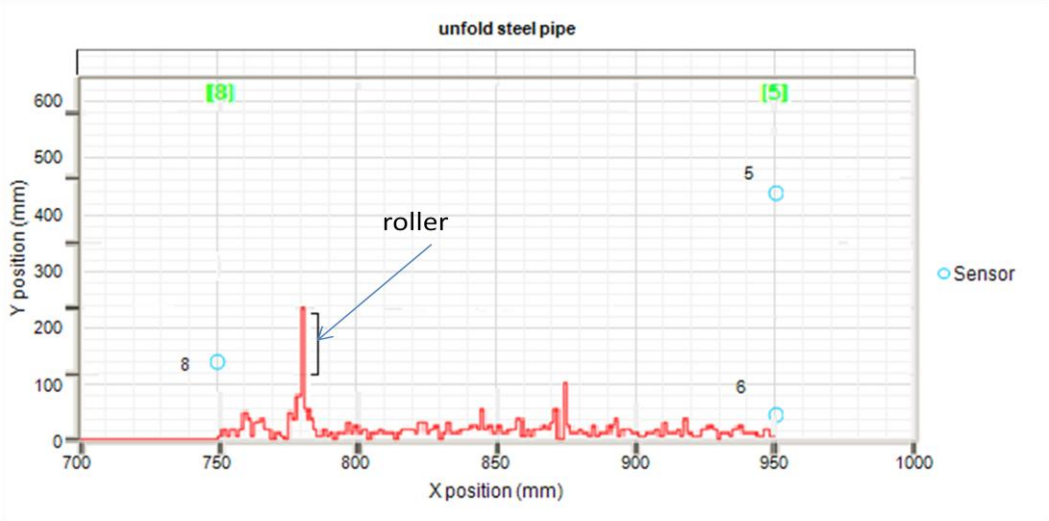

Fig. 5.9 linear location result overlaid on schematic-pipe.

Since high energy and high amplitude are the characteristic of signal from crack surface fretting, it is deducted that the AE signals detected at this location were release from fatigue crack growth initiation at the roller position.

iii) WTML source location fatigue crack growth

The wavelet transform modal location (WTML) methodology was used to locate AE signals from fatigue crack growth. Figure 5.10 shows typical AE waveform of an event from fatigue crack and the wavelet transform of 'clean' signal detected by three channels, 5, 7 and 8 respectively. The meaning of 'clean' signal in this discussion is that the arrival of S_0 and A_0 component can be clearly determined by wavelet transform analysis.

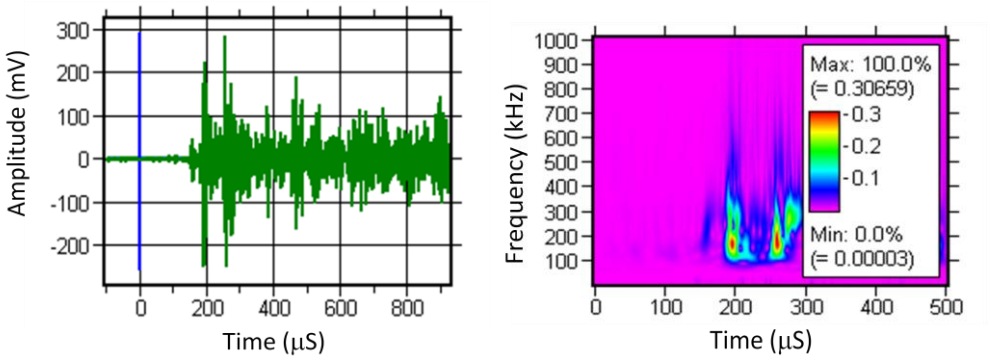

a) Waveform and wavelet signal from channel 5

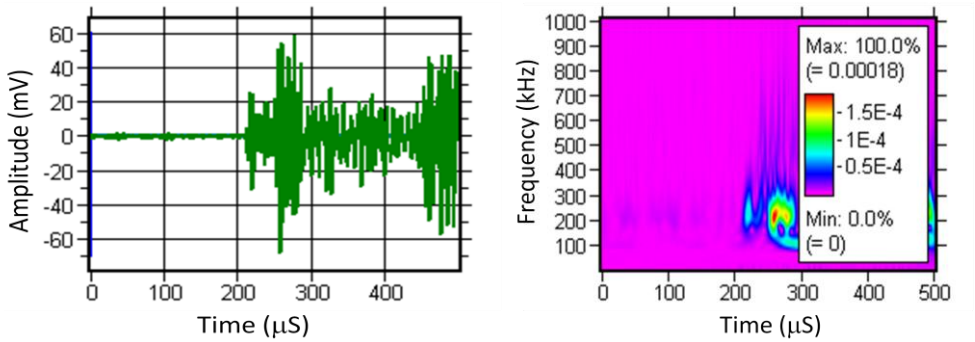

b) Waveform and wavelet signal from channel 7

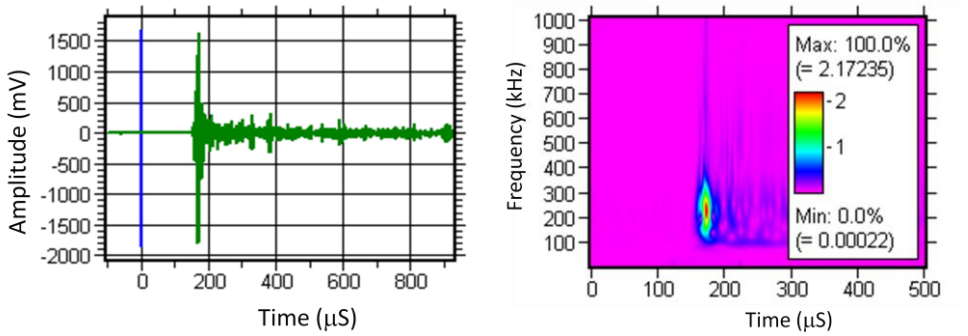

c) Waveform and wavelet signal from channel 8

Fig. 5.10 Example of 'clean' AE signal detected from fatigue crack growth

It is clearly shown in Fig. 5.10 a) and b) that some noise signals appear in the waveform signal detected by channels 5 and 7 just before the arrival of S_0 component, however by using wavelet transform analysis the S_0 component can be clearly differentiated from those noise components. In these cases, temporal separation can be accurately measured by WTML approach. Fig. 5.10 c) shows an AE signal without noise component detected by channel 8. It is clearly shown that temporal separation of S_0 and A_0 component is difficult to be measured just by viewing the waveform signal (as usually done in standard SSMAL approach); however, the temporal separation measurement is still possible by wavelet transform analysis.

Fig. 5.11 shows the wavelet of the waveform used for WT modal location and their modified dispersion curve. These modified dispersion curves were calculated using the WT modal location calculation as an input parameter.

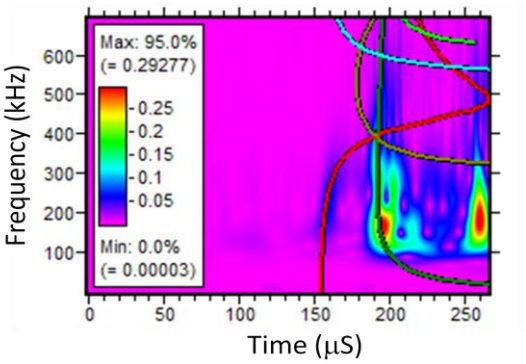

a) WT detected by channel 5 at 60225 cycles

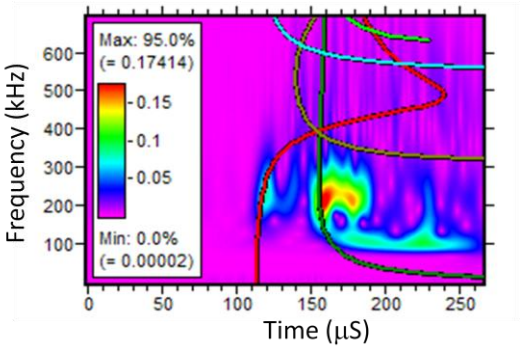

b) WT detected by channel 7 at 60225 cycles

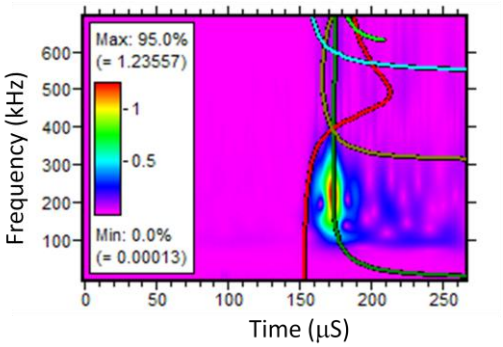

c) WT detected by channel 8 at 60225 cycles

Fig. 5.11 Typical verification result of WT modal location calculation for AE event detected at 60225 cycles.

The solid red, green and grey lines represent the modified dispersion curve of the S_0, A_0 and A_1 components of the Lamb waves. The dispersion curve for S_0 and A_0 were perfectly overlaid on the wavelet component which suggests that the right temporal separation measurement has been used in the overall WTML calculation.

Fig. 5.12 shows the location of a recorded waveform from crack growth using WT modal location method. The solid blue, pink and green lines represent the WTML location for channel 5, 7 and 8 respectively.

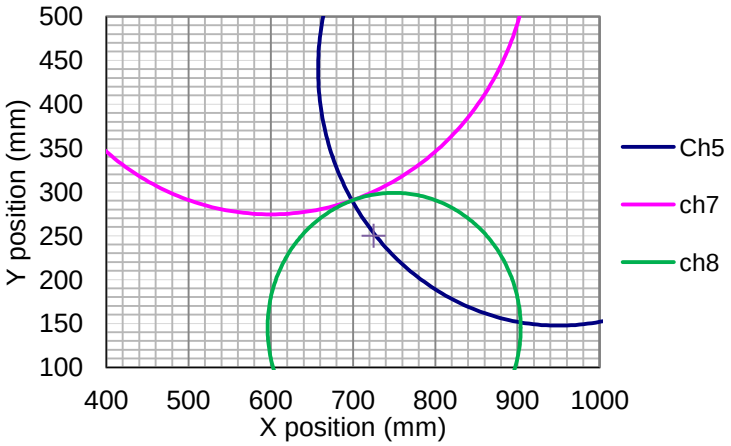

Fig. 5.12 Typical WTML result solved by circle intersection technique (data acquired at 60225 test cycles)

However, not all signals detected from fatigue crack growth area are 'clean'. Some signals are contaminated by noise sources as shown in Fig. 5.13

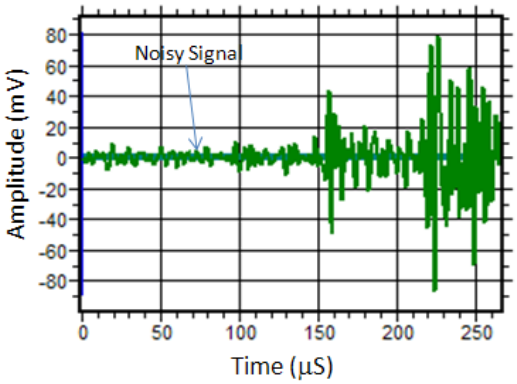

Fig. 5.13 Typical noisy waveform signals.

The typical WTML result from a noisy AE signal using circle intersection technique is shown in Fig. 5.14.

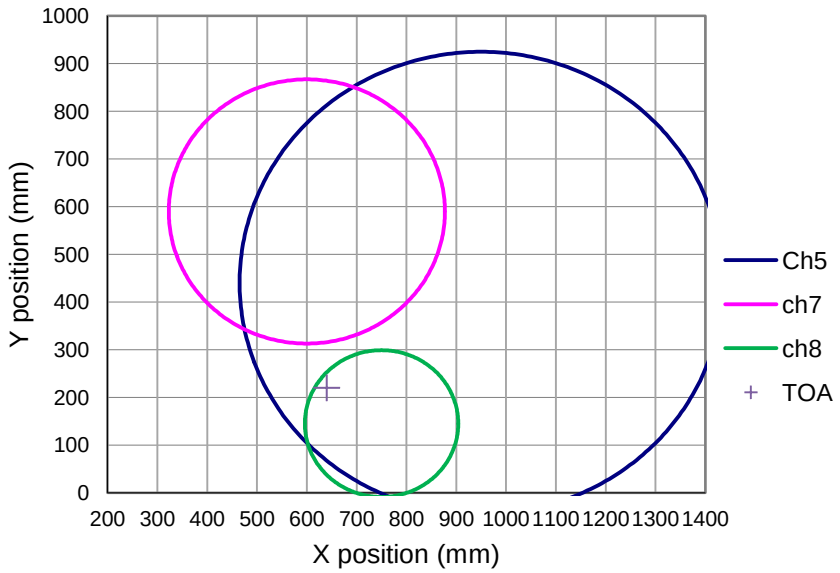

Fig. 5.14 Typical WTML of noisy signal from fatigue crack before signal denoising

The blue, pink and green circle represents the source to sensor location for channel 5, 7 and 8 respectively. It is clearly shown in this figure that three circles do not intersect at one location. Source to sensor location using WTML for channel 8 shows a good agreement with TOA location; however WTML for channel 5 produced a relatively large error. The possible reason for large error in source location is most probably introduced by temporal separation measurement error.

Further investigation into the waveform signal and wavelet diagram has been carried out. The analysis shows that the noise component in the waveform signal as previously discussed was the main contributor for temporal separation measurement error which leads to the WTML measurement inaccuracy as shown in Fig. 5.15.

a) b)

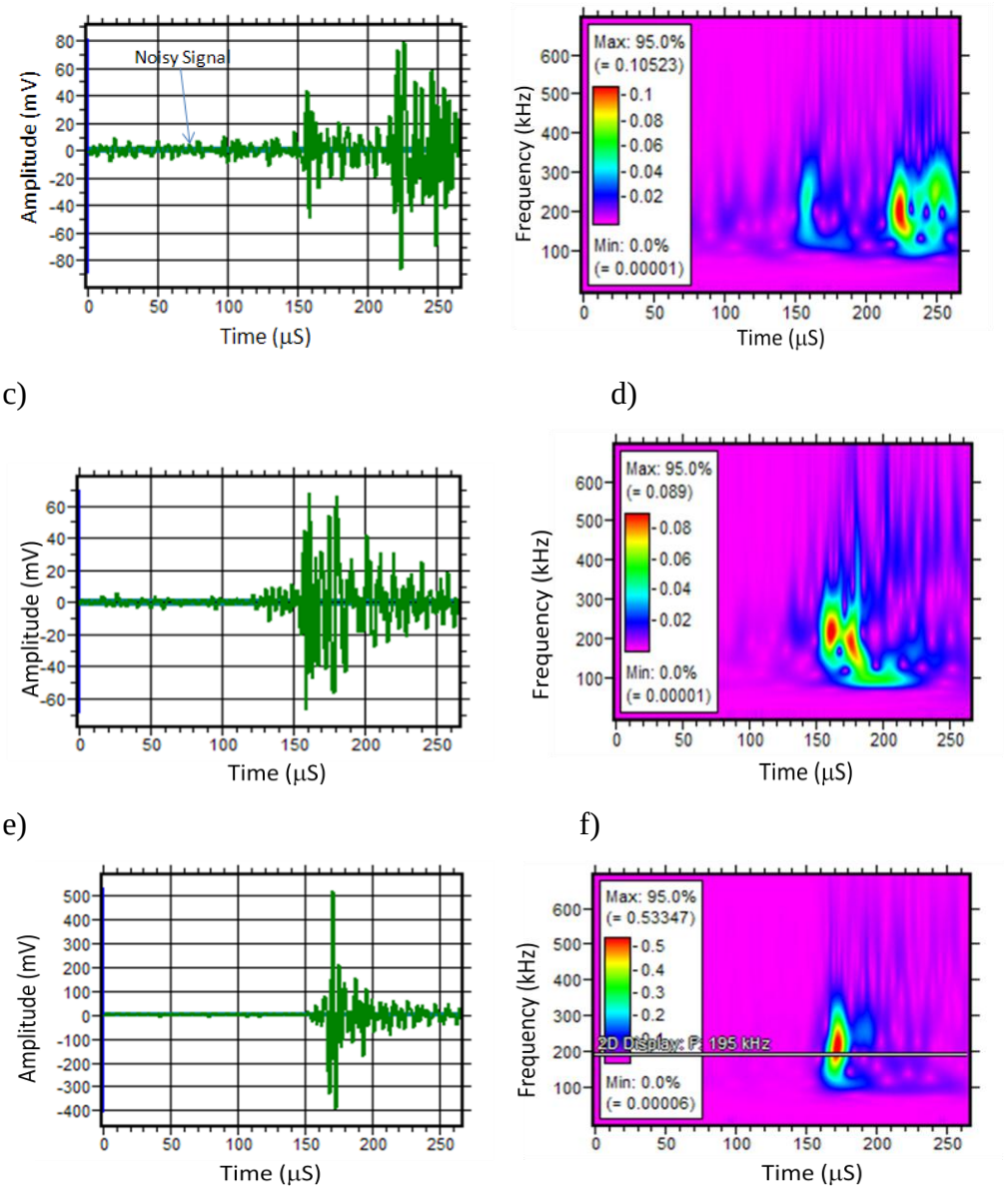

Fig. 5.15 Waveform and their wavelet for AE signal detected by channel 5, 7 and 8 at 136383 cycles.

The noise signal is clearly shown in Fig. 5.15 a) where the low amplitude signal is continuously emitted from 0 to 150 second which makes the arrival of S_0 component difficult to identify. Wavelet transform analysis of this signal (Fig. 5.15 b) shows that this is a low amplitude signal of similar frequency content to the S_0 component. Therefore, it is difficult to discriminate this noise by frequency filtering so that the used of SSMAL approach to determine the source location will produce large error.

A relatively ‘clean’ signal was detected by channel 8 as shown in Fig. 5.15 e) and f). This ‘clean’ signal enables the accurate temporal separation measurement that leads to more accurate source location calculation.

Several authors suggested that the noise signal can be removed from the waveform using discrete wavelet transform (DWT) denoising (Kwon 2000, Takemoto 2000). The DWT denoising was used in this study to remove the noise signal detected by channels 5, 7 and 8 from the above waveform. Fig. 5.16 shows time frequency map of typical noisy AE signal detected from crack growth area.

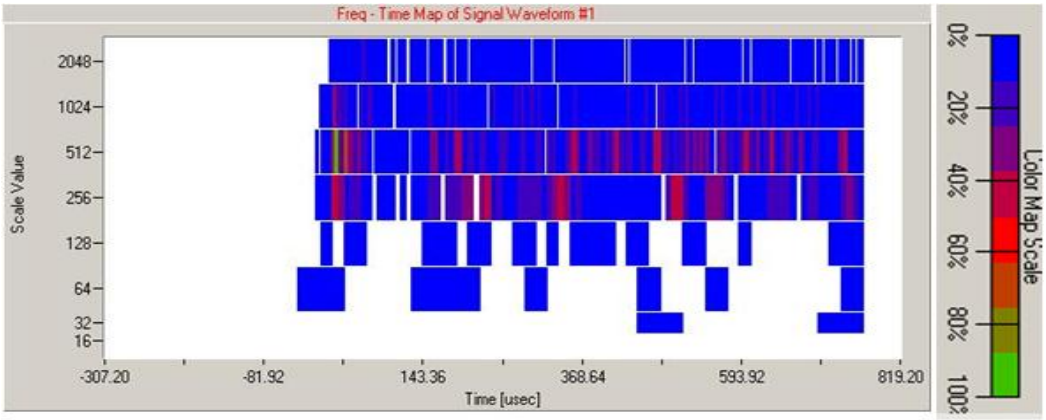

Fig. 5.16 Typical frequency-time map of noisy signal under DWT

Colour map scale represents the percentage of wavelet coefficient of waveform component at a certain frequency and time. The coefficient value represents the significant of those components to the original signal. Coefficient values close to zero are considered insignificant and usually associated with noise components.

The wavelet coefficient ‘thresholding’ of 10% was applied to the noisy waveform to remove any signal component with near zero wavelet coefficients. Fig. 5.17 shows the frequency-time map of ‘clean’ signal after DWT signal noising. It is clearly shown in this figure that most of low and high frequency noise (near zero coefficient) were removed after denoising process.

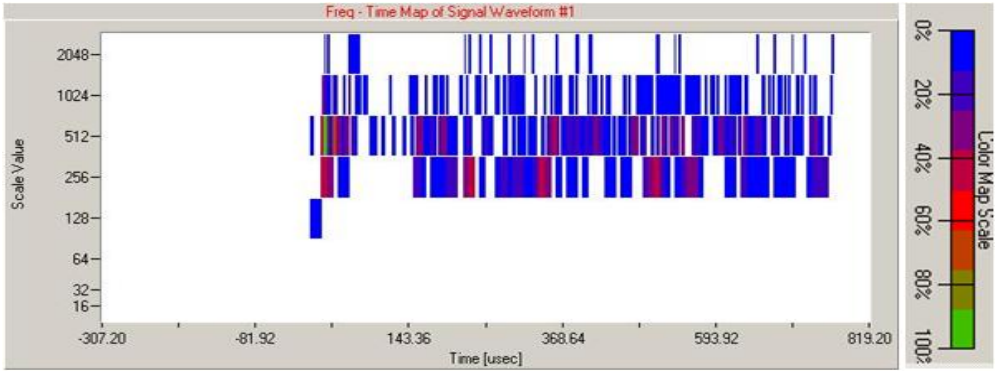

Fig.5.17 Typical Frequency-time map of ‘clean’ signal after denoisiong

The ‘clean’ waveform is than reconstructed using inverse DWT facility in the analysis software. Fig. 5.18b), 5.19b) and 5.20b) show the denoised waveform for AE signal detected by channel 5, 7 and 8 respectively.

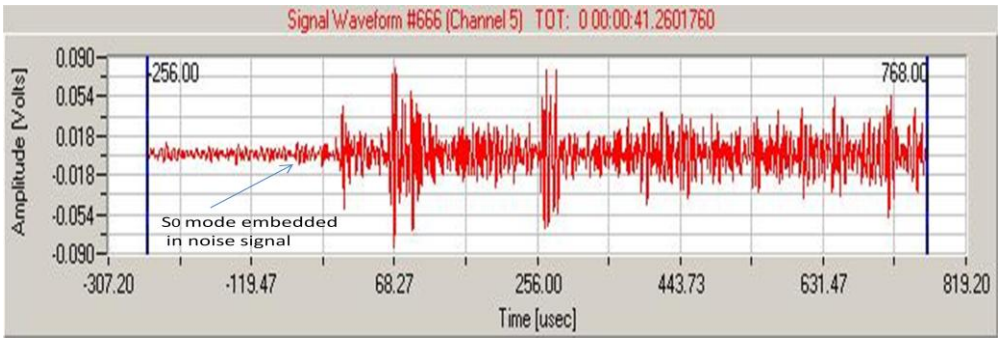

a) Waveform signal before denoising

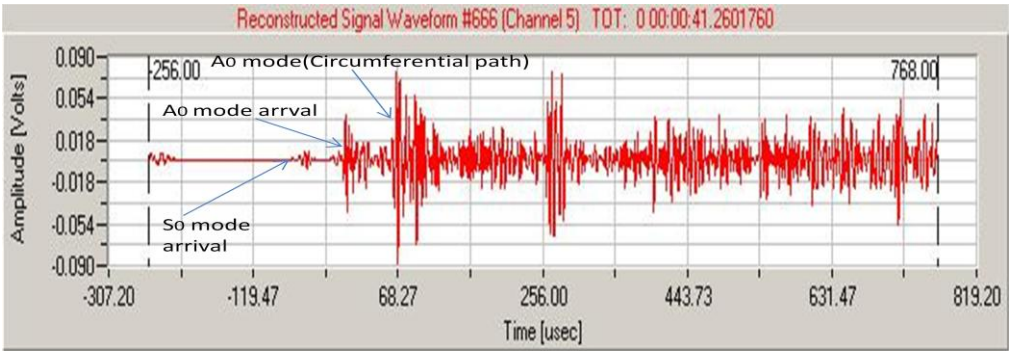

b) Reconstruct waveform signal after DWT denoising

Fig. 5.18 Example of waveform signal from fatigue crack detected by sensor 5

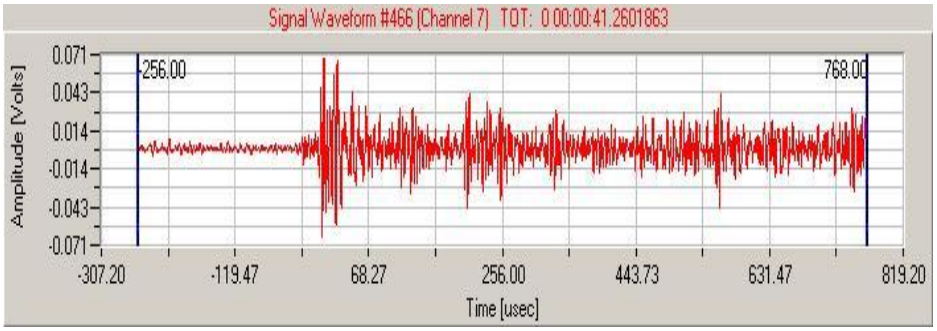

a) Waveform signal before denoising

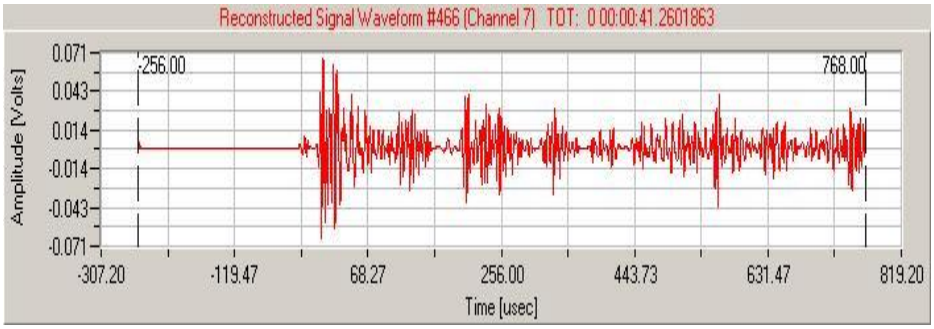

b) Reconstruct waveform signal after WT denoising

Fig. 5.19 Example of waveform signal from fatigue crack detected by sensor 7

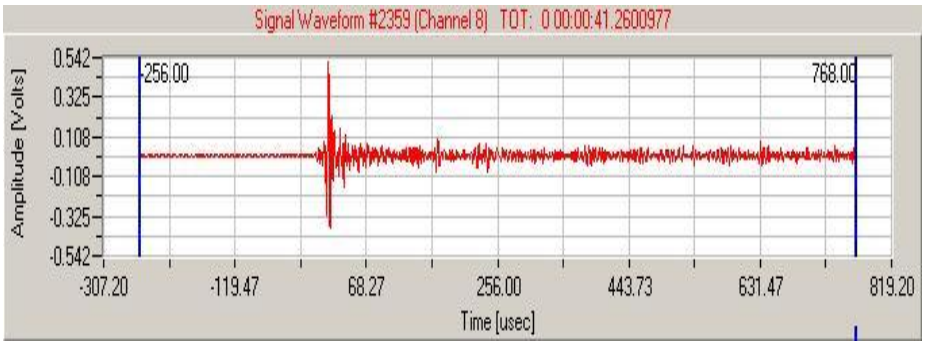

a) Waveform signal before denoisiong

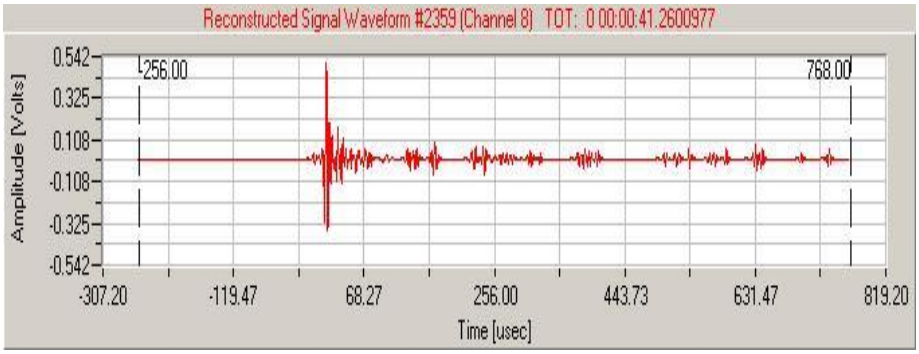

b) Reconstruct waveform signal after WT denoising

Fig. 5.20 Example of waveform signal from fatigue crack detected by sensor 8

It is clearly shown in Fig. 5.18a) that, the arrival of S_0 component couldn't be readily identified from the original waveform due to noise signal. When dealing with a situation like this, SSMAL is difficult to use for accurate source location. However, using WT denoising method, the background noise was successfully removed from the waveform. The arrival of direct S_0 and A_0 mode can be determined from the reconstructed waveform (Fig. 5.18b). This suggests that more accurate temporal separation measurement of a noisy signal can be achieved by the application of DWT denoising method.

As PACshare wavelet software does not have a continuous wavelet transform and wavelet coefficient analysis facility, and therefore WTML method couldn't be carried out on the reconstructed waveform. Temporal separation was determined from the reconstructed waveform and source to sensor distance was carried out using the standard SSMAL approach. The location of an AE event was then determined by the circle intersection technique and the result shown in Fig. 5.21. The result of SSMAL shows a better agreement with TOA planar location result. However, the actual location is unknown due to crack position under rollers.

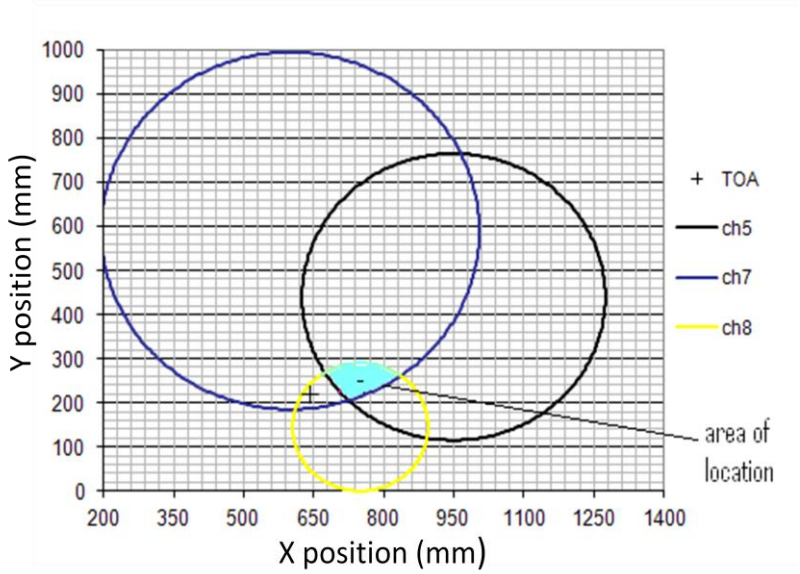

Fig. 5.21 Typical SSMAL of noisy signal from fatigue crack after WT denoising

This investigation clearly shows that high level noise signals will greatly affect the accuracy of AE source location. If noise level has the same magnitude and frequency content as the S_0 component, the arrival of S_0 component cannot be

determined which will affect the temporal measurement accuracy of SSMAL and WTML location. Usually this kind of noise could not be removed by a waveform filtering method; however, this near zero wavelet coefficients signal can be discriminated using wavelet transform analysis.

5.2.4 Conclusions for AE source location in steel pipe

There was no crack signal detected from the notch area due to poor experimental design. However, the AE signals from crack growth were detected at the point loading area. The linear sensors array of AE sensors used in this experiment were able to detect the AE signals from fatigue crack growth and approximately located by TOA source location method.

From these laboratory investigations, it is found that:

- It has been possible to confirm the detection and location of AE associated with fatigue crack growth.
- WD sensors were successfully used to detect AE from fatigue
- AE was well located. TOA linear location provided an invaluable tool for separating AE from fatigue crack growth apart from the AE signal associated with the load point.
- For 'clean' AE signal, WTML was able to locate the fatigue crack signal detected by TOA planar location method and showed a good agreement with TOA planar location result.
- WT denoising analysis was capable of filtering out any unwanted components from noisy waveform signals. SSMAL of de-noised waveform signal shows good agreement with TOA planar location result.

It should be noted that during fatigue monitoring of circumferential fatigue crack growth in actual piping components, mechanisms such as friction between roller and specimen, impact loading from load cell and noise from testing machine will not be present and therefore discrimination of crack signal (crack closure) from point contact loading will not become a big problem. However, turbulence from the liquid flow and water leaking at crack area will act as AE sources and therefore these noise signals can be discriminate by using WT denoising analysis.

5.3 Crack length measurement in steel plate using WTML method

This section discusses a fatigue crack growth study carried out on a mild steel plate specimen in order to provide better understanding of the characteristics of AE signals from fatigue under tensile-tensile cyclic loading and to validate the workability of WTML method to accurately locating such damage.

This research work aimed to:

- Grow the fatigue crack in the mild steel plate using cyclic tensile loading.
- Confirm that fatigue in this mild steel plate can be detected using AE techniques.
- Locate AE from fatigue damage using TOA location with linear and planar sensor arrays.
- Implement WTML method to the AE signal from fatigue crack growth detected by TOA planar location.
- Evaluate the efficiency of WTML for locating the actual data from fatigue crack growth in the pipe.
- Evaluate the capability the AE methods to measure crack length due to fatigue crack growth under tensile-tensile loading.

5.3.1 Specimen geometry

Mild steel plate with dimension of 5mm thick, 790 X 300 mm was used in this study. Seven holes were produced at each ends of the specimen (Fig. 5.22) in order to hold the specimen on the testing machine. Two sharp notches were introduced at both edge of specimen.

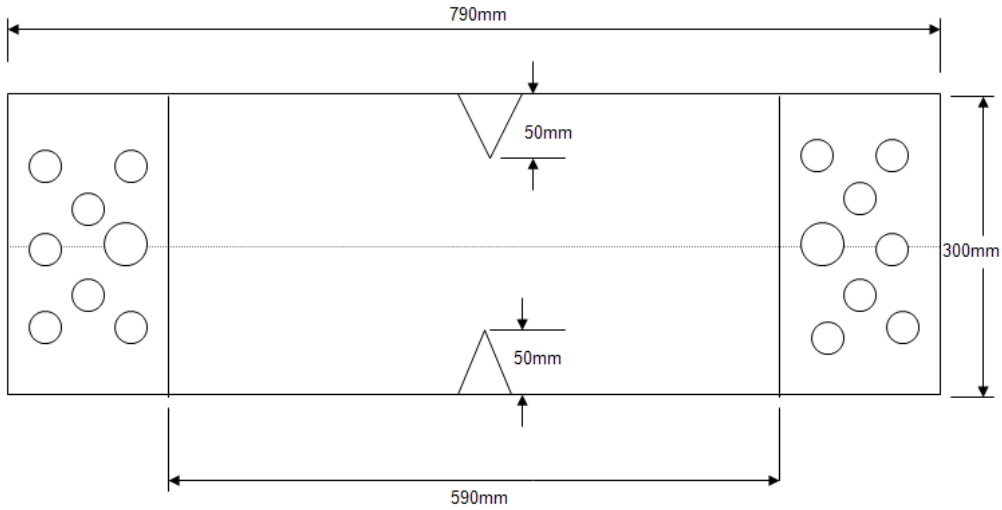

Fig. 5.22 Specimen configurations (all dimensions in mm)

These sharp notches were prepared by wire cutting and are introduced to act as crack growth initiation point and notches dimension were selected based on British Standard 6835-1: 1998 (BS 1998). The dimension of both notches is 40 mm width and 50 mm length and opening angle of 21.8^{o} as shown in Fig. 5.23.

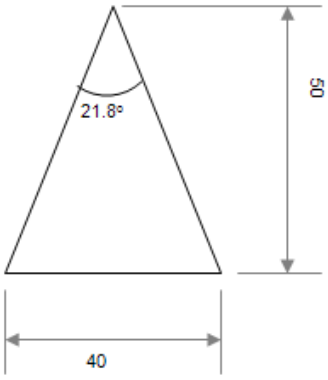

Fig. 5.23 Notch configuration (dimensions in mm)

Four supporting plates were used to grip and hold the specimen to the loading cell in the test rig during this test. These supporting plates was fabricated from mild steel with dimension of 6 mm thick, 300 mm width and 100 mm length as shown in Fig. 5.24.

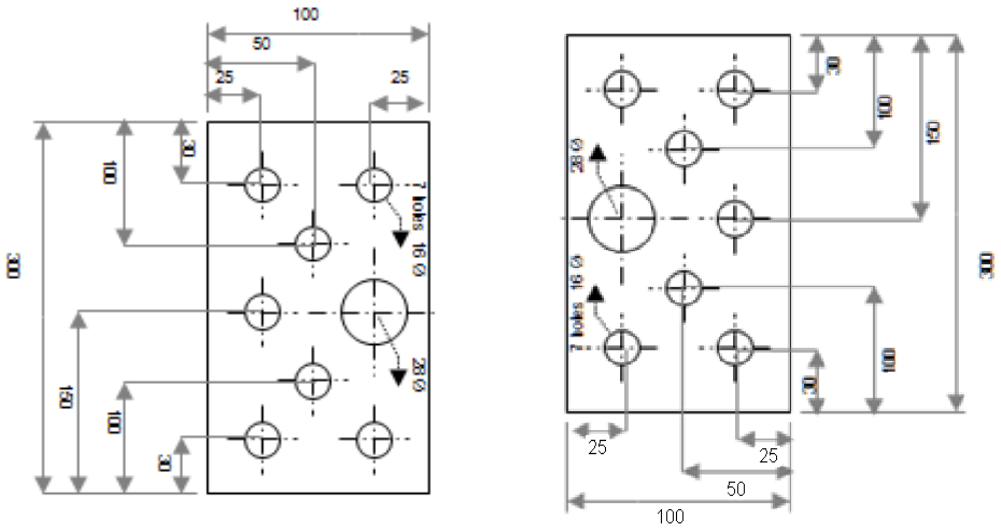

Fig. 5.24 supporting plate configurations for both end of specimen (all dimension in mm)

Seven holes were drilled through these supporting plates, one with 28 mm diameter for loading pin holder and other six with diameter of 16 mm for inserting bolts and nuts for grip the specimen to retain it during failure.

Optimum load values were found to be:

P_{max} = 80 kN and P_{min}=10, where P_{max} is maximum load and P min is minimum load (Shigley,2004).

5.3.2 Experimental equipment, procedure and analytical method

i) Experimental equipment and procedure

The Mistras AE system from Physical Acoustic Corporation (PAC) was used to acquire AE signals released from fatigue crack growth throughout this work. Four wideband (WD) AE transducers with frequency range of 100 to 1000 kHz were used to detect AE signals from fatigue test. These sensors were attached to 2/4/6 preamplifier with working frequency range 20 kHz to 1200 kHz and connected to AE data acquisition system through coaxial cable. The 40 dB threshold level has been used for AE data acquisition and detected events were amplified by 40 dB amplifier. All recorded signals were stored on the computer for further analysis.

All WD sensors were mounted via an acoustic couplant layer of silicon grease and held in position with magnetic holder for 48 hours to secure the couplant layers. Sensor response was verified using the H-N source technique (ASTM 1994).

DeltaT calibration map for the area around the notch and expected crack growth area was developed (details as in section 5.3.2) to determine the location of the crack tip from the crack growth AE signal. The plate specimen was then installed into the test rig as show in the Fig. 5.25.

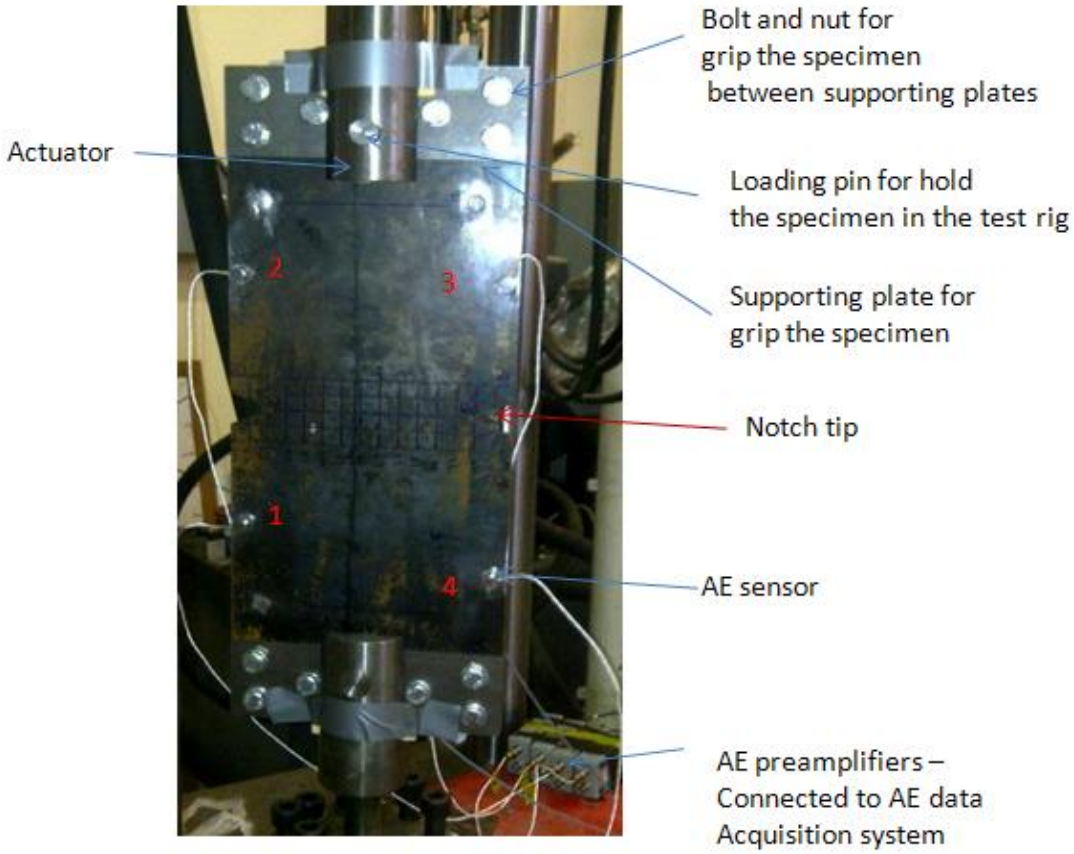

Fig. 5.25 Placement of AE sensors on the specimen and the placement of specimen on the test rig.

The Mayer testing machine with maximum load of 500 kN was used to applied the load to the specimens. Specimen was loaded under tensile-tensile cyclic loading at frequency of 2Hz with maximum load of 80 kN and minimum load of 10 kN. Load data from testing machine was fed to parametric channel of AE data acquisition

system. This load data was recorded simultaneously with the transient AE signals detected during fatigue test and both data were used for AE source mechanism characterisation by correlating AE parameters with the load value.

The crack growth was monitored using crack gauges. Two crack gauges were attached to the specimens at the vicinity of notch tip as described in detail in section 5.3.3.

Before the actual fatigue test is carried out, gridlines for DeltaT training data (8 cm x 30 cm) with a grid resolution of 2 cm x 2 cm was constructed around the notch and expected crack growth area. Four WD sensors were attached on the specimen at location of 1 (250,285), 2 (555,285), 3 (550, 13) and 4 (200, 15) as shown in Fig. 5.26 and 5.27

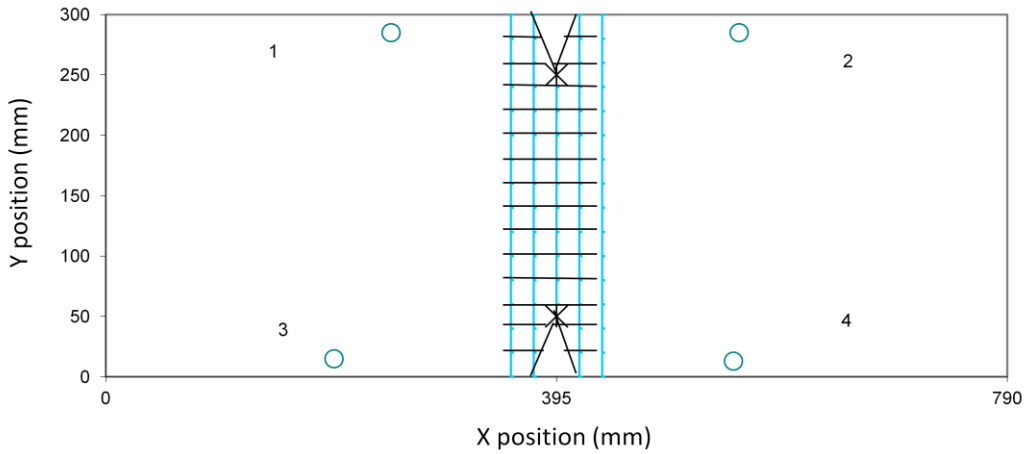

Fig. 5.26 Schematic diagrams of grid lines for training data by H-N source for DeltaT location and position of AE sensors

Fig. 5.27 Actual grid line on the plate specimen

Five H-N sources were conducted at each node and time delays between each pair of sensor were calculated using DeltaT software developed by Baxter (2007). The DeltaT map base on time arrival delay between pairs of sensors was developed as calibration map. Five H-N source were conducted at both notches and location of this notch was compare with the calibration map to assess the performance of the DeltaT map. This map will be used to determine the location of detected signal during crack growth test using DeltaT approach and will be compared with other location methods.

ii) Crack growth monitoring

Crack gauge as described in Chapter 3 (section 3.3.3) was used to monitor the crack growth throughout this work. Crack gauge was attached to specimens at the vicinity of notches tip. This gauge was connected to the power supply box and voltage amplifier through a terminal as shown in Fig. 5.28.

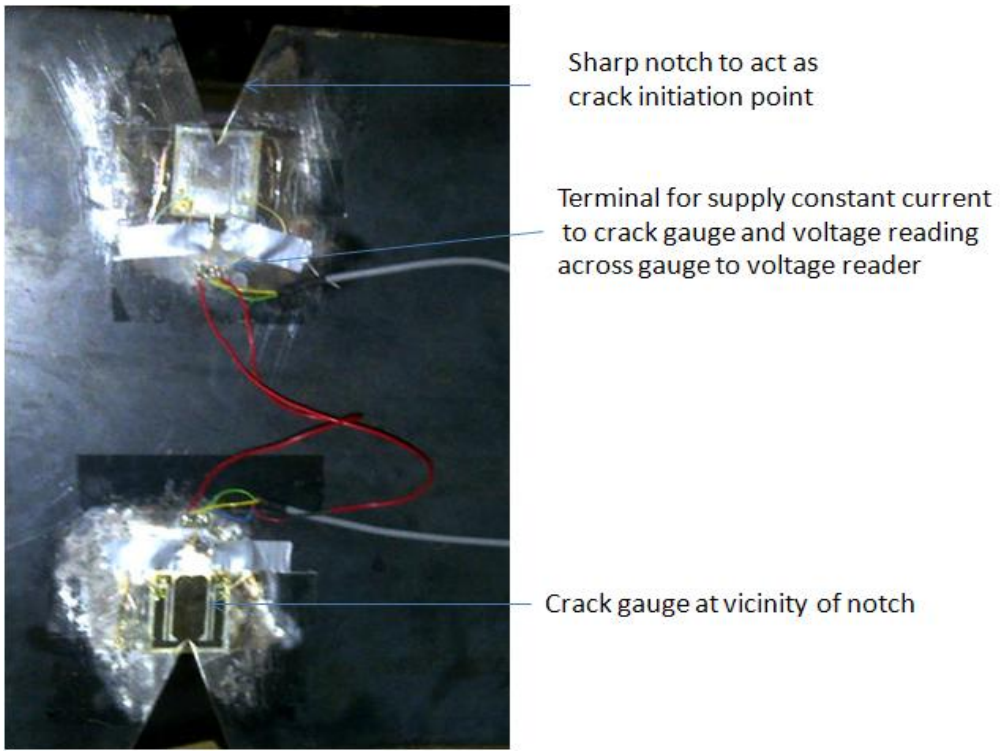

Fig. 5.28 Attachment of crack gauge on the specimen at the vicinity of notch tip

Fig. 5.29 shown the location of the notch and gauge on the specimen when the specimen was loaded inside the test rig.

Fig. 5.29 Location of crack gauges on the specimen inside the test rig.

A constant current (25 mA) was supply from power supply (Fig. 5.30) to the crack gauge and the voltage reading across crack gauge were fed to voltage amplifier through this power supply.

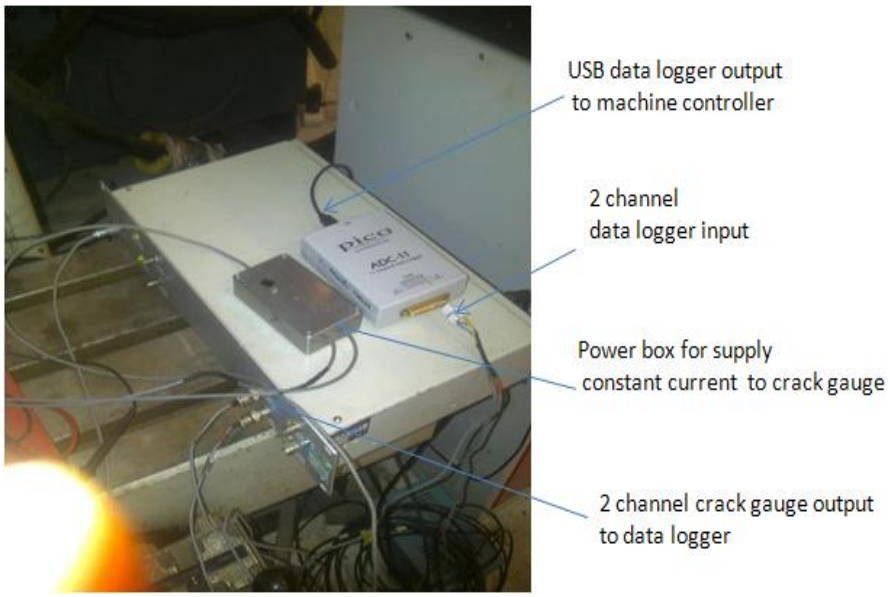

Fig. 5.30 Constant crack gauge power supply and voltage reader

The voltage amplifier was connected to Pico ADC-11 data logger (Fig. 5.31) and Pico data logger software (PicoLog Recorder) has been used to record the voltage across the crack gauge during crack growth. These data were stored inside the Mayer testing machine data storage for further analysis, and analysed using PicoLog Player.

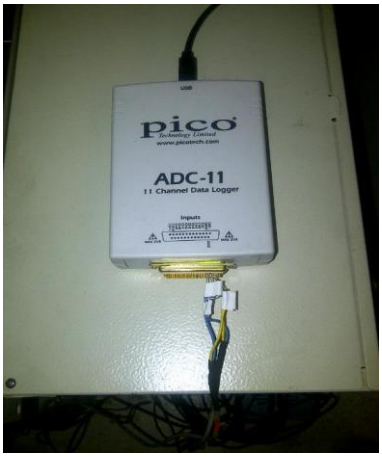

Fig. 5.31 Pico ADC-11 data logger

The test was stopped at certain numbers of cycles during the fatigue test to allow the red dye penetrant test to be carried out for measuring the actual length (the distance of the crack tip to the notch tip). The measured crack length was plot against the voltage across the crack gauge to draw the relationship between the voltage reading and the actual crack length. This correlation was then used to plot the length of crack growth against number of cycles.

In order to accurately locate the fatigue crack growth, the various AE source mechanisms from fatigue crack growth were investigated and characterised using AE data feature. The following procedure was used to analyse and characterise the AE signals detected during fatigue testing.

i. Recorded AE signal was viewed under linear location using PAC software. Any signal released at notch location under this setup is assume to be released by fatigue crack growth activity and was used for further analysis.

ii. Certain AE feature data such as event, amplitude, energy, and rise time were analysed and correlated with load data at different load level such as at peak load and other load value.

iii. AE source mechanisms were determined by AE data feature extraction. At this stage, the AE data features from fatigue area were extracted and the characteristic of AE fatigue signal were determined by selecting the appropriate AE data feature.

iv. AE data were filtered based on AE data feature extraction, load level and position of X-axis.

v. Filtered data file were replay under TOA planar location setup. Five data-files for different crack length were selected for further analysis. Six AE events were extracted from each data-file and saved as new data-files for further location analysis.

AE signals from fatigue crack growth for various crack lengths determined from section 5.3.3 were used for AE source location. The WTML method developed in

this study (as described in Chapter 4) was used to locate the actual signals emitted from fatigue crack growth. The accuracy of this method was then compared with other AE location methods such as TOA, TP Filtering and DeltaT.

For TOA source location, the filtered AE signal from different crack length (about 6 signals in each data file) were replayed under TOA planar location analysis and the results were used for further location comparison. Velocity of 3200 m/s (the fastest velocity of A_0 mode) and threshold level of 45 dB was used for TOA planar location. This velocity and threshold value were chosen with the observation that the amplitude of S_0 mode component and noise signal is less than 45 dB and therefore the AE detection system will be triggered by the arrival of A_0 component.

Triple point source location was carried out by filtering the waveform signals (used for TOA planar location) at 390 to 400 kHz frequency range (triple point frequency is 396 kHz). This narrow range frequency filtering was carried out to select the wave component that propagated close to triple point velocity and the filtered data saved as new data files. These new data files were replayed under TOA planar location. The analysis velocity used is 3170 m/s (triple point velocity for 5 mm steel) and the AE detection system is assumed to be simultaneously triggered by S_0, A_0 and A_1 modes at this frequency range. The threshold level was also reduced to 20 dB during this filtering process. This threshold level was chosen to accommodate the signal attenuation due to high the signals frequency of triple point.

The filtered AE signals (used for TOA planar location) were also located by DeltaT method by comparing the time arrival delay at different sensors pair with the calibration map as described in section 5.3.2.

5.3.3 Results and discussion

i) Crack growth monitoring

Crack growth was monitored throughout this study using crack gauge. The voltage reading across the crack gauge was recorded and red dye penetrant testing has been

used to determine to the physical length of the crack growth. Fig. 5.32 shows the relation of the voltage reading across the crack gauge and the crack length observed using red dye penetrant testing.

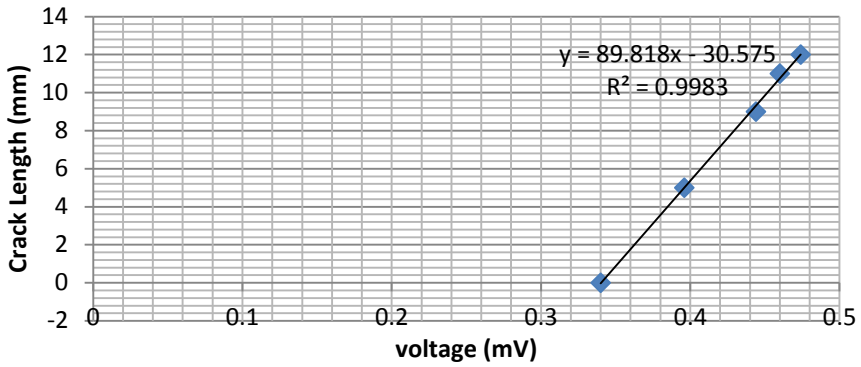

Fig. 5.32 Relation between crack length and crack gauge measurement

A linear relationship between the output voltage across the crack gauge and the crack length measured by penetrant test was obtained with the coefficient of determination (R^2) of 0.9983. This coefficient value suggests that the crack gauge provided a crack length measurement with accuracy of 99.83%.

The relation between crack length and crack gauge reading can be represents by the following equation.

$$y = 89.818\,x - 30.575 \qquad \text{Eq. 5.1}$$

where y is the crack length in mm and x is the voltage reading across the crack length in mV. This equation has been used to determine the length of the crack growth against the number of cycles of fatigue loading throughout the test as shown in Fig. 5.33.

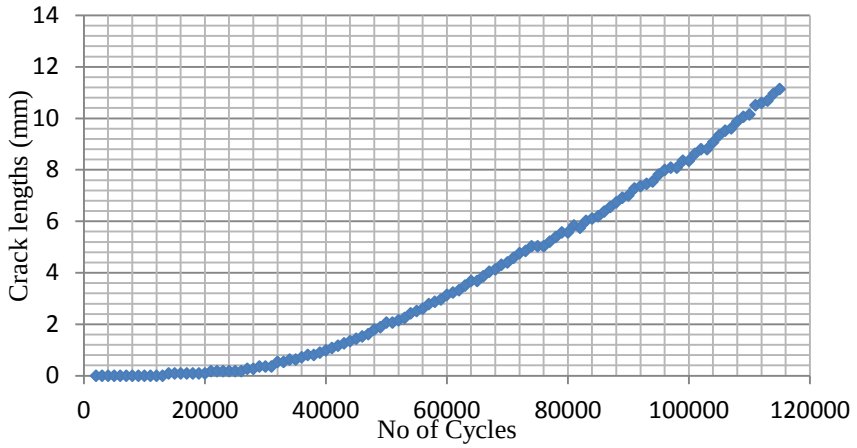

Fig. 5.33 Crack lengths against the number of cycles

The test was stopped at 120,000 cycles of test at a crack length of approximately 11 mm. In actual application of steel piping system in power plant, the crack length should not be more than the thickness of the pipe as described in acceptation and rejection criteria in ASME Code (ASME IX, 2006).

ii) AE signal analysis and fatigue crack growth characterisation

The response to H-N source of the WD sensor was above 98 dB demonstrating that all sensors were mounted correctly. However, not all signal detected during the fatigue test arose from the fatigue crack growth area. Signals may also be due to other sources such as friction between specimen and loading pin or friction between bolts and specimen surface. In order to ensure that only the signal released from fatigue crack growth were used for source location and crack size measurement, the stored AE data were examined under linear location setup. Fig. 5.34 shows the typical linear location result of AE signal from fatigue crack growth test.

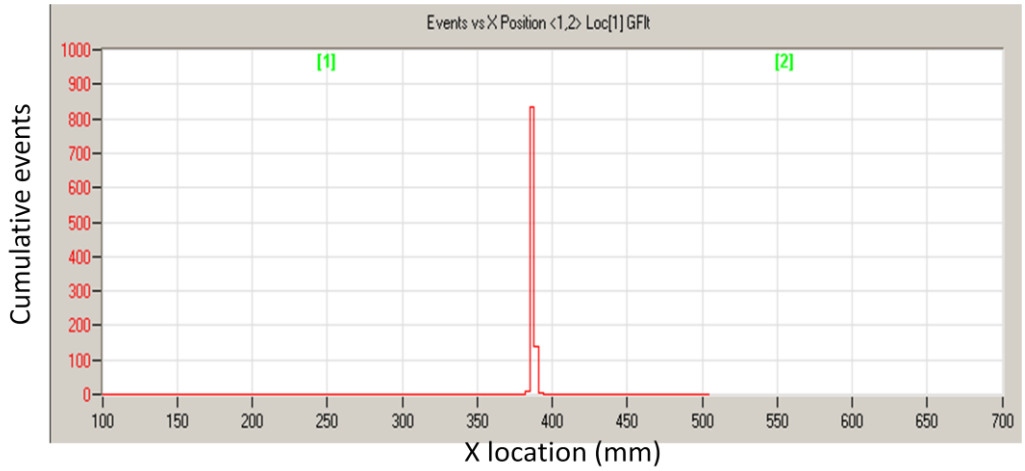

Fig. 5.34 Plot of cumulative AE event against X position

This linear location result shows a very good agreement with the actual notch location (395, 250) which suggest that the detected AE signal were emitted by fatigue crack growth activity in the vicinity of the notch tip.

According to Scruby (1987), the primary sources associated with crack growth are plastic zone extension, plastic opening at the crack tip and elastic crack advance. However, plastic zone extension and plastic opening at the crack tip may not be detectable under slow ductile loading and elastic crack advance can be detected if their mechanism is fast brittle fracture. Most of these sources are generated at peak load value under cyclic fatigue loading.

Secondary events associated with fatigue crack growth are crack face fretting (Scruby 1987). This mechanism also known as crack closure and usually occurs at lower load value (Pollock 2012).

Since the source mechanism of fatigue crack growth is load dependent, load level of detected AE signals was plotted against the duration of test and Fig. 5.35 shows a typical plot of load level of detected signals versus test duration from one of recorded AE data-file.

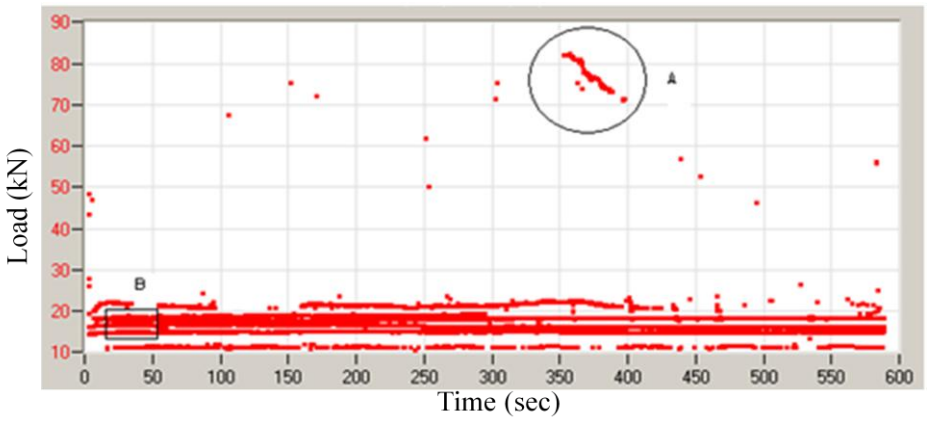

Fig. 5.35 Plot of load level against time

It is clearly shown in this figure that most of AE signal recorded were detected at low load value level (around 18 kN). Only small numbers of AE signal were detected at peak load as shown in circle A in Fig. 5.35. This result suggests that most of AE hits detected in this test come from crack closure and other mechanism associated with it.

In order to gain a better understanding about the mechanisms of AE sources detected at peak load and at around 18 kN, their waveform and data feature were further analysed. Fig. 5.36 shows typical waveform signal detected at peak load (circle A) in the above figure and Fig. 5.37 shows the typical waveform signal detected at around 18 kN (rectangular B).

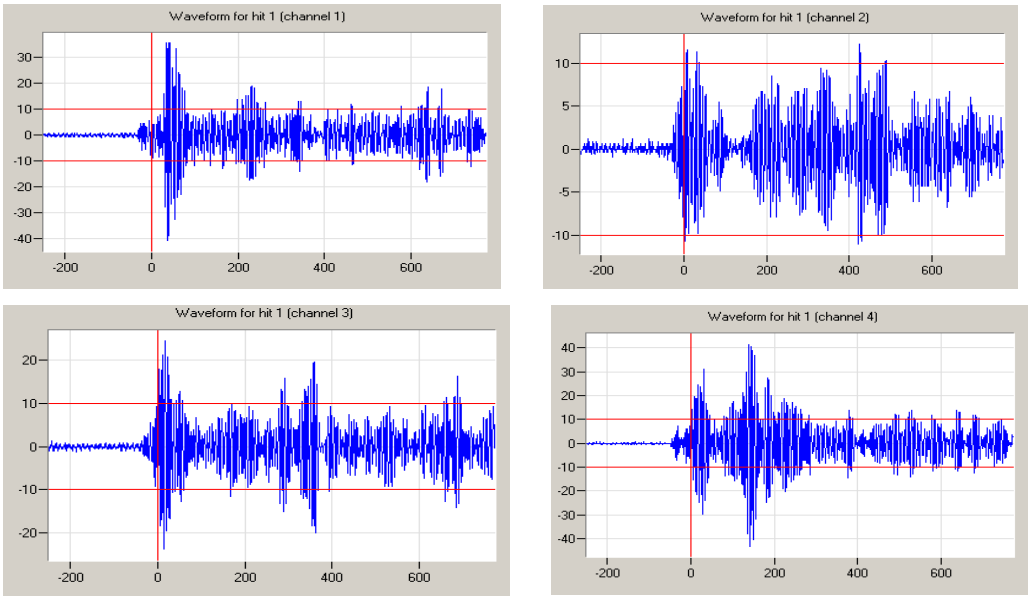

Fig. 5.36 Typical waveform of AE signal released at peak amplitude (circle A)

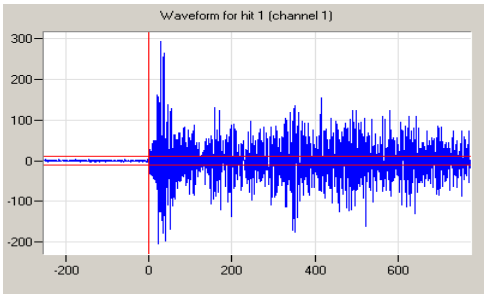

a) Channel 1

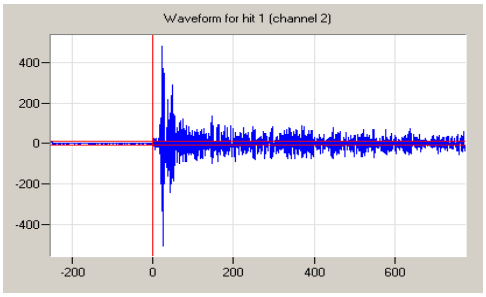

b) Channel 2

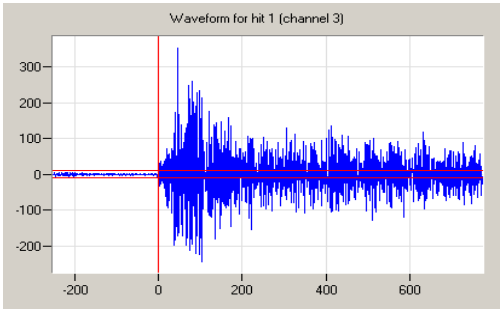

c) Chanel 3

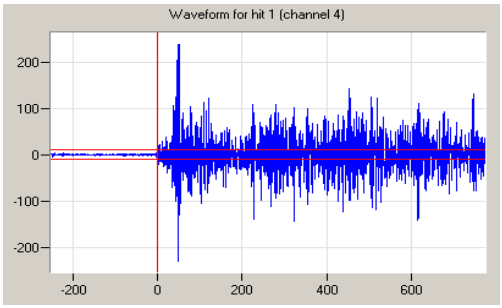

d) Chanel 4

Fig. 5.37 Typical high amplitude signal released at lower load value (around18 kN, rectangular B).

It is found that the amplitude of the AE signal detected at peak load is less than 55dB while the amplitude of AE signal released at 18 kN have various amplitude signal. All high amplitude signals (above 70 dB) were released at this load level.

The low amplitude and small numbers of detected signals at this load level suggest that the primary source associated with the crack growth is difficult to detect in mild steel plate used in this work. The result may also suggest that the crack growth mechanism at the crack tip may be dominated by plastic tearing (Scruby 1987). A few signals with amplitude above the detection threshold (45 dB) detected at peak load may came from the fracture of precipitation material at the grain boundary within the plastic zone (Scruby 1987, Miller and McIntire 2005) and therefore the use of AE signal from crack growth primary source for accurate source location is quite impractical.

All high amplitude signal were detected at a relatively low load level (around 18 kN in this case) which suggest that the signal were caused by the friction of two crack surface during crack closure as suggested by Scruby (1987) and proved by Pollock

(2012). Although the crack closure is considered as secondary event associated with the crack growth, it can be used to accurately locate the crack growth (Scruby 1987). Crack closure usually taking place just after the crack opening at crack tip (crack advancement) due to the abrupt change of stress level associated with the stress relief during crack growth (Miller and McIntire 2005).

Based on this argument, all high amplitude signals detected in this test most probably released by crack closure mechanism. Since crack closure mechanism is much related with the crack opening process, the use of AE parameter from this mechanism is very significant for AE crack growth monitoring. Furthermore, it is impossible to filter the detected signal based on load level in real application of AE crack growth monitoring. Due to this reason, only signal with amplitude more than 70 dB has been used for AE source location and crack length measurement in this study.

iii) DeltaT map and result

DeltaT was claimed to produce improved results compared with TOA method for location of damage in landing gear (Baxter 2007) and therefore it is possible to utilise this method to accurately locate the crack growth and measure the crack length in a plate-like structure.

The accuracy of DeltaT method was also found almost comparable with the WTML (novel method developed in this study) for locating the AE location from H-N source as discussed in chapter four.

However, the nature of actual AE signal released from fatigue crack growth may vary from the standard H-N source, and therefore there is some possibility that DeltaT method can locate the crack growth more accurate than other AE methods. Due to this argument, DeltaT calibration map was developed for this specimen by using H-N sources.

In order to validate the workability of the calibration map, five H-N sources was performed at each notch tip and the location of each source were compared with

calibration map using DeltaT software. The DeltaT locations of H-N sources at notches are shown in Fig. 5.38.

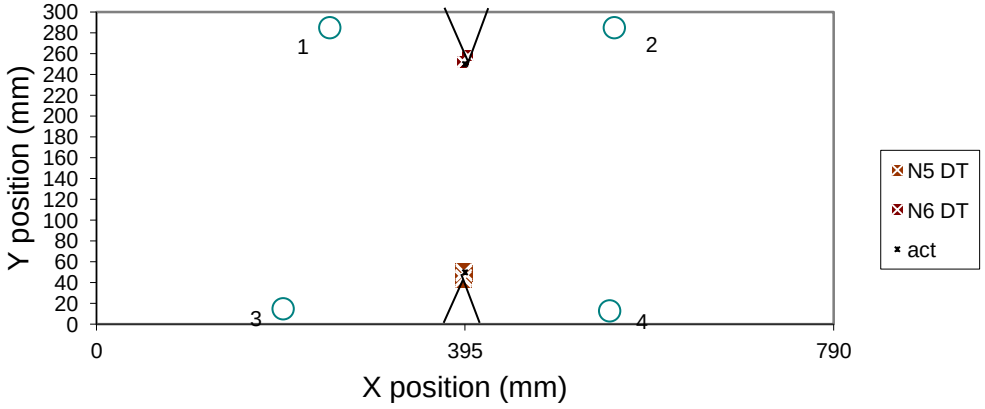

Fig. 5.38 Location of H-N sources at notch using DeltaT location method.

N5 DT is the location of H-N sources at notch tip between sensor 1 and 2 while N6 DT is the location of H-N sources at notch tip between sensor 3 and 4. It is clearly shown in this figure that the location of H-N sources at both notches located by DeltaT method yield a very good agreement with the actual notch tip location and therefore the developed calibration map is very reliable to be use for locating any AE signal from fatigue crack growth in this study.

iv) WTML location result

WTML location was carried out on AE signal detected at five different crack lengths in accordance with the procedure described in Chapter 4. Fig. 5.39 shows a typical result of wavelet transform analysis of an AE waveform from fatigue crack growth.

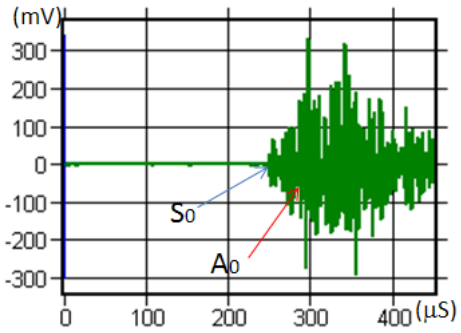

a) Typical waveform signal from crack

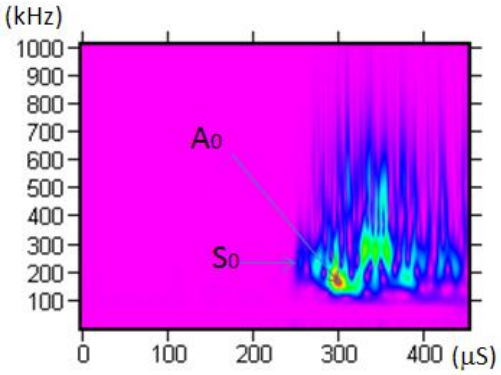

b) Wavelet of the above waveform

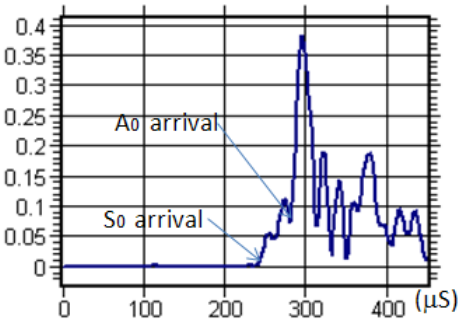

c) Wavelet coefficient of the wavelet

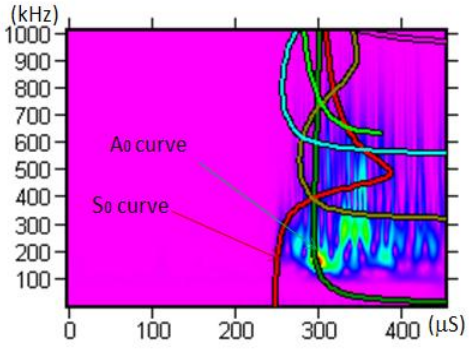

d) Wavelet superimposed with modified dispersion curve

Fig. 5.39 Typical Wavelet transforms analysis result of AE signal from fatigue crack growth

It is clearly shown in this figure that the arrival of S_0 mode from wavelet analysis (Fig. 5.39 b), wavelet coefficient analysis (Fig. 5.39c), is similar with the arrival as shown in original waveform (Fig. 5.39 a). The arrival of A_0 mode can be determined by wavelet coefficient analysis as shown in Fig. 5.39c; however the arrival of A_0 component is difficult to determine by just viewing the time domain waveform signal (Fig. 5.39 a). The temporal separation between S_0 and A_0 mode using wavelet transform analysis was then deployed for source to sensor distance calculation using SSMAL equation (Pullin, 2005).

The modified dispersion curve was constructed based on calculated distance and this curve was superimposed onto the waveform as shown in Fig. 5.39 d). It is clearly shown in this figure that dispersion curves of S_0 and A_0 mode based on this calculation is perfectly matched with correspond modes component in wavelet

transform analysis result. This result suggests that accurate location of fatigue crack growth is obtained using WTML method.

A circle was plotted around each sensor using the calculated source to sensor distance as each radius. The intersection of every circle was then used as the location of the AE sources from fatigue crack growth. Fig. 5.40 shows a typical location of AE event from crack growth sources analysed by WTML location method.

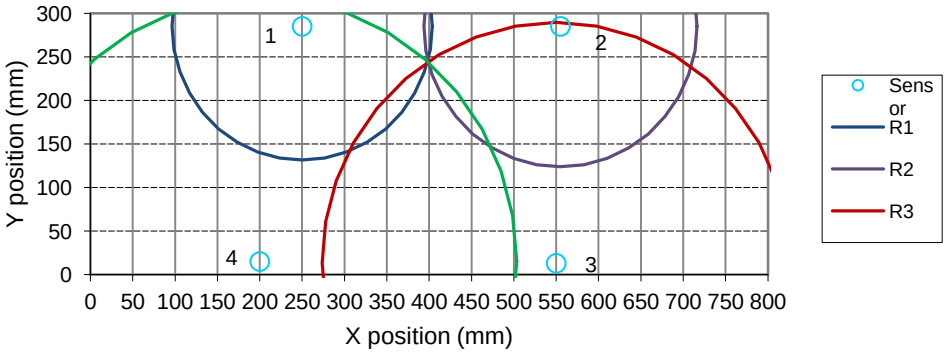

Fig. 5.40 Typical WTML location result of an AE event from fatigue crack shown by circle intersection

Four circles represent the distance of sources from AE sensors calculated by WTML methodology. It is clearly shown that all circles intersect at almost single point suggesting that WTML method developed in this study can accurately locating the AE source from crack growth.

Fig. 5.41 shows typical location of AE events detected around 110,000 cycle of the fatigue crack growth test analysed using WTML, DeltaT, TOA and triple point filtering under planar location setup. The crack length measured by crack gauge at this loading cycle is 2.9 mm.

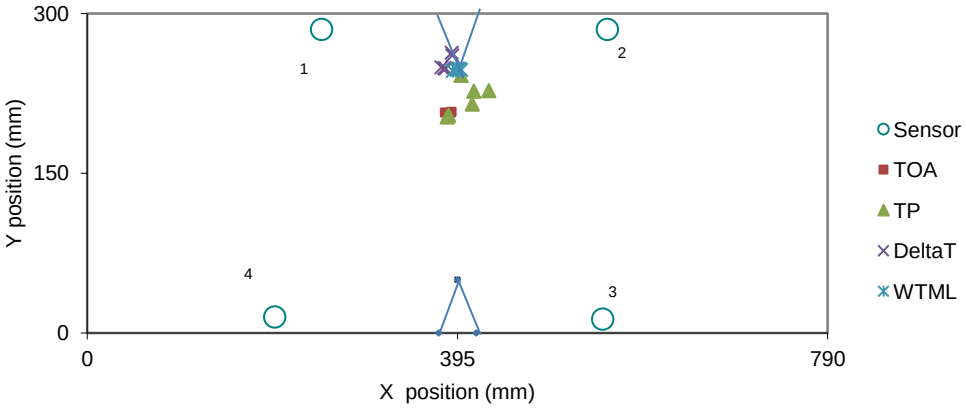

a) AE sources located by various location method

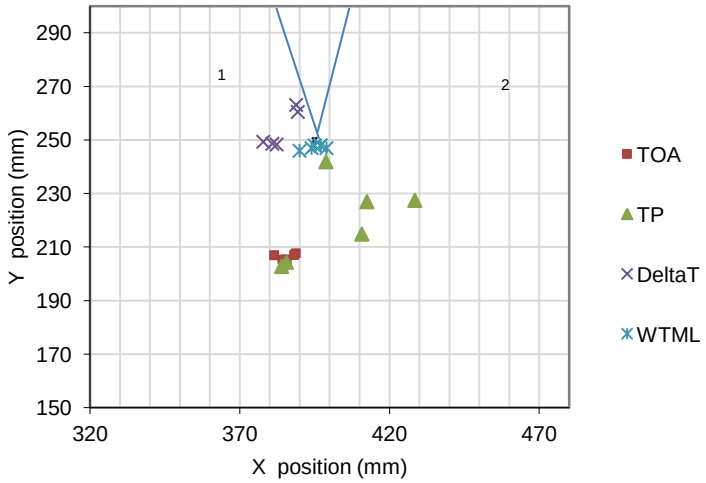

b) Close-up of above figure

Fig. 5.41 Location of five AE events at 110,000 test cycle and b) close-up of AE location

It is clearly shown in the above figure that WTML location yields the most accurate result compared with DeltaT, TP filtering and TOA location methods. The distances between the locations of the sources to the notch were calculated and used as a crack length. This measurement was then compared with the crack length measured by crack gauge and their measurement errors are shown in Table 5.1.

Table 5.1 Source to sensor distance errors for AE data located at 110000 cycles

	Source location error (mm)			
Location method	Actual length (mm)	Average	RMS	STD
TOA	2.9	44.7	41.9	1.1
TP	2.9	35.3	35.1	10.9
DT	2.9	14.1	10.4	1.4
WTML	2.9	3.7	1.7	1.3

It is clearly shown that the source to sensor distance determined using WTML location method produce the smallest error (1.7 mm) compared with other location method. The DeltaT location result produce better location result compared with TP filtering (35.1 mm) and TOA location method (which produces the highest error, 41.9 mm). The TOA error value is considered very high for crack length measurement. However their location results quite precise, with standard deviation about 1.1 mm, which suggest that the error may come from a systematic source. Further investigation was carried out and it was found that the source of error is false triggering as shown in Fig. 5.42.

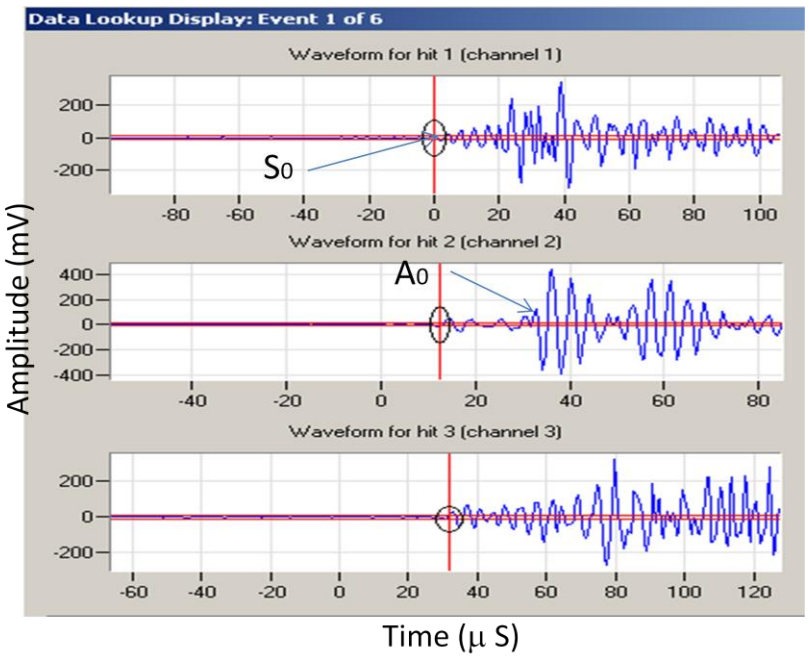

Fig. 5.42 Typical detection threshold triggered by S_0 component

The detection system was triggered by S_0 mode for channel 1, 2 and 3 instead of A_0 as presumed earlier. Since the velocity of S_0 is faster than A_0 mode, the distance between sensors and source calculate based on A_0 velocity will definitely differ from the actual distance which lead to location error.

Fig. 5.43 shows typical location of AE events detected at around 122,000 cycle of the fatigue crack growth test. Crack length measured by crack gauge at this loading cycle is 3.7 mm.

5.4 AE sources located by various location method

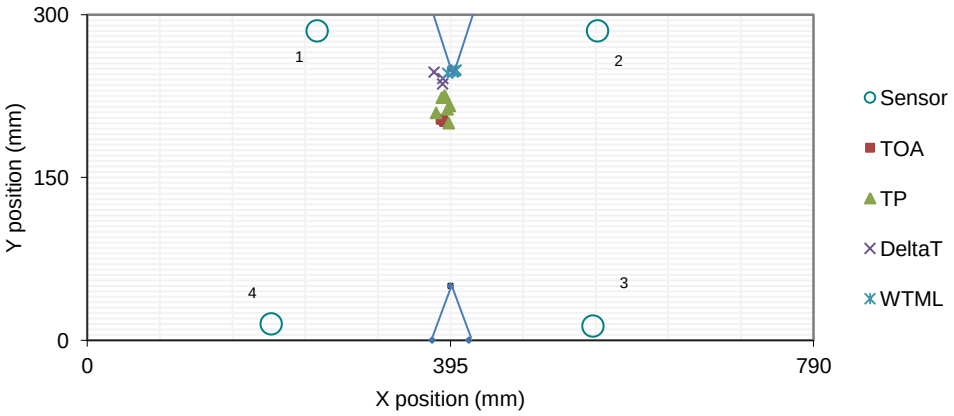

b) Close up of the above figure

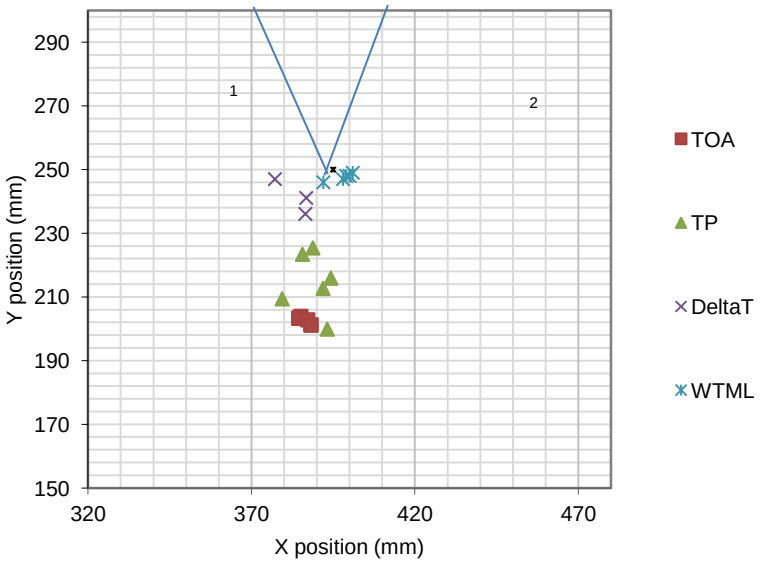

Fig.5.43 Location of five AE events at 122,000 test cycle and b) close-up of AE location

It is clearly shown in this figure that the AE location calculated by WTML method is the closest to the crack tip compared with other location method. The measurement error for each location methods are shown in Table 5.2.

Table 5.2 Source to sensor distance errors for AE data located at 122,000 cycles

	Source location error (mm)			
Location Method	Actual length (mm)	Average	RMS	STD
TOA	3.7	48.2	44.5	0.7
TP	3.7	36.4	33.8	7.2
DT	3.7	15.5	7.8	6.0
WTML	3.7	5.0	1.3	0.6

The WTML location method gives most accurate and precise location result compared with other methods with location error of 1.3 mm and standard deviation of 0.6 mm. DT location result have better location result compare with TP filtering and TOA location methods, however TOA location result give precise result compared with DeltaT and TP filtering method.

Fig. 5.44 shows typical location of AE events detected around 130,000 cycle of the fatigue crack growth test. Crack length measured by crack gauge at this loading cycle is 4.13 mm.

a) AE sources located by various location methods

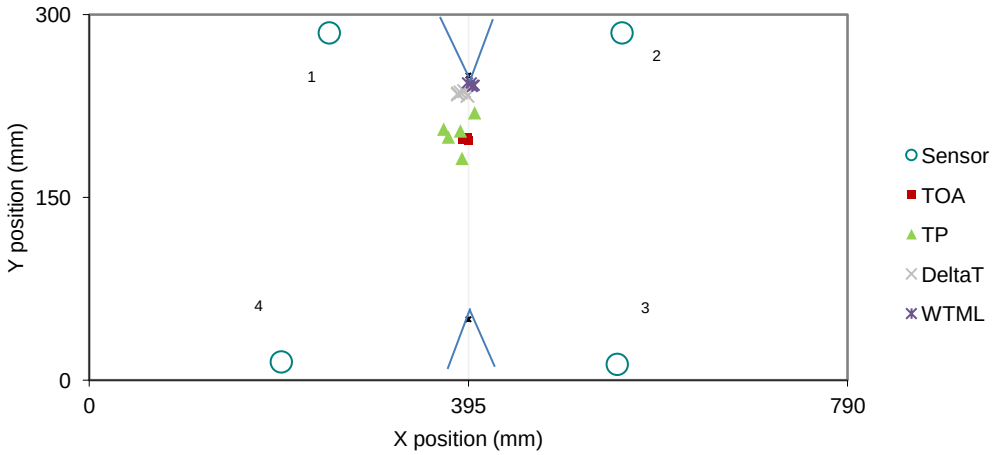

5.5 close-up of the above figure

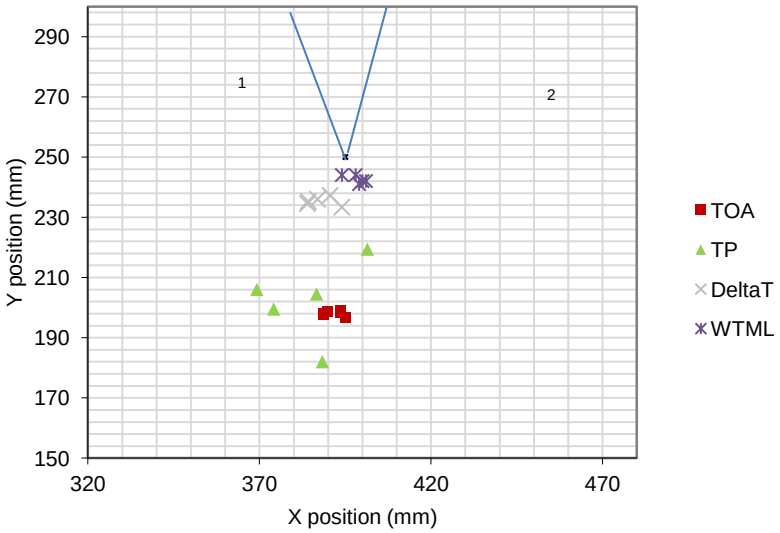

Fig.5.44 Location of five AE events at 130,000 test cycle and close-up of AE location

It is clearly seen in this figure that location trend is same with the previous location analysis with WTML source location give the more accurate location compare with other location methods. AE source location errors for data taken around 130,000 cycles are given in Table 5.3.

Table 5.3 Source to sensor distance errors for AE data located at 130,000 cycles

	Source location error (mm)			
Location Method	Actual length (mm)	Average	RMS	STD
TOA	4.1	52.1	47.9	0.8
TP	4.1	50.3	47.7	9.2
DT	4.1	16.7	10.8	1.5
WTML	4.1	8.4	4.6	1.6

It is clearly shown in this table that WTML location result yield more accurate result compared with other location result.

Fig. 5.45 shows typical location of AE events detected at around 140,000 cycle of the fatigue crack growth test. Crack length measured by crack gauge at this loading cycle is 4.9 mm.

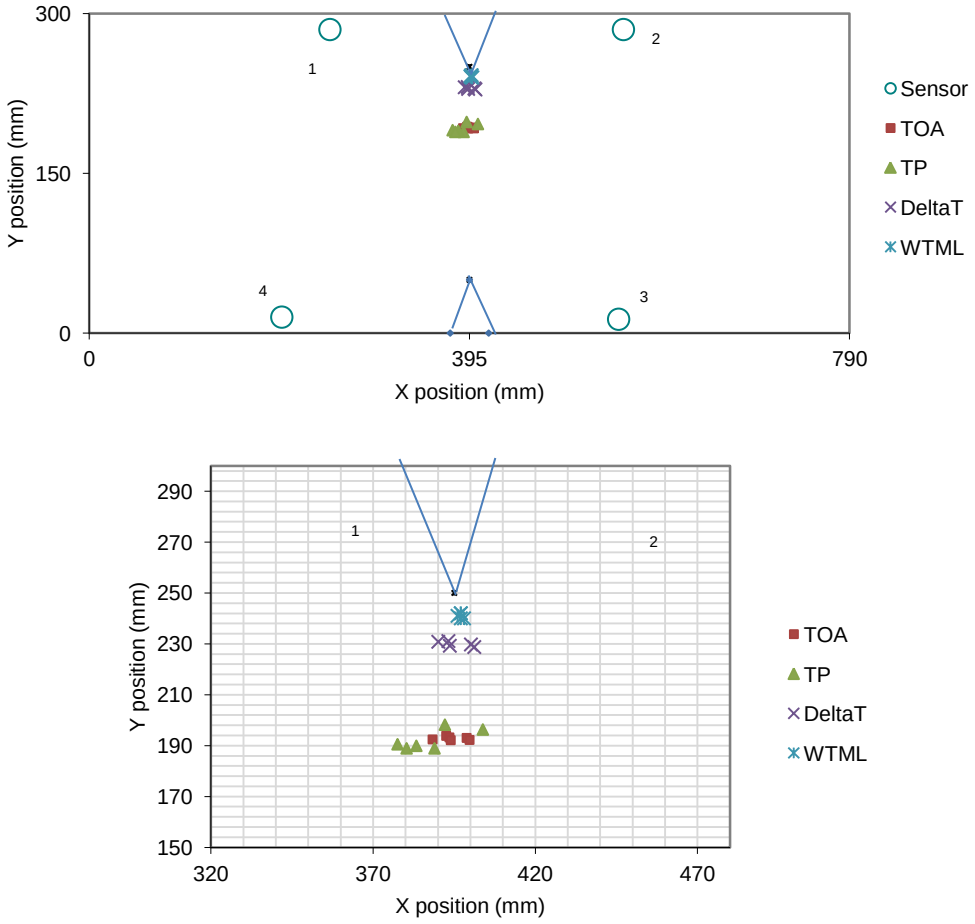

Fig.5.45 Location of five AE events at 140,000 test cycle and close-up of AE location

AE source location measurement error for data taken around 140000 cycles is presented in Table 5.4.

Table 5.4 Source to sensor distance errors for AE data located at 140,000 cycles

	Source location error (mm)			
Location Method	Actual length (mm)	Average	RMS	STD
TOA	4.9	57.3	52.3	0.6
TP	4.9	58.9	54.0	3.9
DT	4.9	20.5	14.2	0.9
WTML	4.9	9.2	3.9	5.5

Fig. 5.46 shows typical location of AE events detected at 155,000 cycle of the fatigue crack growth test. Crack length measured by crack gauge at this loading cycle is 5.7 mm.

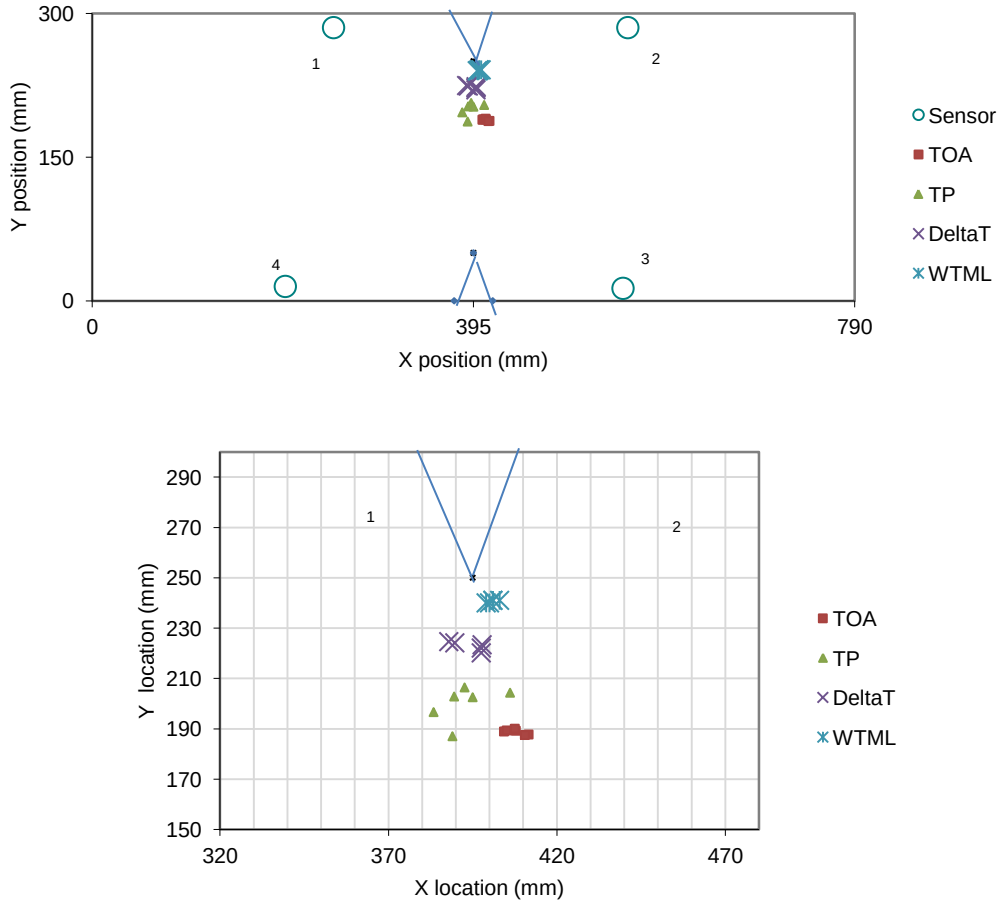

Fig. 5.46 Location of five AE events at 155,000 test cycle and close-up of AE location

Table 5.5 Source to sensor distance errors for AE data located at 155,000 cycles

	Source Location error (mm)			
Location Method	Actual length (mm)	Average	RMS	STD
TOA	5.7	62.6	57.1	1.4
TP	5.7	50.6	45.5	7.2
DT	5.7	27.5	20.1	1.5
WTML	5.7	11	5.0	0.5

Fig. 5.47 shows the plot of crack length calculated by WTML, TP, TOA and DeltaT location method, and that measured by crack gauge against the number of test cycles from the above data.

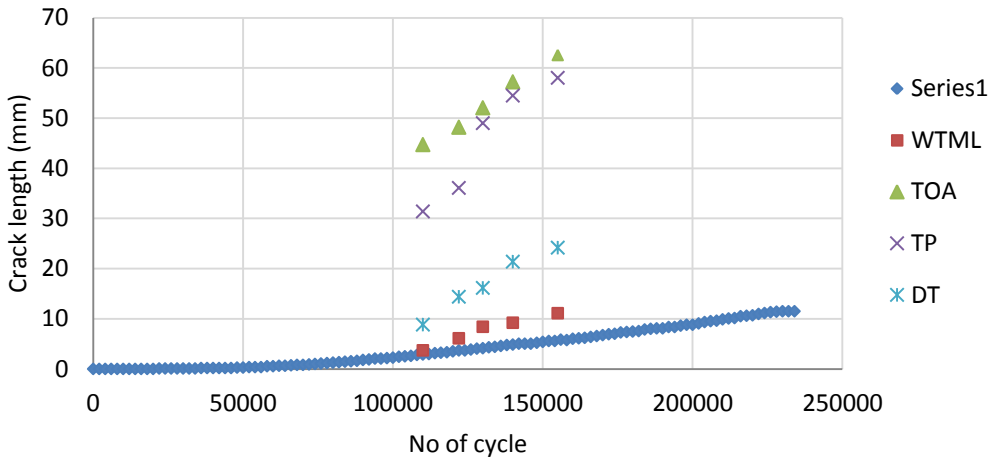

Fig 5.47 Crack length against no of cycle calculated by various AE sources location method.

It is apparent in this figure that WTML location method produced more accurate crack length measurement compared with TOA, TP filtering and DeltaT source location methods. DeltaT location yields more accurate crack length measurement compared with TOA and TP filtering methods. It is clearly shown in this figure that the crack length measurement error using TOA method is very high and it is caused by detection threshold being triggered by the faster S_0 mode instead of A_0 mode component which travels much slower than S_0 mode as previously discussed.

The crack length calculated with WTLM method increases almost linearly as measured by crack gauge while crack length calculated by TOA, TP filtering and DeltaT methods increased exponentially. This measurement discrepancy suggest that a systematic error has been produced during TOA, TP filtering and DeltaT sources location.

Since the previous investigation shows that the main source of TOA location errors came from the triggering due to S_0 mode, the data was then reanalysed using the velocity of S_0 mode instead of A_0 component. Fig. 5.48 shows the plot of crack length calculated by TOA location method using S_0 mode velocity, and that measured by crack gauge against the number of test cycles for the previous data.

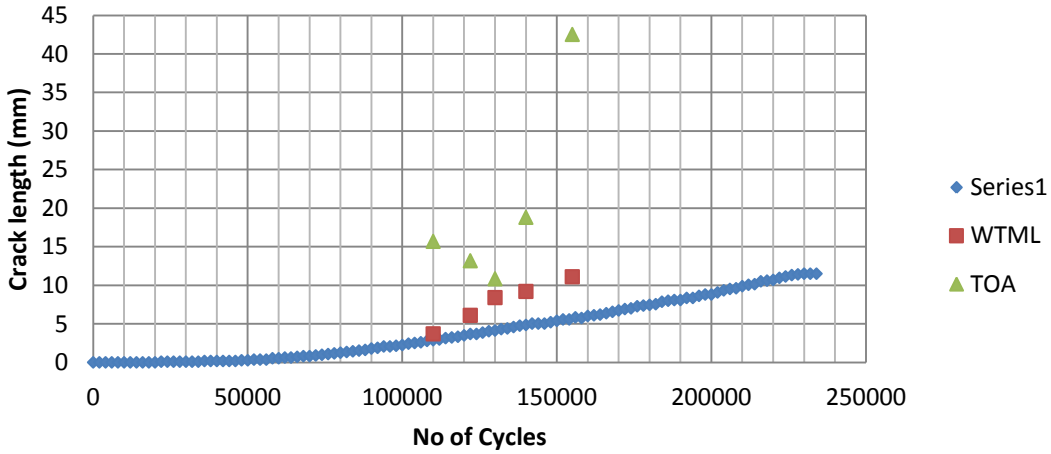

Fig. 5.48 Crack length against no of cycle calculated TOA location using fastest S_0 velocity compared with WTML and crack gauge measurement.

It is clearly shown in this figure that the TOA crack length measurement error was significantly improve compared with the result shown in Fig. 5.47 which uphold the view that the use of correct wave velocity is very crucial for accurate TOA location result. This further supports the case for developing improved location method such as WTML

The triggering issue for TOA was considered to be worthy of further investigation. Fig. 5.49 shows the typical threshold crossing for the AE signal detected around 122, 000 cycles.

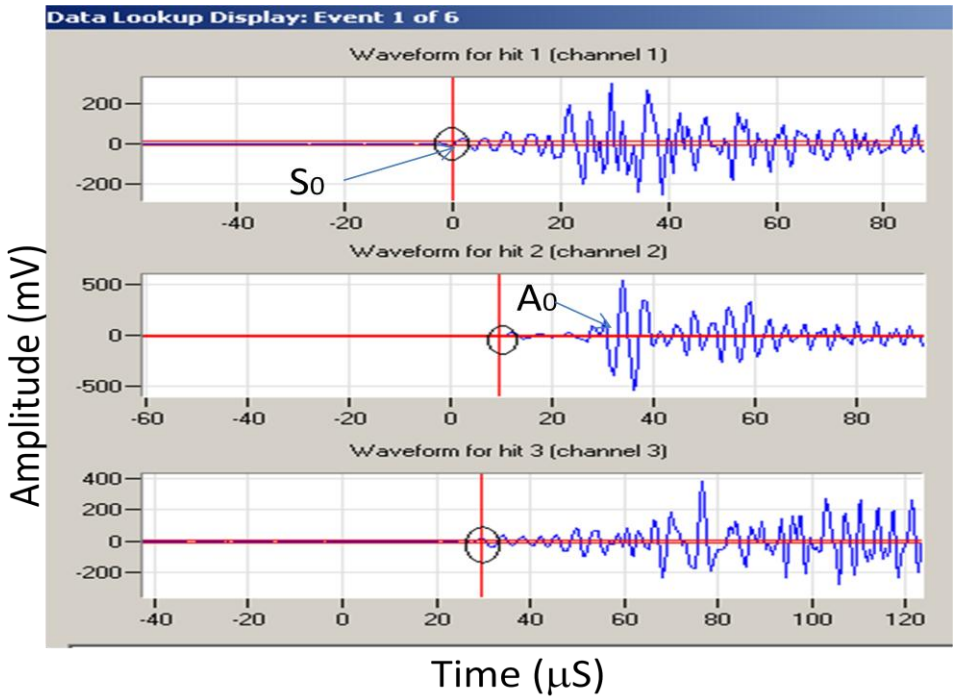

Fig. 5.49 Typical threshold crossing for signal detected around 122,000 cycles

Although the detection threshold were triggered by S_0 component for all detection sensors, however their location accuracy is different from that locate at around 110,000 cycles.

This inconsistency most probably due to the S_0 mode wave velocity is highly dispersed with frequency content of the signal. The frequency of detected AE signals at various locations may be not exactly same to each other; therefore small change in frequency content will cause huge change of propagation velocity. The used of incorrect wave velocity is then led to massive location error.

There also some possibilities that the detection threshold were triggered by other wavemode component that propagates with different wave velocity.

Further investigation has been carried out on the signals detected at 130,000, 140,000 and 155,000 cycles and their results are shown in Fig. 5.50, 5.51 and 5.52 respectively.

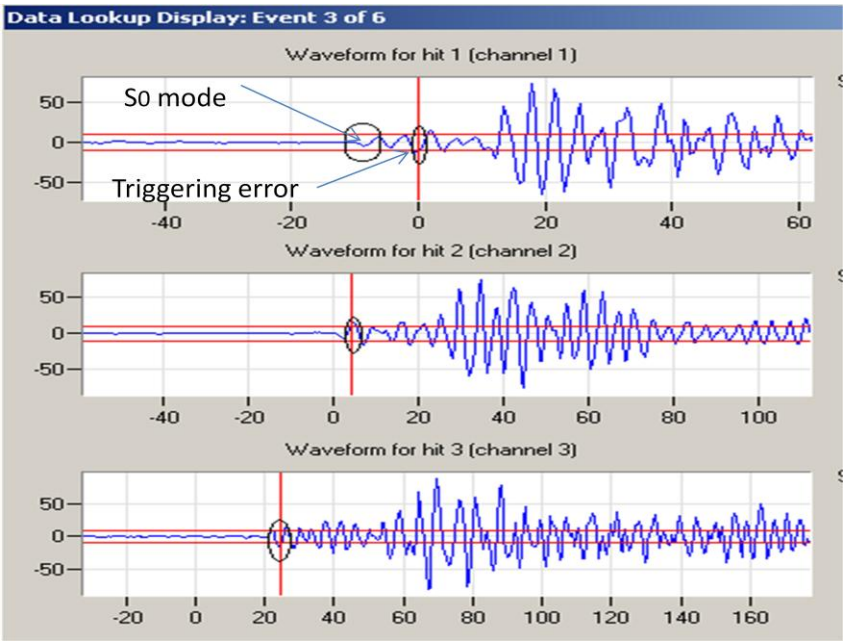

Fig. 5.50 typical threshold crossing for AE signal detected around 130,000 cycles

It is clearly shown in Fig. 5.50 that the detection threshold for channel 1 was not triggered by the fastest S_0 mode; however the detection threshold was triggered by other wave component. This incorrect triggering was then led to the location inaccuracy. In this case, the most possible reason for incorrect triggering is that the amplitude S_0 mode is smaller than the detection threshold, however the reflection of S_0 mode from both sides of the plate interfere at sensor surface. This positive interference may have higher amplitude than detection threshold and therefore triggered the detection system.

If more than one sensor were triggered by incorrect wave mode, the location error from other incorrect triggering will be added to the location error as shown in Fig. 5.51.

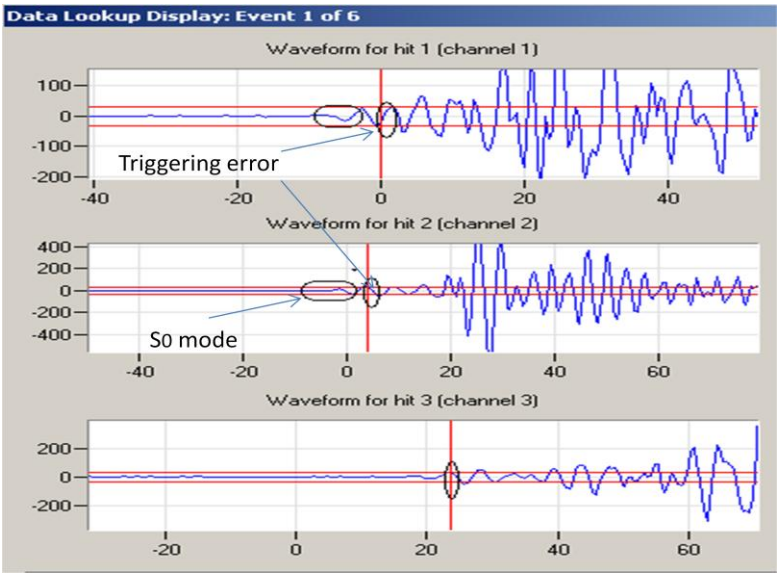

Fig. 5.51 Detection threshold crossing of AE signal detected around 140,000 cycles

It is clearly shown in this figure that the channel 1 and channel 2 were triggered by incorrect wave component while channel 3 was triggered by S_0 mode. These incorrect triggering will increase the location error for AE location at 140,000 cycles. Instead of having incorrect triggering by same source at more than one sensor, it is possible that the detection threshold was triggered by more than one source as shown in Fig. 5.52.

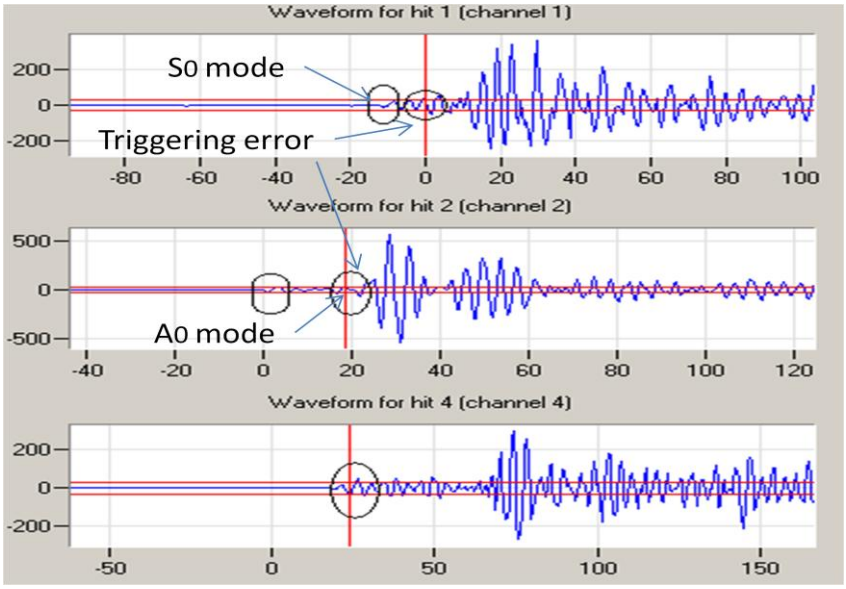

Fig. 5.52 Detection threshold crossing of AE signal detected around 155,000 cycles

It is clearly shown in this figure that the detection threshold was triggered by incorrect wave component suspected from side reflection, channel 2 were triggered

by A_0 component which travel much slower than A_0 component. This multiple source of triggering will cause the location error for AE signals detected at 155,000 cycles is higher than that detected at 140,000 cycles.

It also found in this study that the TP filtering location give a very inconsistent and imprecise result compared with other location techniques. The possible reason for the large measurement inconsistency experienced by TP filtering method is also caused by triggering error. The S_0, A_0 and A_1 modes actually not intersect exactly at the same point.

For waveform filtered in the range of 390 to 400 kHz, there is the possibility that the faster S_0 mode propagates faster than other modes components in this frequency range and therefore triggers the detection threshold. This error can be improve by increase the detection threshold however, since the signal at high frequency range are highly attenuate, the whole signal may be passed the triggering threshold without detected.

Furthermore, DeltaT location method used in this study also work based on first threshold crossing and therefore incorrect triggering may also affect the accuracy of this location method.

5.4 Summary of findings

- AE has been successfully used to detect and characterise the stress wave signals released during tensile-tensile fatigue loading based on AE data feature analysis. It was found that:
    i. The main AE sources mechanisms are crack surface fretting and plastic tearing. Base on AE-load data analysis, high amplitude AE signals (around 70 dB) were released at lower load value (around 18 kN) which suggests that this source is produce by crack surface fretting.

    ii. AE signal released at peak load (80 kN) have relatively lower amplitude (less than 55 dB). These suggest that the crack opening

mechanisms during fatigue crack growth is tearing of plastic deformation area in the vicinity of the crack tip.

- WTML was successfully used to accurately locate the AE signal released from fatigue crack growth. The accuracy of WTML is much better than TOA, DeltaT and triple point filtering location methods.

- WTML was successfully used to determine the crack length in the steel pipe with the maximum measurement error of 5 mm. A step by step guide to WTML methodology to measure the crack length is shown in Appendix 1

- WTML based location technique can be used to measure crack length if accurate enough.

- The TOA location method produces the largest location inaccuracy. The main sources of location errors are triggering error and therefore TOA planar location based on threshold crossing is not reliable to be used for accurately measure the fatigue crack length.

CHAPTER 6: CONCLUSIONS AND FUTURE WORKS

Managing the safety aspect of ageing nuclear power plant is very important to ensure their integrity and functional capability is achieved throughout the entire plant service life. Thermal fatigue is among the major ageing mechanism in nuclear power plant piping system and a through wall crack and leakage are the most likely modes of failure. Acoustic emission (AE) testing can be used to globally locate an active source emitted from cracking area by using an array of sensors.

The cost saving of deploying an AE inspection method can be achieved by minimisation of the time to perform the follow up test due to the localisation of the damage source and the downtime associated with plant shut down.

6.1 Summary of Conclusion

An accurate AE source location methodology has been developed in this work using wavelet transform analysis (WT) and modal location theory. This new method is known as Wavelet Transform analysis and Modal Location (WTML). This novel method utilised the dispersive characteristic of Lamb waves and time-frequency discrimination capability of wavelet transform analysis.

It is possible to use AE technology for measuring the crack length in steel pipes based on the proposed location method. The accuracy of WTML is found to be superior to other AE location methods.

6.1.1 WT Source location of H-N source in steel plate and pipe

- Novel WTML method has been successfully developed. This method utilised modal location theory (velocity of different wave component) and time-frequency discrimination capability of wavelet transform analysis.

- It is found that WTML is more accurate than conventional TOA. WTML overcomes false threshold triggering and time delay between first arrival and first threshold crossing.

- WTML is more accurate than TP filtering. TP is expected to produce more accurate source location than FTC TOA since the detection threshold is triggered by S_0, A_0 and A_1 simultaneously. However, TP occurs at relatively higher frequency at which AE signal highly attenuate, increase the time delay between FTC and first arrival which lead to location inaccuracy.

- WTML improve the accuracy of SSMAL due to the time-frequency discrimination capability of WT analysis which improves the temporal separation measurement error.

- WTML is comparable with DeltaT in term of accuracy, however it is considered superior since the proposed method does not requires calibration of testing area and the sensors can be moved anywhere on the test item. Furthermore, single sensor WTML for monitoring crack growth in nuclear piping especially circumferential crack in welded area is possible.

6.1.2 WT Source location for fatigue crack growth in steel plate

- AE has been successfully used to detect and characterise the stress wave signals released during tensile-tensile fatigue loading based on AE data feature analysis. It was found that:
    - The main AE source mechanisms are crack surface fretting and plastic tearing. Base on AE-load data analysis, high amplitude AE signals (around 70 dB) were released at lower load value (around 18 kN) which suggests that this source is produce by crack surface fretting.

- AE signal released at peak load (80 kN) have relatively lower amplitude (less than 55 dB). These suggest that the crack opening mechanisms during fatigue crack growth is tearing of plastic deformation area in the vicinity of the crack tip.

- WTML was successfully used to accurately locate the AE signal released from fatigue crack growth. The accuracy of WTML is much better than TOA, DeltaT and triple point filtering location methods.

- WTML was successfully used to determine the crack length in the steel plate with the maximum location error of 5 mm. The step by step instruction for WTML methodology to measure the crack length is shown in Appendix 1

- WTML provides improved accuracy over DeltaT, TOA and triple point filtering methods.

- The TOA location method produces the largest location inaccuracy. The main sources of location errors are triggering error and therefore TOA planar location based on threshold crossing is not reliable for accurate fatigue crack length measurement.

6.1.3 WT Source location for fatigue crack growth in steel pipe

- It has been possible to confirm the detection and location of AE associated with fatigue crack growth using WD sensor was successfully used to detect AE from fatigue.

- AE was well located. TOA linear location provided an invaluable tool for separating AE from fatigue crack growth from the AE signal associated with the load point.

- For ‘clean’ AE signal, WTML was able to locate the fatigue crack signal detected by TOA planar location method and showed a good agreement with TOA planar location result.

- WT denoising analysis is capable of filtering out any unwanted components from noisy waveform signals. SSMAL of de-noise waveform signal shows good agreement with TOA planar location result.

6.2 Recommendation for further work

The following work is recommended for further investigation;

i. Conduct a fatigue crack growth test which ensures that the crack can be grown from the notch tip. This is very important for verifying the workability of WTML methodology to accurately locate and monitor the crack length in pipe structures.

ii. Conduct water flow and turbulence to simulations to represent the actual noise sources in nuclear piping. Further development of source characterisation is required for pick the right AE signals from crack growth and eliminate background ‘noise’ signal and ultimately discriminate fatigue crack signal from other sources such as fretting, turbulence, water flow and leaking. This can be achieved by improving the AE signal filtering methodology (either using pattern recognition approach or other methods) or DWT denoising.

iii. Develop automation system for WTML location. The system should include
   - Algorithm for automatic detection of AE signal from crack growth either using proper filtering technique or artificial neural network.

   - Algorithm for compressing the ‘noise’ from the crack growth signals

- Algorithm for SSMAL based on WT analysis

- Algorithm for validate the source to sensor distance using modified dispersion curve and

- Iterative algorithm for determine the intersection point/triangulation point

iv. Further field test should be conducted to allow comparison between current NDT technique and WTML AE testing. It is important to gain confidence in WTML AE technique and provide more case studies for future research.

CHAPTER 7: REFERENCES

Addison, P.S. (2005). "Wavelet transforms and the ECG: a review". Physiological Measurement. 26: R155-R199

Aggelis, D.G, Kordatos, E. Z., Matikas, T.E. (2011). "Acoustic Emission for Fatigue Damage Characterization in Metal Plates". Mechanic Research Communication. **38**:106-110

Alfouri, M and Daqrouq, K. (2008). "ECG Signal denoising by Wavelet Transform Thresholding". American Journal of Applied Science. **5**(3): 276-281

Aljets, D., Chong, A., and Wilcox, S., (2010). "Acoustic Emission Source Location in Plate -like Structures Using a Closely Arranged Triangular Sensor Array". The 29th European Conference on Acoustic Emission Testing 2010, Vienna.

ASME (2006). ASME Boiler and Pressure Vessel Code, Section III.

ASME (2006). ASME Boiler and Pressure Vessel Code, Section XI.

ASTM (1982). "Standard Definitions of Terms Relating to Acoustic Emission" American Society for Testing and Materials, E610-82

ASTM (1994). "Standard Guide for Determining the Reproducibility of Acoustic Emission Sensor Response", American Society for Testing and Materials, E976 – 94

ASTM (1997). "Standard Guide for Mounting Piezoelectric Acoustic Emission Sensors", American Society for Testing and Materials, E650 – 97

ASTM (1995). "Standard Test Method for Liquid Penetrant Examination." American Society for Testing and Materials E 165-95

Atwood, C.L., Shah, V. K., Galyean, W.J. (1999). "Analysis of Pressurised Water Reactor Primary Coolant Leaks Events Caused by Thermal Fatigue." ESREL '99-European Safety and Reliability Conference

Baxter, M.G. (2005). “Detection of Fatigue Crack Growth in Aircraft Landing Gear, 4 Point Bend Test Specimens”. Key Engineering Materials. **293-294**: 193-200

Baxter, M., Pullin, R., Holford, K., Evans, S. L. (2007). “Delta T sources location for acoustic emission, Mechanical system and Signal Processing.” **2**: 1512-1520

Bieniussa, K. W. B, Reck, H. (1999). “Technical Notes. Piping specific analysis of stresses due to thermal stratification”. Journal of Nuclear Engineering and Design. **190**: 239–249

BSI (1998). “Method for determination of the rate of the fatigue grack Growth in metallic materials: Fatigue growth rate of above 10^{-8} m per cycle“. BS 6835 – 1: 1998

BSI (1993). “Methods of Fatigue Testing, British Standard. Guide to general principles”. BS 3518- Part 1: 1993

Chang, H., Han, E.H., Wang, J.Q., Ke, W. (2009). “Acoustic emission study of fatigue crack closure of physical short and long cracks for aluminium alloy LY12CZ”. International Journal of Fatigue. **31**, 403–407

Chang, H., Han, E.H., Wang, J.Q., Ke, W. (2006). “Analysis of modal acoustic emission signals of LY12CZ aluminium alloy at anodic and chatodic polarization”. NDT&E International. **39**:8-12

Daubechies, I. (1990). “The Wavelet Transform Time-Frequency Localization and Signal Analysis”. IEEE Transaction on Information Theory, **36**(5): 961-1005

De Souza (2008). “Conversion from geometrical to electrical model of LVDT”. 16th IMECO TC4 Symposium. Florence, Italy Sept.

EPRI (2005), "*Materials Reliability Program: Management of Thermal Fatigue in Normally Stagnant Non-Isolable Reactor Coolant System Branch Lines (MRP-146)".* Palo Alto, CA: 2005. 1011955.

Gosselin, S.R., Heasler, P.G., Simonen, F.A., Doctor, S.R., (2007). "Fatigue Crack Flaw Tolerance in Nuclear Power Plant Piping".

Fine, M.E and Chung Y.W. (1996). "Fatigue failure in metal." Metal Handbook, 10th ed. ASM international. 19: 148

Ganesan, R., Das, T.K., Sikder, A.K., Kumar, A. (2003). "Wavelet based identification of elimination defect in CMP (Cu-Low k) using non-stationary Acoustic Emission." IEEE Transaction on Semiconductor Manufacturing, **16**(4)

Gorman, M. R., (1991). "Plate Wave Acoustic Emission." J. Acoustic Society of America. **90**(1)

Grondel, S., Delebarre, C., Assad, J., Dupuis, J-P., Reithler, L., (2002). "Fatigue crack monitoring of riveted strap by Lamb waves analysis and Acoustic Emission techniques". NDT&E International. **35**:137-146

Hamstad, M. A., Gallagher, A. O., and Gary, J., (2002). "A Wavelet Transform Applied to Acoustic Emission Signal: Sources Identification". Journal Acoustic Emission. **20**: 39-61

Han, K.S and Oh, K.H. (2006). "Acoustic emission as a tool for fatigue assessment". Key engineering Materials. **306-308**, 271-278

Harker, A. H. (1988). "Elastic Waves in Solids: with applications to the non-destructive testing of Pipelines." British Gas PLC, Adam Higler, Bristol.

Hatrun Corporation (2009). "Krak-gage® Theory of Operation". http://www.krak-gage.com. Download on Tuesday, December 01, 2009.

Hatrun Corporation (2009), "Krak-gage® drawing, specification and selection table". http://www.krak-gage.com Download on Tuesday, December 01, 2009.

Hayashi, M. (1998). "Thermal fatigue strength of type 304 stainless steel in simulated BWR environment". Nuclear Engineering and Design. **184**: 135-144

Heiple, C. R and Carpenter, S. (1987). "Acoustic emission produced by deformation of metals and alloys- a review". J. Acoustic Emission, **6**(4): 215-237

Hirschberg, P., (2000). "Mitigation of Thermal Fatigue in Unisolable Piping Connected to PWR Reactor Coolant Systems (MRP-29)." EPRI, Palo Alto, CA. 1001017.

Holford, K.M. and Carter D.C. (1999). "Acoustic Emission Sources Location". Key Engineering Materials.167-168: 162-171

Holford, K.M., 2000, "Acoustic Emission - Basic Principles and Future Directions", Strain. **36** (2):

Holland, S., Kosel, T., Weaver, R., Sachse, W. (2000). "Determination of Plate Source, Detector Separation from one Signal". Ultrasonic **38**: 620-623

Hsu, N.N. and Breckenridge, F.R. (1979). " Characterization and Calibration of Acoustic Emission Sensors." Material Evaluation. **39**: 60-68

Huang, M., Jiang L., Liaw, P.K., Brooks, C. R., Seeley, R., and Klarstrom, D. L., (1998). "Using Acoustic Emission in Fatigue and Fracture". Materials Research, Journal of Materials. **50** (11):

IAEA (1993). “Applicability of leak before break concept”. International Atomic Energy Agency, Vienna. IAEA-TEC DOC 710

IAEA (2003). “Assessment and management of ageing of major nuclear power plant components important to safety”. International Atomic Energy Agency, Vienna. IAEA-TECDOC-1361

Jeong, H. (2001). “Analysis of plate wave propagation in anisotropic laminates using a wavelet transform,” NDT&E International, **34**: 185-190

Jeong, H. and Jang, Y-S. (2000). “Fracture source location in thin plates using the wavelet transform of dispersive waves,” IEEE Transactions on Ultrasonic, Ferroelectrics and Frequency Control. **47**:612-619

Jeong, H. and Jang, Y-S. (2000). “Wavelet analysis of plate wave propagation in composite laminates,” Composite Structures, **49**: 443-450

Jingpin, J., He, C., Wu, B., Fei, R., and Wang, X. (2004). “Application of Wavelet Transform on Modal Acoustic Emission Source Location in Thin Plates with One Sensor”. International Journal of Pressure Vessels and Piping. **81**: 427-431

Jingpin, J, Bin, W., Cunfu, H. (2008). “Acoustic Emission Source Location Methods Using Mode and Frequency Analysis”, Structural Control and Health Monitoring. **15**:642-651

Khan, M. A, Shoji, T. and Takahashi, H. (1982). “Acoustic from cleavage microcracking in alloy steels”. Metal Science. **16**:118-126

Khan, M. A, Shoji, T., Niitsuma, H, and Takahashi, H. (1982). “Acoustic Emission Rating Parameter for Prediction of Tearing Instability in Structural Materials”. Engineering Fracture Mechanic. **16**(5) 645-658

Krautkramer, J & Krautkramer, K. (1975). “Ultrasonic Testing of Materials”. Springer- Verlag, Berlin, 3rd Edition.

Kupperman, D.S. & Clayton, T.N. (1985). “Evaluation of method for leak detection in reactor primary systems”. Journal of Nuclear Engineering and Design. **89**(2-3): 371-378

Kwon, O. Y. and Lee, K.,(2000), “ Acoustic Emission for Detection of Fatigue Damage” in *Acoustic Emission - Beyond Millennium* edited by T. Kishi, M. Ohtsu and S. Yuyama, Elsevier, Oxford.

Li, Z., Xia, S., Wang, J., Su, X.(2006) “Damage detection of cracked beams based on wavelet transform.” International Journal of Impact Engineering. **32**: 1190-1200

Liaw, P.K, Logsdon, W.A, Roth, L.D., and Hartmann, H.R.,(1985) “Krak–gage for Automatic Fatigue Crack Growth Rate Testing,” A Review, in “ Automated Test methods for Fracture and Fatigue Crack Growth, ASTM STP 877, W.H. Cullen, R.W Landgraf, L.R Kaisand, and J.H. Underwood, Eds., American Society for Testing and Materials, Philadelphia, pp. 177-196

Maji and Sapathi (1995). “Acoustic Emission Source Location Based on Lamb Wave.” Proceedings of Engineering Mechanics. **1**: 597-600

Miller, R. K. and P. McIntire, (2005). Acoustic Emission Testing, Vol. 5, 3rd ed., NDT Handbook, ASNT.

NEA/CSNI/R (2005) 8, (2005). “Thermal cycling in LWR component in OECD-NEA member countries”. Nuclear Energy Agency

PAC (2005). “DiSP with AEwin User’s Manual Rev. 3”. Physical Acoustic Corporation, Princeton, New Jersey, USA.

Park, H.C. & Kim, D.-S. (2001), Evaluation of the dispersive phase and group velocities using harmonic wavelet transform. NDT&E International **34**: 457-467

Pollock, A. A. (1986). “Classical Wave Theory in AE Testing”. Progress in Acoustic Emission 111. The Japanese Society of NDI.

Pollock, A. A., 1989. Acoustic Emission Inspection, Metals Handbook, 9th Edition, ASM International. **17**:278-294

Pollock, 2012. “AE Observation During Cyclic Testing of A572 Steel Laboratory Specimen”. 30th European Conference on AE Testing. Granada.

Prosser W.H, Dorighi, J., Gorman M.R. (1992). “Extensional and flexural waves in a thin-walled graphite/epoxy tube.” J. Compos. Mater. **26**:2016–27

Prosser, W.H., Gorman, M.R. (1994). “Plate mode velocities in graphite/epoxy plates - Part 1”. J. Acoustic Soc. Am. **96**:902–907

Pullin, R., Holford, K.M. and Baxter, M.G. (2005). “Modal Acoustic Emission Signals from Artificial and Fatigue Crack Sources in Aerospace Grade Steel, Key Engineering Materials. **293-294**:217-226

Rindorf, H.J. (1981). “Acoustic Emission Source Location in Theory and in Practice.” Bruel and Kjaer Technical Review. **2**: 3-44

Roberts, T.M., Talebzadeh, M. (2003). “Acoustic emission monitoring of fatigue crack propagation”. Journal of Construction Steel Research. **59** (6), 695- 712

Roberts, T.M., Talebzadeh, M. (2003). “Fatigue life prediction based on crack propagation and acoustic emission count rates”. Journal of Construction Steel Research. **59**(6): 679-694

Rodgers, J.M, Morgan, B.C., Richard M. Tilley, R.M., (1996) ”Acoustic emission monitoring for inspection of seam-welded hot reheat piping in fossil power plants,” *SPIE Conference on Non-destructive Evaluation Techniques for Aging Infrastructure & Manufacturing*, Vol. 2947.

Scruby, C. B. (1987). “An Introduction to Acoustic Emission”, J. Phys, E: Sci. Instrument. **20**: 946-953

Shigley, J. E., Mischke, C. R. and Budynas, R. G. (2004) “Mechanical Engineering Design, 7th Edition, mcgraw-Hill

Singh, P. J., Mukhopadhyay, C.K., Jayakumar, T., Mannan, S.L., Raj, B. (2007). “Understanding fatigue crack propagation in AISI 316 (N) weld using Elber’s crack closure concept: Experimental results from GCMOD”. International Journal of Fatigue, **29**, 2170–2179

Surgeon, M. and Wevers, M. (1999). “One sensor linear location of acoustic emission events using plate wave theory”. Materials Science and Engineering. A265: 254–261

Takemoto, M., Nishino, H., Ono, K. (2000). “Wavelet Transform-Application to AE signals analysis” in *Acoustic Emission - Beyond Millennium* edited by T. Kishi, M. Ohtsu and S. Yuyama, Elsevier, Oxford

Talebzadeh, M. (2001). “Assessment of Structural Integrity based on Acoustic Emissions”. PhD Dissertation. Division of Structural Engineering, University of Wales Cardiff

Theobald, P., Zeqiri, B., Avison, J., (2008). “Couplants and their influence on AE sensor sensitivity”. J. Acoustic Emission, **26**: 91-97

Vallen, H. “AE Testing Fundamentals, Equipment, Applications,” NDT.net - September 2002, Vol. 7 No.09.

Vallen (2009). “Vallen System website.” http://www.vallen.de, Download on Tuesday, June 23, 2009, 12:01:40 PM

Zhihao, J., Dan, W., Wen, J. (2009). “The wavelet transform in the acoustic emission signal feature extraction of the rubbing fault”. DOI 10.1109/DBTA.2009.164

Zhao, J. R., Ma, Y. and Gao, H. (2000). “Denoising method of AE signal by using wavelet transform”. (download from http://www.ndt.net/ on 10 May 2010)

Ziola, S. M., and Gorman, M.R. (1991). “Source Location in thin plates using cross correlation.” Journal of Acoustical Society of America. 90(5):2551-2556.

Appendix A: Wavelet Transform Analysis

Fundamental of Wavelet Transform

A wavelet transform is a time-frequency representation technique which describes a signal by using the correlation translation and expansion (rescaling) of a function called a mother wavelet. Fig. A1 shows how multi resolution is achieved by wavelet transforms analysis when compared with STFT.

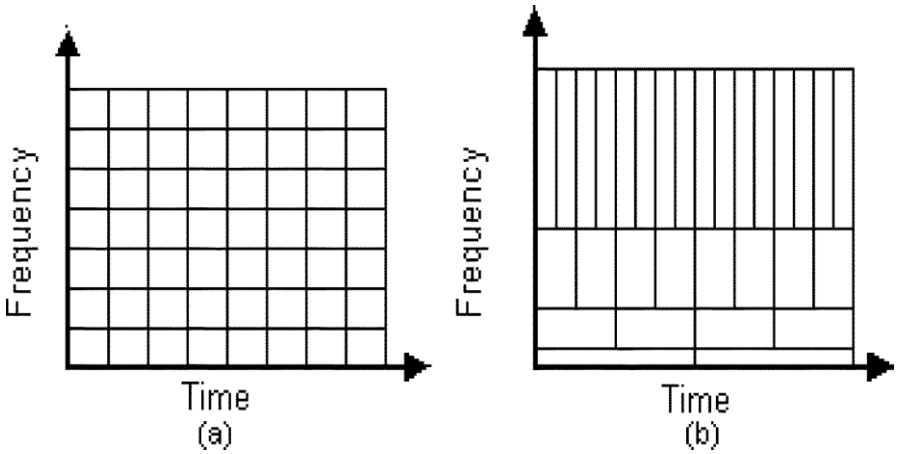

Fig. A1 (a) STFT with fix window and (b) WT with variable aspect window (Ganesan et. al 2003)

Temporal analysis is performed with a contracted high frequency mother wavelet, while frequency analysis is performed with dilated, low frequency of the same mother wavelet. The translation operation allows signal features to be isolated in times while the dilation operations allow identifying signal features that exist at different frequencies. In this way, the wavelet transform represents a signal as a sum of wavelets with different frequency components (Takemoto 2000, Addison 2005).

Wavelet transforms analysis can be divided into two categories, continuous wavelet transform and discrete wavelet transform (DWT). The continuous wavelet transform is calculated by the convolution of the signal and wavelet function (Addison 2005).

Continuous wavelet transform

A wavelet function $\psi(t)$ is a small oscillating wave. This analysing function contains both the analyzing shape and the window. This function can be considered

as wavelet if they satisfying the following condition (Addison 2005, Jianping 2004 and Jeong 2001):

$$\int_{-\infty}^{\infty} |\psi(t)|^2 dt < \infty, \qquad \text{(A1)}$$

$$\int \frac{|\Psi(\omega)|^2}{|\omega|} d\omega < \infty, \qquad \text{(A2)}$$

where $\Psi(\omega)$ is the Fourier transform of $\psi(t)$. The equation (A1) indicates that a wavelet must have definite energy, and equation (A2) is the admissibility condition which indicates that the wavelet has no zero frequency components. The wavelet function ψ (t) is also known as the mother wavelet. Any basic wavelets that meet the admissibility condition (A2) can be chosen as mother wavelet. The Gabor function was adopted by the software utilised in this work because it provide better resolution in both frequency and time domains compared with other wavelets (Vallen 2009).

The Gabor function is expressed as (Jeong 2000, Jianping 2004);

$$\psi_g(t) = \frac{1}{\sqrt[4]{\pi}} \sqrt{\frac{\omega_0}{\gamma}} \exp\left[-\frac{(\omega_0/\gamma)^2}{2} t^2 \right] \exp(i\omega_0 t), \qquad \text{(A2)}$$

and its Fourier transform is

$$\Psi_g(\omega) = \frac{\sqrt{2\pi}}{\sqrt[4]{\pi}} \sqrt{\frac{\gamma}{\omega_0}} \exp\left[-\frac{(\gamma/\omega_0)^2}{2} (\omega - \omega_0)^2 \right] \qquad \text{(A4)}$$

where ω_0 and γ are positive constants.

The Gabor function (A3) can be considered as a Gaussian window function centred at $t = 0$, and its Fourier transform (A4) centred at $\omega = \omega_0$. The function $\Psi_g((t-b)/a)$ is then centred at $t = b$ and then its Fourier transform is centred around $\omega = \omega_0/a$. Jeong (2000) set $\omega_0 = 2\pi$ such that $1/a$ is equal to the usual frequency f= $\omega/2\pi$.

If $\psi(t)$ satisfies the condition described above, then the wavelet transform of a real signal *f(t)* with respect to the wavelet function $\psi(t)$ is defined as (Jiao, 2004; Jeong, 2000):

$$WT_f(b,a) = \frac{1}{\sqrt{a}} \int_{-\infty}^{\infty} f(t) \psi^*\left(\frac{t-b}{a}\right) dt, \qquad \text{(A5)}$$

where ψ* denotes the complex conjugate of ψ, and this is defined on the open (a, b) half plane(a>0 and b∈R). Parameters *a* and *b* stand for rescale and shift of the basic wavelet function.

The analysis function for WT can be defined as

$$\psi_{a,b}(t) = a^{-\frac{1}{2}}\psi(\frac{t-b}{a}), \qquad \text{(A6)}$$

which mean that every wavelet is generated by shifting and rescaling a basic wavelet $\psi(t)$.

$$WT(b,a) = (t)\int_{-\infty}^{\infty}\psi^*(t)f(t)dt, \qquad \text{(A7)}$$

when function ψ(*t*) satisfies the admissibility condition (A2), the original signal *f*(*t*) can be obtained from the wavelet transform *WT*(*b*,*a*) by performing wavelet inversion.

Discrete wavelet transforms (DWT)

The discrete wavelet transform and its inverse transform are defined as follows (Addison, 2005):

$$WT_{m,n} = \int \psi^*_{m,n}(t)f(t)dt, \qquad \text{(A8)}$$

$$f(t) = \kappa_\psi \sum_m \sum_n WT_{m,n}\psi_{m,n}(t), \qquad \text{(A9)}$$

where κ_ψ is a constant value for normalisations.

In the discrete domain, the scale and shift parameters are generally discretised as $a = a_0^m$ and $b = nb_0$ and the analysing wavelets are also discretised as follows:

$$\psi_{m,n}(t) = a_0^{-\frac{m}{2}}\psi(\frac{t-nb_0}{a_0^m}), \qquad \text{(A10)}$$

where m and n are integer values.

Wavelet Coefficient

Wavelet analysis is fundamentally a correlation method. The wavelet coefficient, $\psi_c(t)$, provides information about the structure of input signal, $f(t)$, and its relationship to the shape of the analyzing wavelet, $\psi(t)$. The wavelet coefficient is defined by the following correlation (Park, 2001):

$$\psi_c(t) = \int_{-\infty}^{\infty} f(t')\psi^*(t'-t)dt \qquad \text{(A11)}$$

Where $\psi^*(t)$ is the complex conjugate of $\psi(t)$ (pair of complex number, both having a same real part, but with imaginary parts of equal magnitude and opposite sign). When $f(t')$ correlate well with $\psi^*(t'-t)$, $\psi_c(t)$ will be large, but when they do not correlate, $\psi_c(t)$ will be small. Any wave shape may be used for the wavelet if it is localised at particular time (Park, 2001).

Gabor Wavelet

Gabor wavelet has been used in the analysis of AE signals due to its good resolution in both time and frequency domain. The frequency component in the output signal has been extracted from the output of the envelope of WT (Jeong 2001, Jingpin 2008):

$$\left|WT_u(x,t)\right| = \sqrt{2a}\left|\psi_g(a\omega_c)\right|\left[1+\cos(2\Delta kx - 2\Delta\omega b)\right]^{1/2} \qquad \text{(A 12)}$$

Where $|WT_u(x,t)|$ is the magnitude of WT of signal x, $\psi_g(\omega)$ is the Fourier transform of the basic wavelet, the parameters a and b stand for scale and shift of the basic wavelet, k is the wave number corresponding to frequency ω. The magnitude of WT takes it maximum value at a = ω_0/ω_c and b = $(\Delta k/\Delta\omega)x = x/c_g$. In other words, the location of the peak on the (a,b) plane indicates the arrival time of the group velocity c_g at frequency $\omega_c = \omega_0/a$, i.e., $f = 1/a$.

Appendix B: Flow chart for WTML AE Crack Length Measurement